FLEXIBLE SOLAR CELLS WITH IMPROVED EFFICIENCY BY INTEGRATION OF LIGHT-TRAPPING NANOSTRUCTURES

A DISSERTATION IN CANDIDACY FOR THE DEGREE OF
MASTER OF SCIENCE IN ENGINEERING

YINGHUI LIU

SUPERVISOR: MORTEN MADSEN

May, 2012

SYDDANSK UNIVERSITET
UNIVERSITY OF SOUTHERN DENMARK

RECOMMENDED FOR ACCEPTANCE

BY NANOSYD,

MADS CLAUSEN INSTITUTE,

UNIVERSITY OF SOUTHERN DENMARK

Information to Users

The quality of this reproduction is dependent upon the quality of the copy submitted. Broken or indistinct print, poor quality illustrations and photographs, print bleed-through, substandard margins and improper alignment can adversely affect reproduction.

ABSTRACT

Solar cells made from organic materials typically incorporate nanostructured blends (bulk-heterojunction) of electron donor and acceptor materials, which efficiently separate electron-hole pairs generated during photo-excitation. From diverse candidate materials, P3HT (regioregular 3-hexylthiophene-2, 5-diyl) has been proofed as an excellent donor material while PCBM (fullerene [6,6] phenyl C61 butyric acid methyl ester) has been verified as a qualified charge carrier acceptor. Therein, a novel, potentially high-efficient blend, namely P3HT:PCBM is proposed for utilizing within organic thin film solar cells. With additional transparent charge carrier collecting layer, viz, the conductive thin PEDOT:PSS (poly(3,4-ethylenedioxythiophene) poly (styrenesulfonate)) film, and appropriate transparent holding substrate, a new type organic solar cell can be obtained. Furthermore, if the holding substrate performs with good flexibility, then the inspiring flexible organic thin film solar cell can be realized. According to plenty of fruitful work, a kind of polyimide - PI2525, is quite proper for meeting the requirements. Hence, it is also utilized in this project. However, comparing to inorganic solar cell, this novel flexible organic thin film solar cell is still weak in power conversion. But, if we can enhance light absorption with applying periodically nanostructured electrode, the solar cell's performance can be further improved. This novel combination of flexible organic solar cell and application of periodic nanostructures is the main objective of this project.

As an experimental starting point, all the organic solar cells were built on rigid BK7 glass substrate. Basing on the experience from the rigid samples, same architecture was applied on the flexible PI2525 substrate, followed by peeling-off from Si handling wafers subsequently.

In order to achieve the combination of nanostructured electrode and the flexible organic thin film solar cell, some necessary tests were performed in this project. With an advanced technique -- electron beam lithography (EBL), optimal functional patterns for light-trapping have been realized, and the light-trapping function of this specific solar cell also turned out to be highly effective. In a word, this achievable combination has been verified to be able to lead the bendable organic thin film solar cell with enhanced power conversion efficiency.

As the essential components of this thesis, all of the related experimental phenomena and outcomes are disserted. Moreover, a summary is given in the last chapter, an outlook which could kindle some inspirations for the future work is included as well.

PREFACE

This dissertation is a part of the requirements for achieving master degree at the University of Southern Denmark (SDU). This work has been fulfilled at the Mads Clausen Institute at SDU in Sønderborg, in the NanoSYD group. Morten Madsen is the supervisor of this project. One related publication was made during the project and has been listed in the bibliography at the end of this dissertation.

I sincerely thank all the fellows which have been supporting me during the whole project, especially my supervisor Morten Madsen my co-supervisor Roana Melina de Oliveira Hansen. Much appreciate to their theoretical instruction and practical guidance. Owing to their help in many aspects, I did learn a lot, I am so delighted to have those profound mentors. Moreover, I also acknowledge Mr. Horst-Günter Rubahn and other fellows in our NanoSYD group, including Kasper Thilsing-Hansen, Jakob Kjelstrup-Hansen, Manuela Schiek, Jacek Fiutowski, Michal Radziwon, Xuhai Liu, and all my classmates, thank these benevolent mates for their helpful support.

In addition, I would like to thank my family for their constant support and comprehension all along, In spite of the thousands of miles distance.

GLOSSARY

AC- Alternating Current

AFM- Atomic Force Microscopy

AM- Air Mass

BHJ- Bulk-Heterojunction

BK7- Borosilicate Crown Glass

CT- Charge Transfer

CTC- Coefficient of Thermal Conductivity

CTE- Coefficient of Thermal Expansion

DMSO-Dimethyl Sulfoxide

D/A- Donor/Accepter

EBL- Electron Beam Lithography

EQE- External Quantum Efficiency

FF- Fill Factor

HOMO- Highest Occupied Molecular Orbital

IPA- Isopropyl Alcohol

LUMO- Lowest Unoccupied Molecular Orbital

MIBK- Methyl Isobutyl Ketone

NREL -National Renewable Energy Laboratory

OPV- Organic Photovoltaic

P3HT- Regioregular 3-hexylthiophene-2, 5-diyl

PCBM- Fullerene [6, 6] Phenyl C61 Butyric Acid Methyl Ester

PCE- Power Conversion Efficiency

PCPDTBT- Poly[2,1,3-benzothiadiazole-4,7-diyl[4,4-bis(2-ethylhexyl)-4H-cyclopenta[2,1-b:3,4-b']dithiophene-2,6-diyl]]

PEDOT:PSS- Poly(3,4-ethylenedioxythiophene) poly (styrenesulfonate)

PI- Polyimide

PMMA- Poly (methyl methacrylate)

PPM- Parts Permillion

PV- Photovoltaic

RPM- Revolutions per Minute

RT- Room Temperature

SEM- Scanning Electron Microscopy

SDU-Syddansk Universitet (English: University of Southern Denmark)

TCO- Transparent Conductive Oxide

TWh- Terawatthours

UV- Ultraviolet

TABLE OF CONTENTS

LIST OF FIGURES

LIST OF TABLES

CHAPTER 1.

INTRODUCTION TO ORGANIC SOLAR CELLS

Incontestably, organic solar cells have been playing more and more important roles in our era. Due to the progress in the past decades, it is well reasonably to believe that its bloom is forthcoming. Comparing to the inorganic ones, organic solar cells are environmentally friendly, low-cost, easy to process, amply large, potentially unbreakable or flexible, etc.[1-4] Regarding these unexampled properties, organic solar cells have been widely applied in plenty of fields, such as commercial building systems or residential home systems (Fig.1.1), PV(photovoltaic) power plants, water pumping, space power supply, telecommunication, automobiles, public system power supply, other digital consumption and military uses as well.[1, 3]

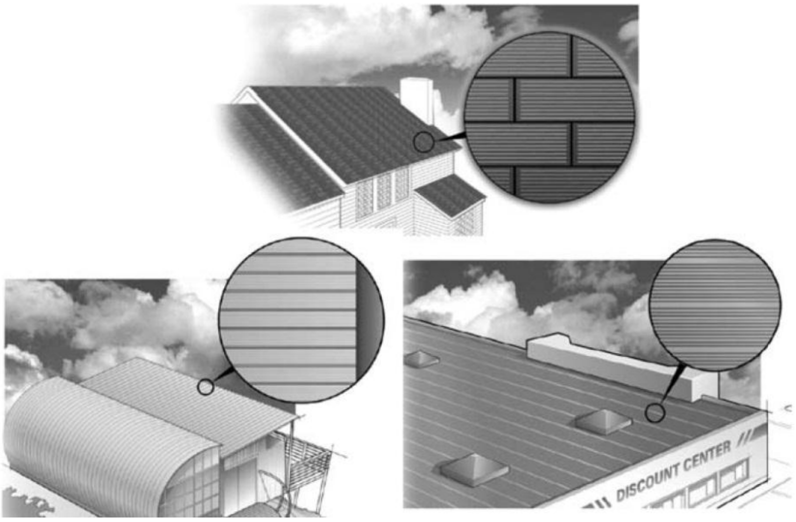

Figure 1.1 New flexible solar modules are integrated, rather than installed, into existing or new buildings. (adapted from Konarka)

Besides, the rapidly increasing high consumption of the traditional fossil fuel results in the inevitable global energy deficiency, plus the environmental pollution which accompany with warming, lightening and powering us up is becoming more and more furious at the same time. People are being eagerer to find renewable, clean, safe energy with high conversion efficiency to instead the old-fashioned ones than any time in history. All in all, the economic, environmental and societal critical factors require us to make a move on the upcoming energy issue. So the cheap and abundant solar energy is doubtlessly the first option which comes to us. A foreseeable prospect is that solar power products based on PV will be popular in the global energy market in the next couple of decades and become a predominant sector by 2040 (Fig.1.2). [1] Therefor we can surely claim that we are entering the solar age presently.

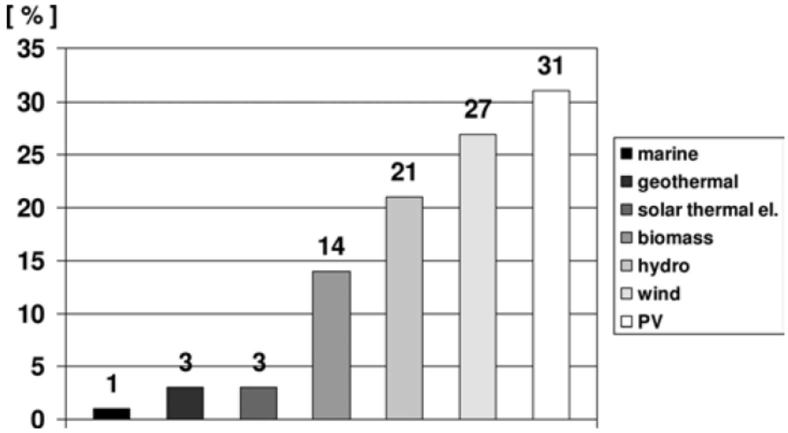

Figure 1.2 Predicted market share scenario of diverse power sources by 2040. Out of a total electricity consumption of 36.346 TWh (from 15.578 TWh in 2001, IEA) renewable energy sources will cover 29.808 TWh, with solar energy becoming largely predominant. (Source: EREC).

Comparing to the conventional solar cells with rigid substrates, a new kind of flexible solar cells is even more potential to be applied in the future. First of all, the mechanical flexibility makes it could be conveniently installed and employed in many specific occasions since it is welcome for all PV applications onto curved surfaces for architectural integration. This property also makes utilizing the utmost room in limited spaces possible and reachable. Secondly, the cost of fabrication, preservation and installation are also minimized in a fairly financial range. Thirdly, the organic stacks make wholly or semi-transparent solar cells conceivable and realizable. We may imagine this kind of "glass": which is harvesting solar energy and transferring it to electricity while being seen through, that could kindle many novel ideas and being utilized in foreseeable aspects in the future. [3]

Even though the flexible organic solar cells have so many merits, it still can't evade the efficiency limitation, the power conversion efficiency (PCE) has always been its blind side. Comparing to the inorganic solar cells, whose PCEs can be up to 20% or even higher, [6, 7] while the organic ones' efficiencies are smaller in some way. But an encouraging breakthrough in realizing higher efficiencies has been achieved by integrating an appropriate mixture of "donor" and "acceptor" polymers to the organic photovoltaic cells' configurations. [2, 3, 5] For the sake of this method and some other effective enhancements, the best record has been rewritten all the time. Fig.1.3 shows all the best research solar cells' efficiencies in the past decades which reported by NREL (National Renewable Energy Laboratory, Colorado, US). We can see that the best efficiency record of emerging OPV is increasing with a rapid rate (the red solid dot-lines in the lower right corner). The Plextronics, US, used P3HT and derivatives of C_{60}, achieved the 5.4% PCE in 2007 and 7.0% PCE in 2010. [8] Both of the Heliatek, Germany, and the Konarka Technologies, US, successfully produced the organic solar cells with the 8.3% PCE in 2010. [9, 10] But the best record which has been admitted by now is the 9.26% PCE which was declared by the Mitsubishi Chemical, Japan, in March of 2011. [11] The increasing up-to date best record has motivated more and more researchers dedicate their wit and sweat to this prospective work and triggered the commercial market being blooming as well.

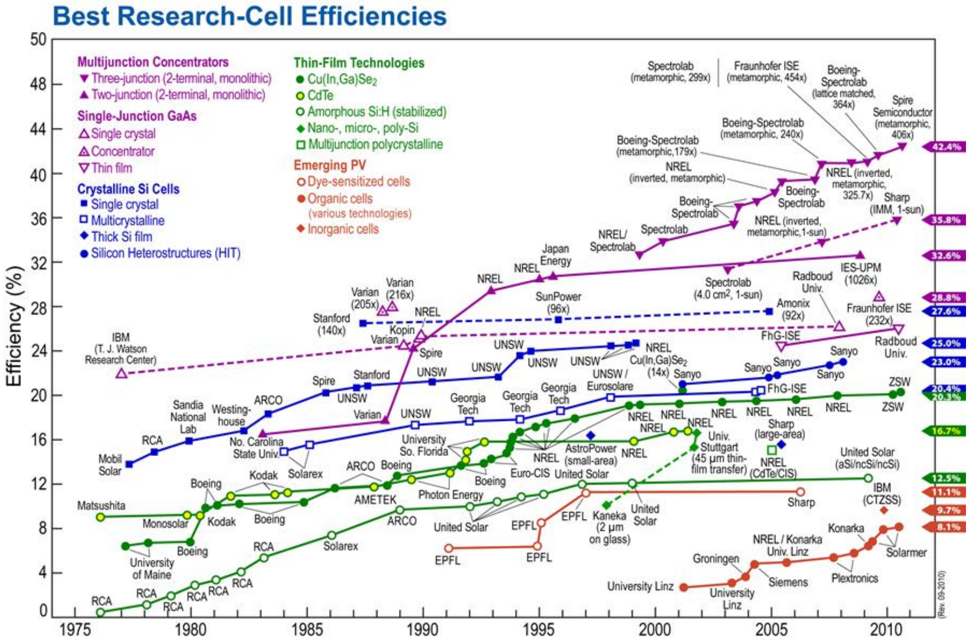

Figure 1.3 Best research solar cell efficiencies reported by NREL (©2010 NREL). From the common crystalline silicon to the exotic and experimental organic polymer cells, there are diverse materials which can be used for producing solar cells. In this graph, we can have a glimpse of their promising future.

This thesis is composed of these five following interconnected chapters: Chapter 1 gives a brief introduction of organic solar cells, the potential value of organic solar cells which inducing a promising future, and, a clear outline of the content in this thesis is included as well. Then, expected objectives are presented in Chapter 2. In Chapter 3, the state-of-the-art, some theoretical interpretation and necessary information are presented. Compendious concepts of the organic thin film solar cells of this very project are given to the readers after going through this chapter. As a good analogically processable mode in Chapter 4, the fabrication and optimization parts of the solar cells which built on rigid glass substrates are included. All the performance of rigid-substrated organic solar cells is presented in this chapter in order to make a profound comparison with the up-coming flexible-substrated organic solar cells depicted in the next chapter. The next chapter, Chapter 5, is an essential part to the entire thesis, the fabrication of flexible polyimide substrate, nanostructures making process with EBL method are disserted; morphologies of each structural part are investigated; moreover, the characterized results from experiments verify the expectant aim of this project. As the last part of the main content, a good conclusion is given in Chapter 6. Meaningful prospects are imagined and inspirations are kindled with realizable methods and paths. I did my endeavour to manifest the working track of this meaningful and promising project within this thesis, hopefully the endeavour will give you an impressive concept of the optimized organic thin film solar cells and also let you realize how valuable and prospective this subject will be.

CHAPTER 2.

OBJECTIVES OF THE PROJECT

This very thesis mainly focuses on developing a method for integrating nanostructured bottom electrode in the solar cells which built on flexible polyimide (PI) substrates, in order to obtain high light absorption in order to improve the power conversion efficiency (PCE). All the necessary theories, assumptions, experimental processes, actual phenomena, mathematical calculations, statistics, analysis and relevant discussions are all included in this thesis. Moreover, this project is also expected to propose some inspirations for overcoming current defects or limitations and give a brief outlook for the future work.

The efficiency limitation of the current organic thin film solar cells is a very important issue, and it's also one of the most discussed points in this thesis. Ideally, if we want to obtain higher power conversion efficiency, that we must make the cells absorb more light, namely elongate the transmission path of light in the cells and coupling the light in a reasonably wide range of the solar spectrum. Because a corrugated metal back surface is able to alter propagation direction of incidence, so that applying periodic nanostructures to trap light in order to further increase the conversion efficiency is feasible. In this way, the enhanced light absorption results in improved conversion efficiency. If we can make a further combination of the nanostructured metal electrodes and a flexible organic substrate, then the imagined target, viz, flexible high-efficient with low cost organic solar cells will be achieved.

Aiming to improve the PCE, I present quite a few inspired ideas of optimising and improving the quality of organic thin film solar cells with experimental results within this thesis. Including trapping light with periodic nanostructures, application of bulk-heterojunction materials, flexible substrates, unconventionally inverted architectures, etc. All these processing methods or inspired applications above were proposed to overcome the potentially conquerable defects and flaws of the current flexible organic solar cells, and all realized with precise and convictive experiments as well. For achieving these ideas, some up-to-date techniques were employed during the entire project process. Electron beam lithography (EBL) was used for fabricating the desired nanostructures on bottom metal electrodes; bulk-heterojunction materials were mixed due to the extended interface and specific properties; a proper procedure of making polyimide substrate was deduced and tested in order to functionalize the flexibility, and so on. Regarding the fruits which presented within this thesis, all the theoretical analysis and practical work was turned out to be worthy and meaningful.

CHAPTER 3.

ORGANIC SOLAR CELLS

3.1 ORGANIC SEMICONDUCTORS

Comparing to the metal materials, semiconductors take advantages of photovoltaic to fulfil the current creation process. Since the band gap of most semiconductors is within the range of 1~3eV (Fig.3.1), the energy of photons will be absorbed by electrons so that make them transit over the narrow band gap in order to generate consecutive current. Besides, the light which can be absorbed is usually visible and infrared, namely the conversion efficiency could much greater than metals; moreover, the excited carriers is not only the electrons but also the holes, that could lead stronger current and further increase the efficiency as well.

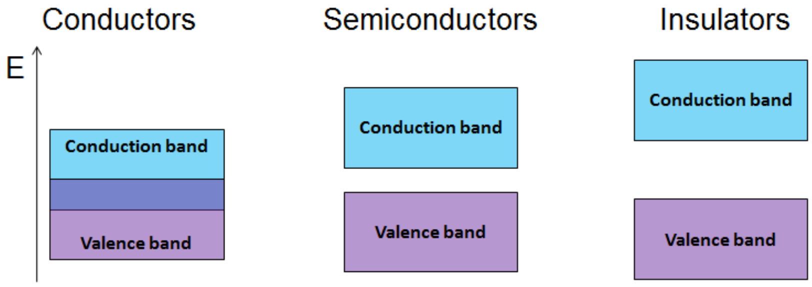

Figure 3.1 Schematic energy band gap diagrams of conductors, semiconductors and insulators. Commonly, conductors' conduction band and valence band overlap each other; semiconductors' band gap is narrow (about 1~3eV); insulators have a broad band gap (usually greater than 9eV).

The specific properties make the semiconductor to be a good choice for carrier generation of solar cells.

Normally, the conjugated architecture of organic photovoltaic (OPV) cells is quite different from the structure which is applied in inorganic ones, this is due to the different electric energy generation mechanisms. For organic solar cells, photon absorption leads the creation of tightly bond excitons or electron-hole pairs, on the contrary to the generation process of free carriers in inorganic materials. Furthermore, the carrier mobility of organic material is low (typically 10^{-7} to 2 $cm^2\ V^{-1}\ s^{-1}$) and the excitons diffusion length isn't too long as well (L_D< 40nm). [12] Nevertheless, most of the organic materials still can be processed to be very thin film due to the high absorption coefficients, making the highly effective light absorption possibly kept.

In organic semiconductor materials, the delocalization of electrons across π-π bonds between neighbouring molecules can provide charge conduction. The π orbital with lower energy is usually called the highest occupied molecular orbital (HOMO) and the anti-bonding π* orbital with higher energy is called the lowest unoccupied molecular orbital (LUMO). [12] When the organic solar cells are working, photon absorption which happens within organic semiconductor materials prompts the electrons from the HOMO level to a higher level, for instance, the LUMO level. That leads to a Coulomb attraction between the remaining electrons and the remaining holes in the HOMO. This bi-particle state is usually referred to as an exciton, and it always presents in three typical modes in materials, the Frenkel, charge-transfer (CT) and Wannier-Mott exciton, which are schematically shown in Fig.3.2. [12] The Wannier-Mott mode is usually found in inorganic materials but the other two modes commonly exist in organic materials. For inorganic semiconductor materials, both the dielectric constants and the delocalized electron densities are high, that results in the spatially dispersed excitons with the radius far greater than a, and the Coulomb binding energy is about a few meV (Fig.3.2(a)). But for the organic semiconductor materials, on the contrary, the radius is shorter so that the binding energy is much higher than in the inorganic ones. For instance, The Frenkel exicton consists of an e-h pair in the same molecule, where the binding energy is commonly from 0.2 to 1eV. [12] The binding energy in a CT mode exciton might be slightly lower than in Frenkel mode. The difference of binding energies between inorganic and organic semiconductors can be potentially reasoned to interpret the power conversion efficiency's difference between inorganic and organic solar cells.

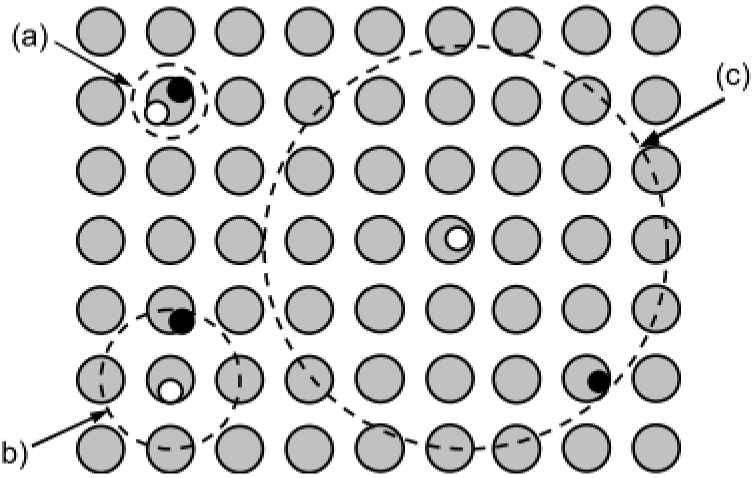

Figure 3.2 Schematic drawing of the three typical types of excitons in solid: (a) a Frenkel exciton in a single molecule; (b) a charge-transfer(CT) exciton, delocalized with a radius roughly comparable to the lattice constant; (c) a Wannier-Mott exciton, highly delocalized with a radius covering several lattice constant length. These three types are plotted in the same drawing; whereas they don't coexist in the same material for sure. This graph is extracted from Ref[13].

3.2 FUNDAMENTALS OF ORGANIC PHOTOVOLTAIC SOLAR CELLS

Due to the sunlight absorption within classical inorganic solar cells, weak Coulomb bound pairs of charge carrier (an electron and a hole) are generated. However, in organic semiconductors, the screening of opposite charges is even much weaker as the dielectric constant is lower. That results in a much stronger interaction of the photogenerated positive and negative charges. Hence, a single exciton, namely a highly bounded e-h pair, becomes the primary optical excitation in organic semiconductor materials. Since this binding is barely overcome in inorganic solar cells, so that the concept of organic solar cells has to be dissimilar. Besides, the most of organic semiconductor materials are amorphous so that charge transfer is much more difficult than in the materials like crystals, that is the another significant difference.

However, there is still a marked advantage, namely the ability to synthesize tailor-made organic substance. Which allows appropriate tuning of the absorption range and the charge transport properties to be possible, moreover, self-assembly can be also fulfilled through nanochemistry techniques. These are prominent advantages which are able to make organic solar cells to be potentially employed regarding various conditions.

The naissance of the first-generation organic solar cells took place in mid 1980s. Two exceedingly notable concepts have come into people's mind since then, these are the donor and the acceptor materials of the organic solar cells theory. [14]

Incident light is usually absorbed chiefly in the donor material, which provides charge carriers, per se. The acceptor, which can accept the charge carriers from the donor, is usually strongly electronegative. That makes the interface between the donor and the acceptor presents like a p-n junction. The photogenerated single excitons diffusion commonly takes place around the interface area formed by the two materials, namely the p-n junction, and always within the donor towards to the acceptor. A good example of the acceptor material is the buckminsterfullerene (C_{60}) with a low LUMO level.

An exciton moves by diffusion heads to the donor acceptor heterojunction, where is very energetically attractive to the transfer of the electron to the acceptor molecules (Fig.3.3). The charge transfer is usually pretty fast, might take time shorter than 100fs in polymerfullerene systems. Meanwhile, it is very efficient as well, due to the slower alternative loss mechanism. [15]

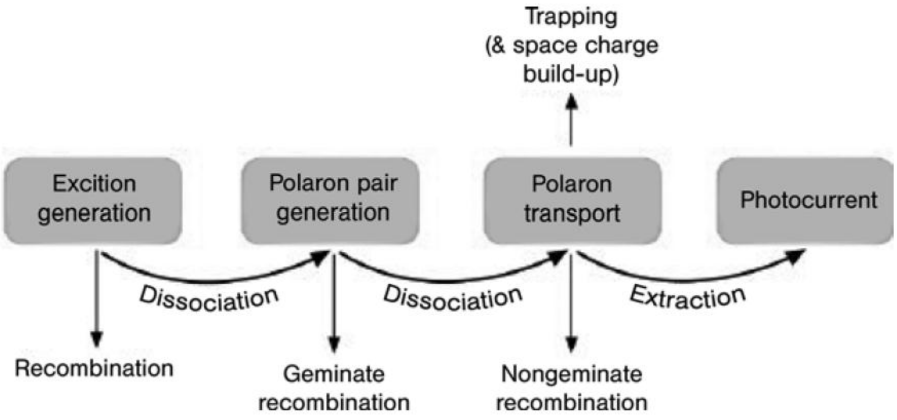

Figure 3.3 Steps from exciton generation to photocurrent in organic solar cells. (Image courtesy of Dr. C. Deibel, http://blog.disorderedmatter.eu).

Since the holes have to stay on the polymer, now the exciton is dissociated. Even if the holes and electrons are locating in sunder, they are still Coulomb bound, regardless of the clearly lowered recombination rate (commonly, the recombination takes place within a blink, from micro- to milliseconds) as compared to the single exciton (the life time can down to nanoseconds).

In order to dissociate the final charge pair and avoid the recombination of monomolecules, an electric field which can overwhelm the Coulomb attraction is in need. And it is an internal field, which can be impacted by the built-in potential due to the difference between the electrodes' work functions.

As shown in Fig.3.4, an OPV solar cell is composed of organic active layers (organic D/A) sandwiched between the top and bottom electrodes. In Fig.3.4 the underlying electrode which is made of transparent conductive oxide (TCO) or translucent polymer layer pre-deposited on clean see-through glass substrates is assigned to collect holes, so the anode it is. For the top contact cathode, which is often made of metal materials (mono- or multilayers), designed for collecting the photogenerated electrons. The anode and cathode materials are chosen to have significantly different work functions for the sake of enhancing appropriate charge separation. Normally, the charge separation happens in the organic D/A interface.

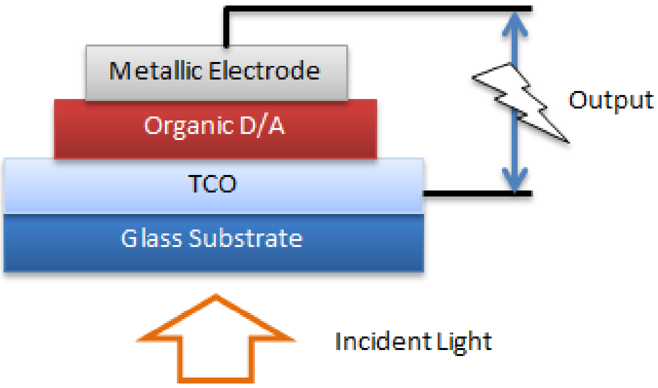

Figure 3.4 A typical OPV cell with the conventional structure.

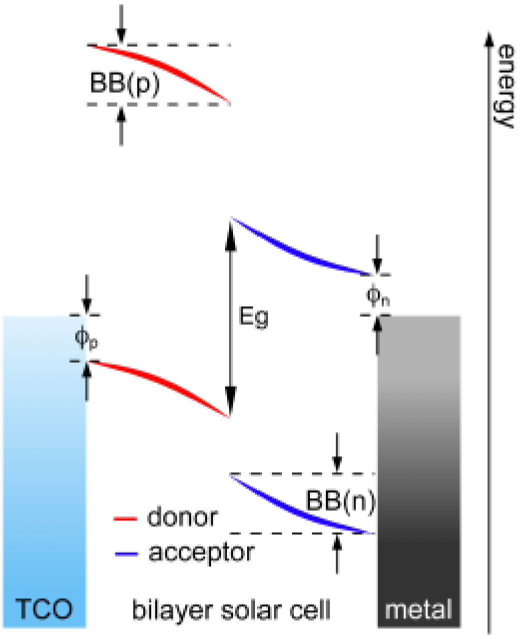

Figure 3.5 Schematic energy level diagram of a bilayer OPV solar cell (φ: workfunction, Eg : bandgap: BB(n): depletion width). (Image courtesy of Dr. C. Deibel, http://blog.disorderedmatter.eu).

Fig.3.5 shows the schematic energy level diagram of a typical bilayer OPV solar cell, the configuration according to Fig.3.4. The TCO anode is followed by the organic donor/acceptor layer, and covered by a metallic top cathode. Now we assume the process happens in this disordered bulk-heterojunction organic solar cell.

Excitons are photogenerated in the donor domains, sequentially diffuse to and dissociate at the D/A interfaces due to the energy offset between the HOMO level of the donor and the LUMO level of the acceptor. After dissociating, the photogenerated excitons turn into oppositely charged polarons. The positive charge polarons, namely the holes, head toward the TCO anode; whereas the negative charge polarons, viz, the electrons, dash to the metallic cathode. An effective band gap is necessary for energetically separating these resulting polaron pairs.

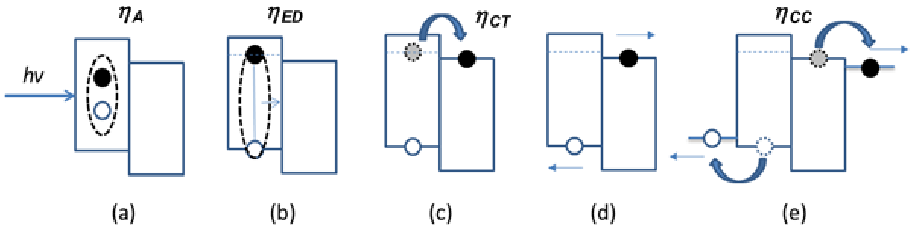

Figure 3.6 Excitonic transformation and transportation. The horizontal lines to the right and left of each graph correspond to the Fermi energies of the cathode and anode, respectively. The boxes refer to the acceptor and donor energy gaps (between the LUMO and the HOMO levels), respectively. Here, the dark dots represent the electrons whereas the white dots stand for the holes. (a) A photon is absorbed by the donor. It is always good to have a material that absorbs as intensely and broadly as possible across the solar spectrum; (b) Excitons diffusion, the exciton which composed of e-h pair diffuses in the donor phase. This process is much related to the exciton's travelling length L_D and lifetime τ. According to the equation $L_D = \sqrt{D\tau}$,[16] the larger the diffusion coefficient, the longer the lifetime, which means the further the exciton can go before it decays back to the ground state. It is better if the exciton has a long travelling length since that allows the exciton to have a higher possibility of achieving the D/A interface with the acceptor in its lifetime. However, if this process doesn't occur, then no charge carriers will be generated so that the exciton will decay back to the ground state. This decay may present in the form of either heat, vibration, or releasing the photons it once absorbed - also known as photoluminescence, but that is the exact contrary process which we don't expect. (c) Charge carriers disassociation. Once the electron and hole have separated, the built-in potential cause the electron to drift toward the cathode and the hole to drift toward the anode. But, if there was by any chance no built-in potential, then the electron and the hole will form a disorderly diffusion. (d) Charge carriers'

motion toward electrodes. (e) The charge carriers will be collected efficiently at their respective electrodes, enter the external circuit and form current at last.

In Fig.3.6, η_A is the light absorption efficiency within the donor domains, η_{ED} is the exciton diffusion efficiency to a dissociation site, η_{CC} is the charge collection efficiency by the electrodes, and η_{CT} is the efficiency of charge carriers transfer. By all of these efficiencies in differential phases, the external quantum efficiency (EQE), η_{EQE} can be calculated. Defined as the ratio of the number of e-h pairs collected at the electrodes to the number of incident photons:

$$\eta_{EQE} = \eta_A \times \eta_{ED} \times \eta_{CC} \times \eta_{CT} \tag{3.1}$$

Normally, $\eta_{CT} = 1$ in organic solar cells since the process is very fast (~10-100fs). Hence, an estimation of η_{EQE} only depends upon the other three parameters, η_A, η_{ED} and η_{CC}.

But why do the charge carriers flow to cathode or anode automatically? What is motivating their directional motion? To answer these questions, we need to consider the difference of work functions in advance. The work function, actually is the minimum energy needed to remove an electron from a solid to a point immediately outside the solid surface. The work function refers to the Fermi level [17]) that is the potential of the two electrodes. When a system is in equilibrium, it has the tendency to keep the chemical potentials to be the same across the entire system. For achieving this equilibrium, the system will tend to make charge redistribution. That is the exact reason to explain why the charge carriers can flow directionally. The charge redistribution, therein increase chemical potential on the anode side and decrease the potential on the cathode side so that the two chemical potential levels can be aligned.

3.3 BULK-HETEROJUNCTION STRUCTURE (P3HT:PCBM)

A heterojunction is the contact of two materials with different electrical properties. The essential character is that the donor is electron richer than the acceptor. Solution-processed bulk heterojunction (BHJ), is widely applied in fabricating organic solar cells. It has drawn a serious attention during the last few years. The advantages like the low-cost, easy to handle, relatively higher efficiency and so on may make it lead the development of photovoltaic technologies in the near future.

Bluk-heterojunctions are able to efficiently dissociate excitons over the entire extent of the solar cells so that can generate e-h pairs everywhere in the thin organic film. But, due to its disordered configuration, it is somehow difficult to separate those e-h pairs; besides, that also increase the possibility that the trapped charge carriers recombine with the mobile ones.

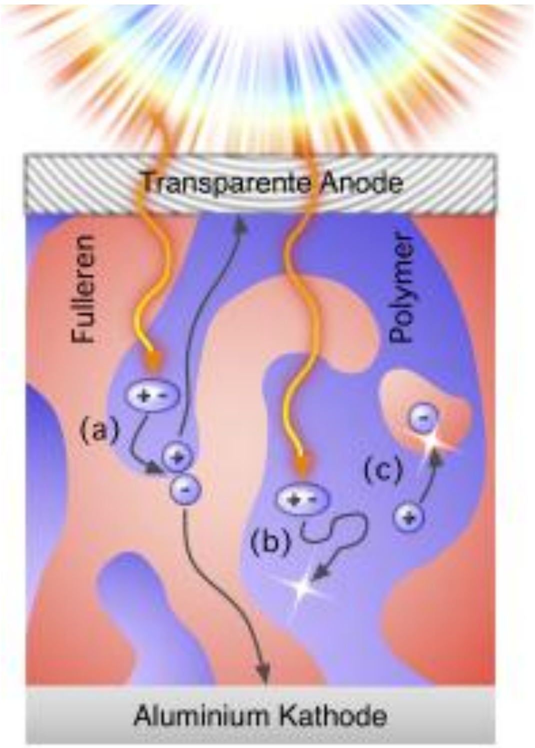

Figure 3.7 Charge carriers' generation and recombination in disordered bulk-heterojunction organic solar cells. (Image courtesy of Dr. C. Deibel, http://blog.disorderedmatter.eu)

The main process of charge carriers' generation and recombination in disordered BHJ organic solar cells can be seen in the above Fig.3.7 In the linear heterojunction formation, donors and acceptors' interaction only take place in the geometrical interface between the conjugated polymer and fullerene layers. However, in the bulk heterojunction formation, the interactions could happen in the entire volume, and meanwhile, with a shorter travelling length (3~10nm). That can be used to explain why this configuration is able to rise the short circuit current (Isc). In Fig.3.7, (a) shows an exciton diffuses to a D/A interface and dissociates into an e-h pair or maybe transforms to a radiative recombination (b). Once e-h pairs are generated, they could be separated with the application of an external electric field, those isolated, free electrons or holes could further hop to the corresponding electrodes to form photocurrent like shown in (a), or might recombine with the other mobile or trapped charge carriers like shown in (c).

According to plenty of scientific articles, a promising mixture of regioregular 3-hexylthiophene(P3HT) and fullerene [6,6] phenyl C61 butyric acid methyl ester (PCBM) is verified as a good bulk heterojunction material and has become prevailing due to their specific properties: P3HT can be used as a good donor material and PCBM is suitable for accepting charge carriers. Therein, in this project, for the photoactive layer, I chose the mixture of regioregular poly(3 hexylthiophene)(P3HT) blended with fullerene [6,6] phenyl C61 butyric acid methyl ester (PCBM) with the ratio 1:1, and dissolved in 1,2-dichlorobenzene.

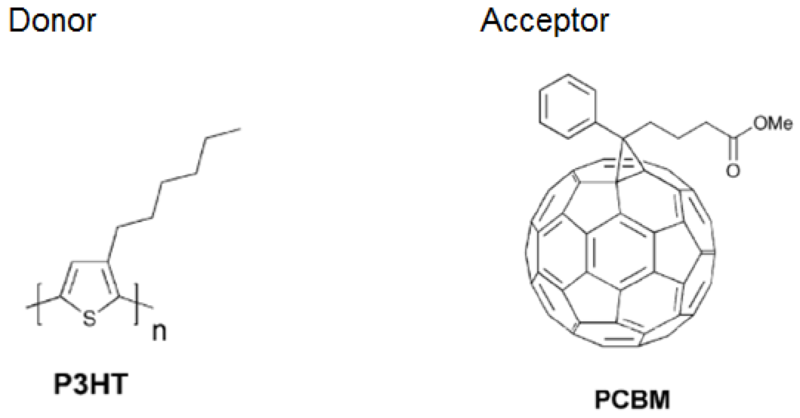

Figure 3.8 Structural diagrams of the donor material regioregular 3-hexylthiophene (P3HT) and the acceptor material fullerene [6,6] phenyl C61 butyric acid methyl ester(PCBM).

Ratio to PCBM (weight)	Layer thickness (nm)	Solvent	Max EQE (%)	Voc (V)	FF (%)	Jsc (mA/cm²)	Eff (%)
1:3	350	-	76	0.58	55	8.7	2.8
-	≈110	DCB	70	0.55	60	8.5	3.5
1:1	-	CB	58	0.61	53	9.4	3.0
1:1	63	DCB	-	0.61	62	10.6	4.0
1:1	≈220	DCB	63	0.61	67	10.6	4.4
1:0.8	-	CB	-	0.65	54	11.1	4.9
1:0.8	-	CB	-	0.63	68	9.5	5.0
1:1	175	CB	70	0.6	52	12	4.4
1:0.8	-	CB	88	0.61	66	11.1	5.0
1:1	320	DCB	82	0.56	48	11.2	3.0
1:1	≈220	DCB	87	0.64	69	11.3	5.2
3:2	80	CB+NtB	-	0.66	-	10.5	4.3

Table 3.1 Non-certified performance data of P3HT-PCBM solar cells as reported in literatures. CB in the fourth left column is the abbreviation of chlorobenzene and DCB stands for dichlorobenzene. Reproduced from Ref [5].

Table 3.1 gives a non-exhaustive survey of investigating efficient OPV cells based on P3HT:PCBM blends. Here we can easily tell that the application of this promising blend has been turned out to be a good way to increase the conversion efficiency. Actually, we can also tell the carrier-donating ability of P3HT and the carrier-accepting ability of PCBM from the molecular structural diagrams (Fig.3.8). Date back to the first report of the solution processed BHJ solar cells which was authored by Yu et al, [18] PCBM, this highly soluble fullerene derivative [19] was considered as an excellent material to achieve sufficient percolation of charges through both components. Remarkably, after so many years of acceptor material investigation, PCBM is still one of the best candidate material of acceptors, the offbeat performance makes it the most popular electron acceptor for organic solar cells.

Another aspect that we must take into account, is the BHJ's morphology, plenty researches have been done on this very point. According the beneficial researching fruits of Ying Zheng and Jiangeng Xue's work, [22] a mixed BHJ cell usually has a higher short-circuit current density than a planner cells does (with other identical conditions), because the excitons generated in the mixed HJ can easily reach a nearly hetero-interface and dissociate to create separated electrons and holes. Naturally, the small dimension also causes less material consumption. These can be taken as specific advantages of the BHJ organic solar cells.

3.4 SOLAR CELLS' PERFORMANCE AND ENERGY CONVERSION

A good solar cell should have a high, steady and reliable power output with high conversion efficiency. Regarding the organic solar cells' intrinsic properties, we may evaluate their performance from a few aspects. These aspects, or might be called parameters, are usually used as criterions to judge the organic solar cells' capability of energy conversion.

For demonstrating these important parameters, we use Fig.3.9 to previously illuminate the organic solar cells' working mode. To power AC devices, an organic can be added as a power resource in a closed-loop electric circuit since it owns an equivalent function which a battery has (Fig.3.9). But, an essential difference is, the power delivered to a load by battery is relatively constant, whereas the power delivered by solar cell is more dependent on the incident light intensity comparing to the load. [15] In this point, we may say that batteries can be taken as voltage source whereas solar cells can be regarded as current source (Fig.3.10). So essentially, the solar cells' can be only functionalized when they are being exposed to incident light. But what if without light's shining? What is the difference the cells make? It is necessary and very important to investigate.

In the dark circumstance, the basic bulk-heterojunction organic solar cells with donor, acceptor, and sandwiched by anode and cathode is a diode. Since the current is roughly proportional to the illuminated area, so basing on the common I-V curve, with considering the generated current in per unit of area, a J-V curve, namely a "voltage vs. current intensity" curve is obtained (Fig.3.11). Positive and negative charge carriers are injected in a certain way depends upon whether a forward bias or a reversed bias is to be achieved. Under reversed bias the electrons can hardly form current when they are going from the anode to the cathode. Nevertheless, on the other hand, if the electrons are able to overcome the injunction barrier, then they can form a constant current from the anode to the cathode when a forward bias is applied. So, the dark curve is a typical I-V or J-V plot of a diode. A reversed bias will produce almost no current which can be negligible but a forward bias is able to produce a relatively high current as long as overcoming the threshold.

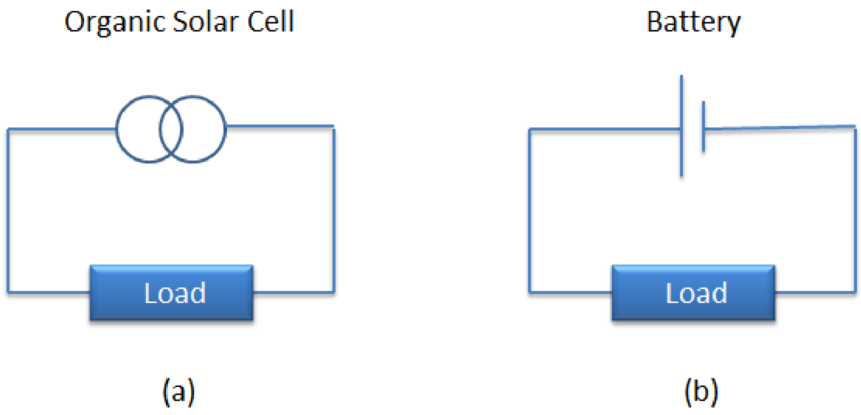

Figure 3.9 A solar cell can be regarded as a battery in a closed-loop electric circuit.

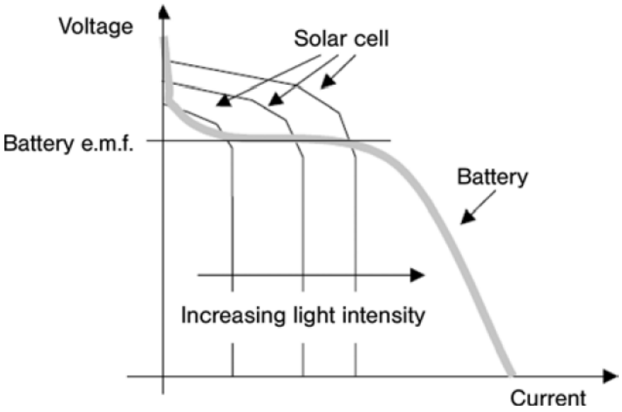

Figure 3.10. A battery is actually a voltage source but a solar cell is a current source. Because batteries are made to offer constant voltages to the load, however solar cells are intending to deliver constant current for any given illumination. The voltage across a solar cell is quite depended upon the load's electric resistance. The "e.m.f." ,viz, the "electromotive force". (Reproduced from Ref [20].)

When incident light coming into the organic solar cells, that would be different from the phenomena above. The curve with hollow dots lower than the dark J-V curve shown in Fig.3.11 stands for the light-on situation. Under illumination, incident photons are absorbed in the donor domains, as depicted in former context the built-in potential cause the charge carriers' dissociation at the D/A interface so that the electrons will go toward the cathode while the holes will go toward the anode then a reversed current which is usually called "photocurrent" will be observed. Under illumination, although there is no external voltage is applied, the solar cells can still fulfil the duty of a battery thus regarded as a power supply.

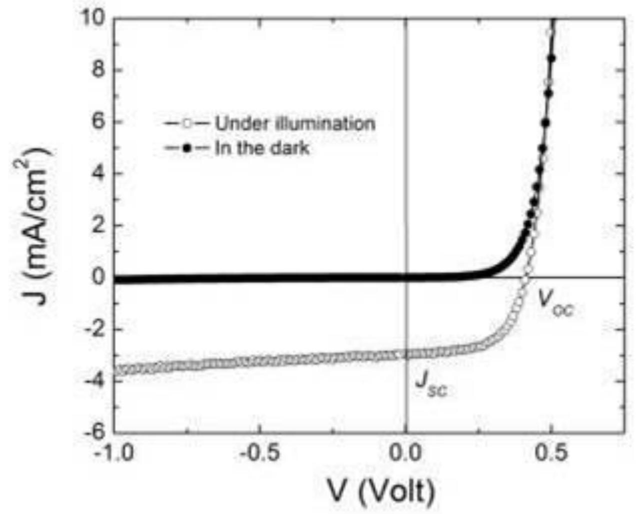

Figure 3.11. A plot shows the relation between the voltage (V) and current intensity (J). The curve with solid dots represents light-off condition and the curve with hollow dots stands for light-on condition.

In the light-on condition, the crossing point of the curve and the vertical J axis stands for the "short circuit current intensity", usually written as Jsc. That is the real-time current intensity without any external applied, can be considered as if it was a short circuit in the whole system. When a forward bias is being applied, it is starting compensating for the reversed photocurrent and there must be a point where the photocurrent becomes zero. The voltage value of this very point, Voc, is known as the "open-circuit voltage". It refers that even an external voltage is applied, there is still no current, equal to an open electric circuit. According to the Ohm's Law, for any intermediate load resistance R_L, the circuit supplies a voltage between 0 and Voc and delivers a current I(V) that satisfies the relationship $V = I(V)R_L$.

The electromotive force (e.m.f.) is actually caused by a temporary change in the electrochemical potential, and that is due to the incident light's shinning. From the cells' external quantum efficiency η_{EQE} which is presented in formula (3.1), we can deduce another formula to calculate Jsc, that is,

$$Jsc = q\int b_S(E)\eta_{EQE}(E)dE \qquad (3.2)$$

Where q is a single electric charge, and $b_S(E)$ is the flux density of the incident photons. From the formula (3.2), we can tell that Jsc is obtained by integrating the product of the photon density and η_{EQE} of the photon energy.

Another important parameter is the Fill Factor (FF). But before describing it, we need to consider the output power density delivered by solar cells. Normally, at the voltage V with a corresponding current density J, the output power density is defined as the area of the operating regime.

$$P=JV \tag{3.3}$$

When P reaches the maximum point (V_m, J_m), as shown in Fig.3.12, then the actual maximum output power intensity is obtained. However, according to the short-circuit current Jsc and open-circuit voltage Voc, the ideal output power intensity could be up to their product. So, here comes the definition formula of Fill Factor (FF),

$$FF = \frac{P_m}{P_{ideal}} = \frac{J_m V_m}{J_{sc} V_{oc}} \tag{3.4}$$

Apparently, we want to have an FF as high as possible. Hence, maximizing the FF, is always a goal which has been pursued by researchers for a long term.

If we can further take the power density of incident light, P_S, into account, then the conversion efficiency of a solar cell actually is the power density delivered at the operating point as a fraction of it, namely,

$$Eff = \frac{|J_m V_m|}{P_S} \tag{3.5}$$

Furthermore, since the conversion efficiency is quite related to Jsc and to Voc through the FF, then,

$$Eff = FF \cdot \frac{|JscVoc|}{P_S} \tag{3.6}$$

By now, the four quantities Jsc , Voc , FF and Eff which determine the performance of a solar cell, have been described. Thus, these four parameters are vital to evaluate the quality of a solar cell.

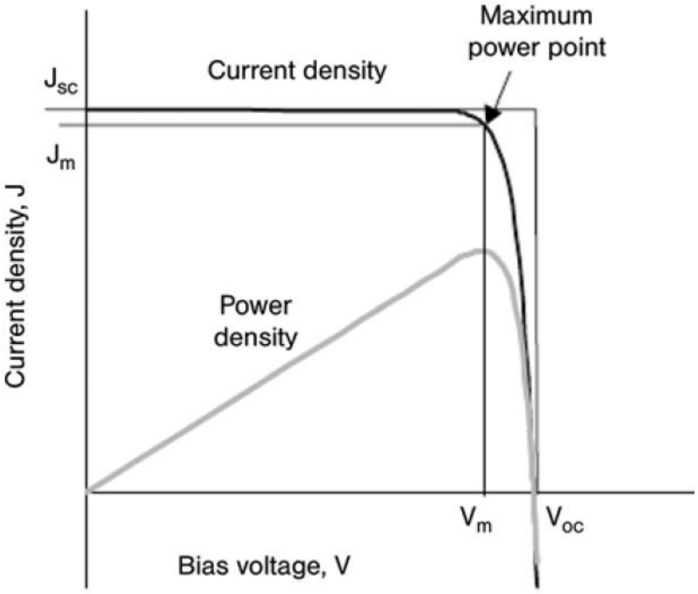

Figure 3.12. The black curve stands for the current voltage while the grey curve represents the power voltage of an ideal solar cell. The max bias Vm is close to the Voc. The maximum power density Pm which can be actually achieved is given by the area of the inner rectangle, whereas the ideal power density can be also calculated by the outer rectangle's area. Ideally, we expect the Fill Factor as high as possible. Assuming if the FF is equal to 1, then the inner and outer rectangles were coincided with each other. (Reproduced from Ref [20].)

3.5 PERIODIC NANOSTRUCTURES FOR IMPROVING LIGHT-TRAPPING

For achieving higher output power and further increase the conversion efficiency, one possible way is trapping more light and elongate the light's travelling path within the multi-layer organic solar cells. An inspired idea for realizing this light-trapping in organic thin film solar cells is the utilization of metallic nanostructures. If these structures can be engineered properly, then the incident light can be scattered, and meanwhile, "folded" into thin bulk-heterojunction active layers, therein more light can be absorbed and converted into electric power.

Basing on this analysis, elongating light travelling path with applying periodic nanostructures was proposed and explored. The structures with tiny dimension behave as back reflectors on top of the bottom electrodes in the solar cells, Fig.3.15(a) is the schematic diagram of this configuration. The grating equation states as following,

$$m\,\lambda = np(sin\,\alpha + sin\,\theta) \tag{3.7}$$

In the formula (3.7), m is the diffraction order in integers and λ is the incident wavelength; n is the refractive index of the grating material; p is the period of grating; a and θ are the incidence and diffraction angles, respectively. If p=λ/n, for normal incidence, m can take values of 0 or ±1. If the etch depth of rectangular gratings is t=λ/4n, the zeroth-order reflection will be highly suppressed so that the ±first-order diffractions are altered by 90°, due to this change of the light propagation direction, the optical path length can be significantly increased.[21]

For maximizing this specific function, the periodic dimension of the structures must be adequately small to meet the light spectrum and some other factors, normally varies from dozens of nanometres to hundreds of nanometres.

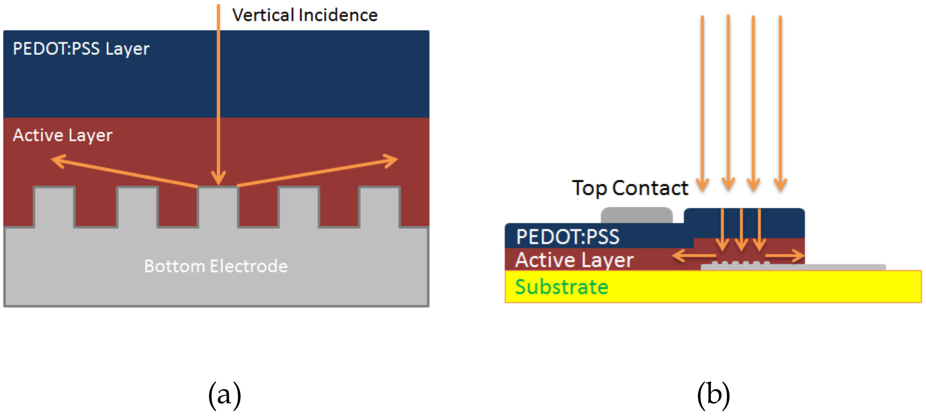

Figure 3.13 Schematic drawings of light scattering in organic thin film solar cells with normal incidence. (a) partially magnified schematic; (b) overall configuration.

With the enhancement from the nanostructures, more incidence can be "reserved" within the thin film solar cells and further increase the conversion efficiency. For the sake of the tiny dimensional structures, the physical thickness of the photovoltaic layers can be reduced in a proper range, that makes the solar cells lighter, cheaper, and optimises the efficiency as well.

In this project, the method which for achieving highly qualified nanostructures is electron beam lithography (EBL) with using the efficient, stable and reliable equipment settled in the cleanroom, Alsion, a Hitachi S-4800 SEM with a Raith ELPHY Quantum module. More detailed information of the application of the nanostructures' enhancement will be presented in the following chapters (Chapter 4 and 5).

3.6 DISCUSSION AND SUMMARY

In general, organic thin film solar cells would be a promising option to achieve energy conversion with barely harmful to the environment. Due to the extraordinary capabilities on absorbing light, transferring charge carriers and generating electric power, multi organic semiconductor thin layers are utilized to fabricate solar cells, and they can also be optimised to potentially improve the conversion efficiency and other characteristics if the thickness can be engineered in an appropriate level. Thanks to the novel bulk-heterojunction configuration, those characters can be further improved as well. According to the state-of-the-art and the precious experience supported by the other researchers, P3HT, is a good candidate of donor material well PCBM plays an offbeat role as acceptor material. At this rate, a mixture of them with a proper ratio turns out to be a good option to form the bulk-heterojunction configuration. Despite now we are still in the researching and optimising period, but a good prospective industrialization of applying bulk-heterojunction in making organic thin film solar cells is foreseeable.

And, regarding to the objectives of this project, an inspired combination of periodic nano-structures and flexible substrates is proposed. Aiming to enhance the light absorption and in order to improve the properties of the organic thin film solar cells, the nanostructures are analysed, investigated and realised with some specific techniques and methods. Thus, making semi- or wholly transparent, highly efficient, qualified and reliable solar cells, has been proved to be feasible in this thesis. Nevertheless, the organic thin film solar cells still have the potential to be further improved from some other aspects, such as the working temperature, working humidity, vibrations, etc. All of these could also be investigated and researched as the follow-up work after this very project.

CHAPTER 4.

FABRICATION AND OPTIMIZATION OF ORGANIC THIN FILM SOLAR CELLS ON RIGID SUBSTRATES

4.1 CATEGORIES OF THE APPLIED ORGANIC MATERIALS

In general, a good candidate of the active material in organic solar cells must have reasonable HOMO level and LUMO level positions and high charge carrier mobilities. People have been searching qualified and reliable active materials with good performance all along. Plenty of materials have turned to be feasible as the component of active layers. There some small molecules of active materials generally used in organic solar cells are listed in Table 4.1, the schematic molecular structures, HOMO & LUMO levels and charge carrier mobilities which under the room temperature are all included.

Table 4.1 Organic molecules commonly used in solar cells

Material[*]	**Molecular structure**	**HOMO (eV)**	**LUMO (eV)**	**Carrier mobility ($cm^2V^{-1}s^{-1}$)**
CuPc	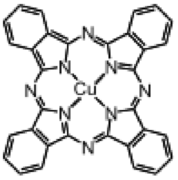	5.2	3.2	$\mu_h=7x10^{-4}$

pentacene	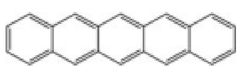	5.1	3	$\mu_h>1$
SubPc	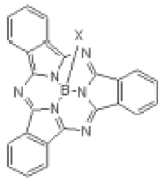	5.6	3.6	N/A
C_{60}		6.2	3.6	$\mu_e=5\mathrm{x}10^{-2}\sim7\mathrm{x}10^{-1}$
PTCBI	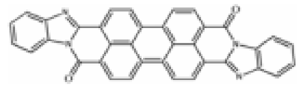	6.2	3.6	$\mu_e=2\mathrm{x}10^{-6}$
PTCDA	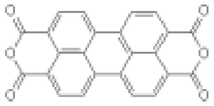	6.8	4.6	$\mu_e=9\mathrm{x}10^{-3}$

*CuPc = Copper Phthalocyanine, SubPc = Boron Subphthalocyanine Chloride, PTCBI = 3,4,9,10-Perylenetetracarboxylic Bisbenzimidazole, and PTCDA = Perylene-3,4,9,10-Tetracarboxylic-3,4,9,10-Dianhydride.
* Reproduced from Ref[12].

According to plenty of academic articles, the promising mixture of regioregular 3-hexylthiophene-2,5-diyl (P3HT, produced by the Rieke Metals, Inc.) and fullerene [6,6] phenyl C61 butyric acid methyl ester (PCBM, produced by NANO-C, Inc.) has been verified as a good bulk heterojunction material, P3HT as the donor material whilst PCBM as the acceptor material, per se.

P3HT is a kind of stiff polymers, but the flexible side chain of the molecule introduces a good solubility in organic solvents. P3HT crystalizes so that produces long, narrow fibrils, and those fibrils from a network which is able to create good percolation paths for the charge carriers' transportation (The row of P3HT in Table 4.2). This leads to the high carrier mobility. Differing from the P3HT, PCBM is a derivative of Buckminsterfullerene, it has a high electron affinity which makes it a qualified electron acceptor material in the organic thin film solar cells (the row of PCBM in Table 4.2).[24, 25]

So in this project, I chose them as the active materials and make the mixture P3HT:PCBM with a proper ratio. Meanwhile, for the testing solar cells based on rigid substrates, I also tried with another promising active mixture of the new low band-gap co-polymer Poly[2,1,3-benzothiadiazole-4,7-diyl[4,4-bis(2-ethylhexyl)-4H-cyclopenta[2,1-b:3,4-b']dithiophene-2,6-diyl]] (PCPDTBT) (produced by the Sigma-Aldrich Logistik GmbH, Germany) and PCBM, just for comparing the fill factors (FF) and power conversion efficiencies (PCE) of them. The schematic molecular structures, HOMO & LUMO level and charge carrier mobility under room temperature of these three kinds of material are all present in Table 4.2.

Table 4.2 Organic molecules used for rigid substrates in this project

Material	Molecular structure	HOMO (eV)	LUMO (eV)	Carrier mobility (cm^2/Vs)*	Reference
P3HT	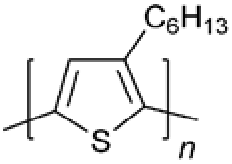	5.2	3.2	$\mu_h=2\mathrm{x}10^{-4}$	37
PCPDTBT	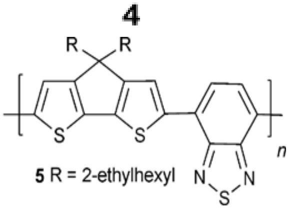	4.9	3.5	$\mu_h=2\mathrm{x}10^{-2}$	24, 25
PCBM	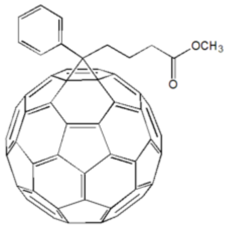	6	4.2	$\mu_e=3\mathrm{x}10^{-3}$	37

*The charge carrier's mobility are measured under the room temperature (RT).

There is another kind of material that I have to mention, which is used as the colourful-transparent electrode, Poly(3,4-ethylenedioxythiophene) poly (styrenesulfonate) (PEDOT:PSS-PH1000, produced by the Ossila Limited, UK), which can be used as a transparent, conductive polymer with high ductility in many applications.

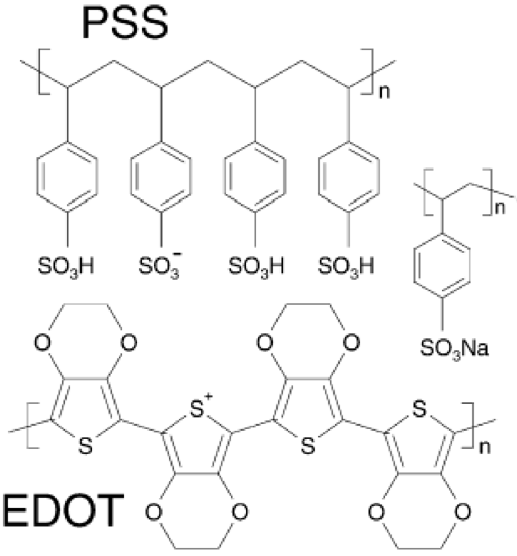

Figure 4.1 The molecular structure of PEDOT:PSS. The upper one is the structure of PSS while the lower one shows the PEDOT's molecular structure.

Due to the transparency and conductivity, PEDOT:PSS is used as the top electrode in this project. However, since it is easy to get physical damage, e.g., penetrated by the measuring probes, I overlaid silver paste to increase the conductivity as well.

4.2 PROCESSING METHODS

4.2.1 THE BLEND OF P3HT:PCBM

For the blends of P3HT and PCBM, a proper component ratio is in demand, people have been working on it all the time and some fruitful outcomes have been demonstrated already. According to the reported work of A. Baumann and J. Lorrmann, et al [26], various ratios turned to be feasible with good quality. In my case, I use the verified ratio 1:1 by physical weight (200mg, respectively), then, mix the P3HT and PCBM in the solvent chlorobenzene or 1,2-dichlorobenzene (10mL) in a containing vial. Afterward, place the sealed containing vial on a rotating hot plate, at the rotating speed 600 RPM (revolutions per minute), 65°C, and leave it for overnight (or over 20h) with being wrapped by aluminium foil.

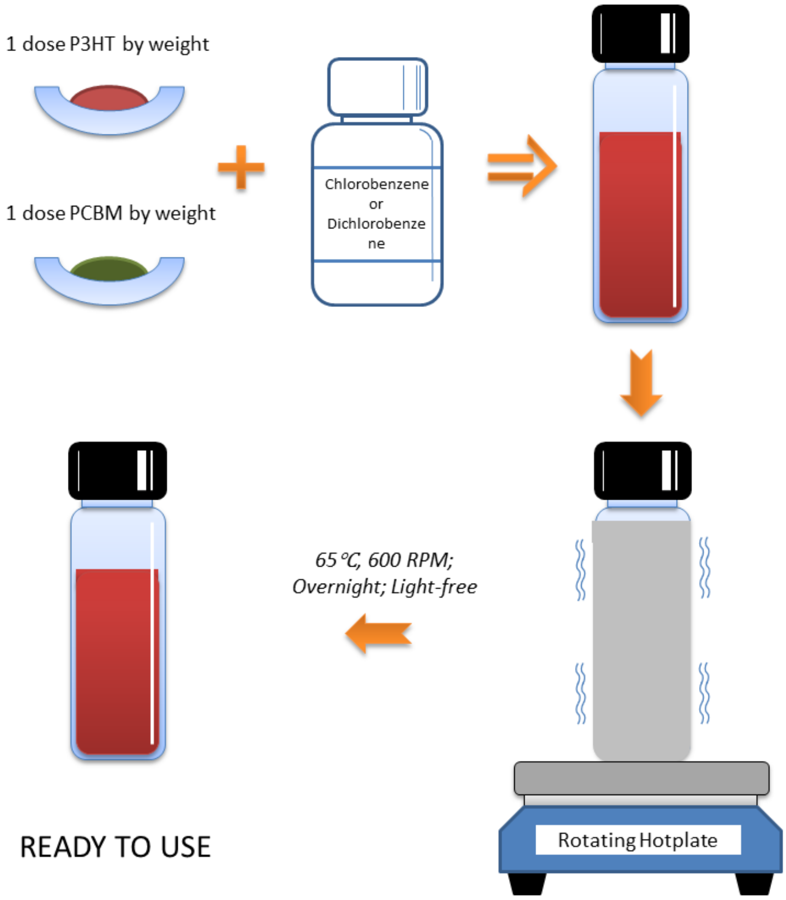

Figure 4.2 Main procedures of making the P3HT:PCBM blend.

4.2.2 THE PEDOT:PSS

The conductive Poly(3,4-ethylenedioxythiophene) poly (styrenesulfonate) (PEDOT:PSS-PH1000) thin layer is employed as an electrode material. It is able to serve several functions, not only due to its hole-transporting and electron-blocking ability, but also can be used to smooth the electrode's surface, seal the underlay active layer from oxygen and induce light due to its transparency. Normally, the PEDOT:PSS layer is spin-coated on top of active layers.

However, somehow the PEDOT has a relevantly high hydrophobicity, that makes it can't form an uniform thin layer on top of the P3HT:PCBM layer. For this reason, I mix another PEDOT, namely CPP:PEDOT (CLEVIOS P Form. CPP105D, produced by the Heraeus Clevios GmbH, Germany) into the PEDOT:PSS. Because the CPP:PEDOT has less hydrophobicity and it's miscible in the PEDOT:PSS so that can provide a good adhesion to the active layer, moreover, due to the small sheet resistance, the conductivity of the well-mixed PEDOT can be improved as well. The PEDOT:PSS/CPP:PEDOT mixing ratio is 3:1, 5% dimethyl sulfoxide (DMSO) was added to the solution and stirred overnight at rotating speed 300 RPM under room temperature.[24, 27]

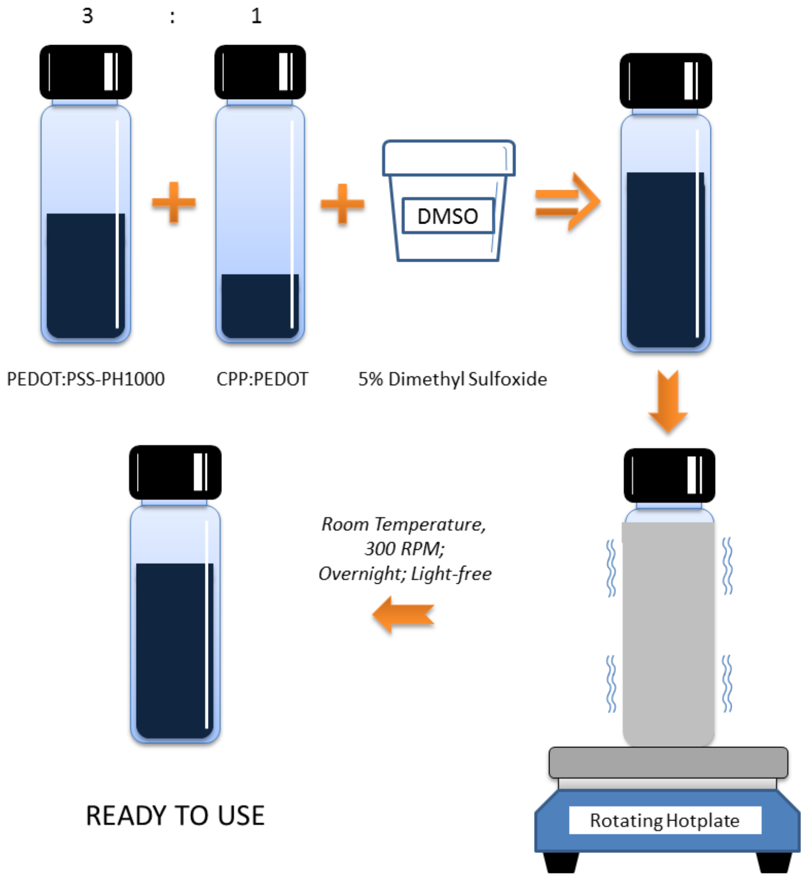

Figure 4.3 Main procedures of making the mixed PEDOT:PSS solution.

4.3 FABRICATION OF THE SOLAR CELLS

4.3.1 SOLAR CELLS' ARCHITECTURES

As the description in Chapter 2, the configuration of the solar cells in this project is unconventionally inverted. Comparing to the conventional geometry (Fig.3.4), the inverted one always generates current in the contrary direction (Fig.4.4).

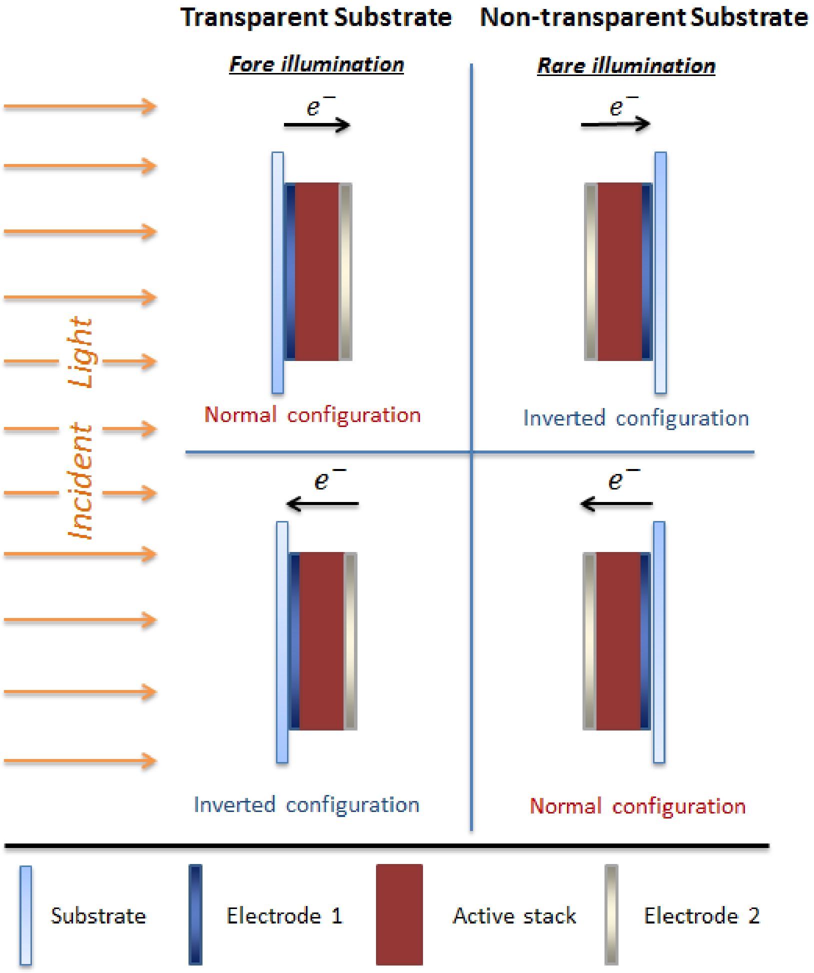

Figure 4.4 Different current directions due to different cells' configurations

Besides, thanks to the different geometries, the lifetimes of the conventional and unconventional cells are different as well. Since the active layer and the PEDOT:PSS layer are sandwiched in the conventional structure, the working lifetime more depends on the moisture condition. However, in the unconventional structure, the PEDOT:PSS layer is partially or wholly exposed to the external circumstance, so the lifetime more depends upon the ambient oxygen level. Thus, an appropriate annealing to minimize the O_2's impact is indispensable (Table 4.3).

Table 4.3 The two typical stacks of organic thin film solar cells

Architecture	**Configuration**	**Lifetime**	
		H_2O	**O_2**
Normal (conventional)	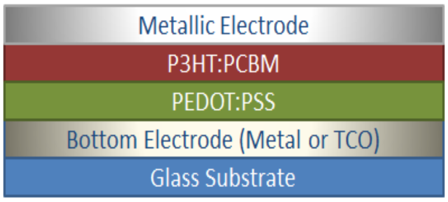	Short	Long
Inverted (unconventional)	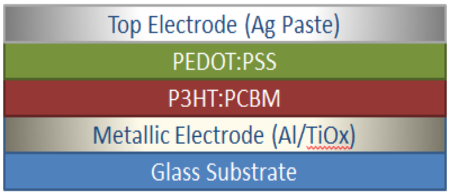	Long	Short

In this dissertation, most of the experimental outcomes are from the solar cells with inverted configuration, all the relevant characterizations, optimizations and discussions are beads on them as well, because my aims are rooted in these specifically structured organic solar cells. The experimentally inverted solar cells' architecture is present in Table 4.3.

4.3.2 BOTTOM ELECTRODES DEPOSITION AND CHARACTERIZATION

In this part, the handling substrates are polished BK7 (borosilicate crown glass) wafers, the bottom electrodes are fabricated on them by photolithography, the processing procedures are depicted in Appendix III. The initial structure of the electrodes is Ti (3nm)/ Al(80nm)/Ti(20nm), later on I also tried Al (80nm)/Ti(2nm) bilayer according Ref[28]. The metal deposition was performed with electron-beam deposition at rate of 2 Å/s and background pressure in the 10-6 mbar range. The top Ti layer is not only designed for avoiding the possible oxidation of in-between Al layer but also for forming a thin utmost top oxide layer (around 2nm thick) due to TiOx's hole-blocking and electron-collecting ability as good cathode materials. [29] Hence, the electrodes need to be exposed to the ambient air for a proper period (normally over 12hs). So the final structure of the initial electrodes is Ti(3nm)/Al(80nm)/Ti(≈18nm)/TiOx(≈2nm) whilst the latter one is Al(80nm)/TiOx(2nm), actually. (Table 4.4)

Table 4.4 Comparison of the Initial & Latter Electrodes' Configurations

	The Electrodes' Configuration
The Initial One	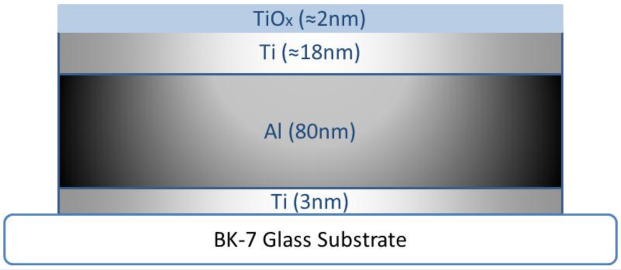
The Latter One	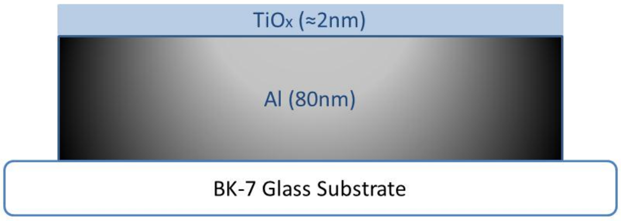

With the application of atomic force microscopy (AFM), the morphologies of the initial and the latter electrodes are investigated. In this dissertation, I use the root mean square (Sq) of the numerical vertical height of surface to present the roughness level. The Sq values are calculated by an image-analysing software: SPIP.

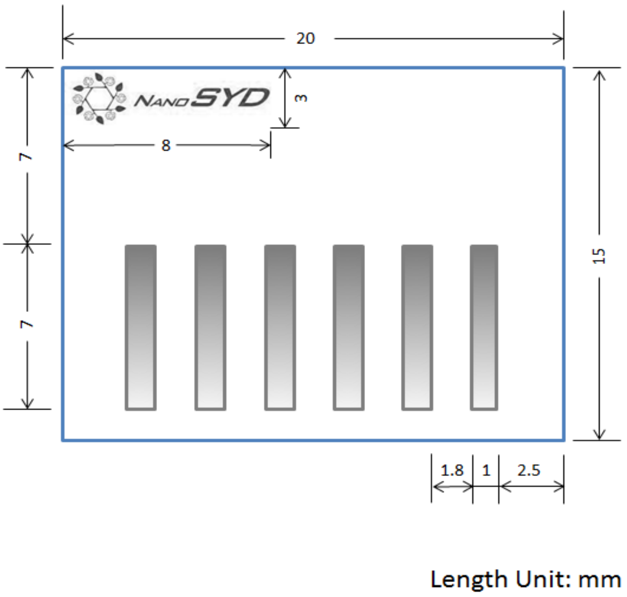

Figure 4.5 Blueprint of the bottom electrodes on BK-7 glass substrate with marked dimensions

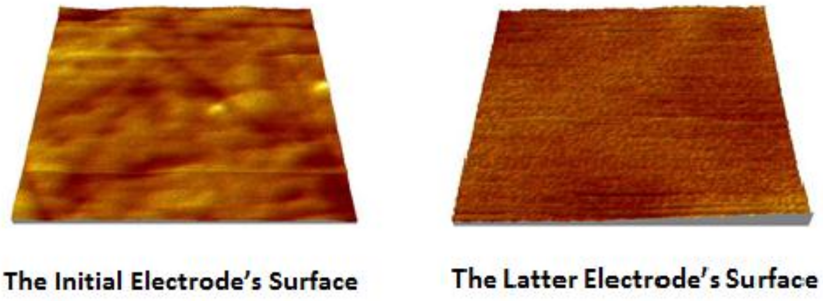
The Initial Electrode's Surface

The Latter Electrode's Surface

Figure 4.6 The 3D images showing the bottom electrodes' morphologies given by atomic force microscopy (AFM). The scanning area's dimension is 10 x 10 μm^2. The left one shows a 4-layer (bottom-up: Ti/Al/Ti/TiOx) electrode's top surface, the Sq is 0.688nm given by SPIP; the right image represents a bilayer (bottom-up: Al/TiOx) electrode's top surface, the Sq is 0.289nm given by SPIP.

4.3.3 ACTIVE LAYER SPIN-COATING AND MORPHOLOGY

After the preparation of the bottom electrodes, let's move on to the formation of active layer. According to the theoretical interpretation, a proper thickness of the active layer turns out to be very important to the solar cells' characteristics. Because we have to reduce the thickness of the active layer in order to shorten the travelling path of the separated charge carriers to avoid the possible carriers' recombination. However, on the other hand, if the active layer's thickness is quite small, then it will be too thin to absorb more light which can also disqualify the solar cells. So due to the reasons above, we need to make a compromise that can even both of the negative influences and maximise the quality of the organic solar cells. Basing on a plenty of experiments' data and theoretical proofs, the dimension range of a few hundreds nanometres can be accepted.

In this project, the active material (P3HT:PCBM blend) is spin-coated on top of the bottom electrodes (rotation: at 1000~1500 RPM for 45 seconds, formed thickness is around 200nm), but since the electrodes are supposed to connect to the external measuring devices, a small part of each single electrode has to be saved, so that a plastic tape with no sticky glue is employed (Fig.4.7).

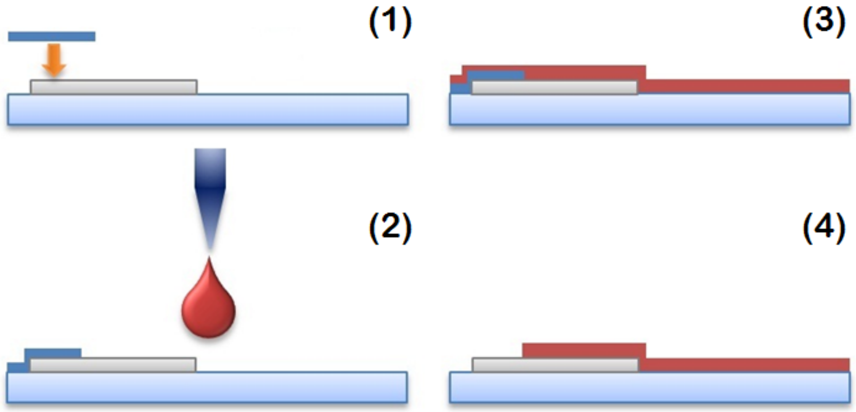

Figure 4.7 The process of forming active layer on the glass substrates with bottom electrodes. (1) Placing a tape to partially cover the electrodes; (2) Vertically dropping a proper dose of P3HT:PCBM blend onto the substrate (with a plastic sucking pipe); (3) Spin-coating the active material; (4) Peeling the tape off (with a pair of tweezers) and the substrate is ready to be sent for

the first annealing. For fulfilling these operations effectively, a well-sealed glove-box is quite in demand.

In reality, to get rid of the negative impact caused by oxygen, all the procedures presente in Fig.4.9 needs to be fulfilled in a glove-box (Fig.4.8). The glove-box is full of nitrogen, which can be used as an oxidization-proof gas. Normally, before starting the experiments, I open the valve to induce the N_2 into the glove-box in order to flush all the remaining gas from the former experiments so that can make the glove-box always at a good state. For further removing the residual oxygen within the active material, an annealing is in demand, more relevant discussion will be introduced and presented in section 4.4 and 4.5. The spin-coater placed inside the glove-box is WS-400BZ-6NPP/LITE (produced by the Laurell Technologies Corporation). For obtaining an uniform active layer, the rotation is usually at 1000~1500 RPM for 45 seconds, and the post-annealing thickness measured with using a Dektek profiler, is around 200nm.

Figure 4.8 A glove-box is necessary to the fabrication process of organic solar cells.

In some researches, the morphologies belonging to different components in organic thin film solar cells are quite related to the cells' performance so that it is necessary to be investigated. Essentially, non-uniform morphology of active layer is detrimental to solar cells' performance as it shortens exciton diffusion length, and degrades hole transportation.[30] According to some lately researches,[7, 30, 31] a good, uniform active layer is able to provide high Jsc, FF and PCE. On the other hand, another effect which was reported by Travis L. Benanti et, al. that the casting solvent on device morphology is rather related to the organization of the conjugated polymer chains.[7]

By using AFM, the morphology of the active layer's surface can be investigated. Figure 4.9 shows the morphology of the P3HT:PCBM thin layer's surface. Here, we can tell the parameter Sq is 0.923nm.

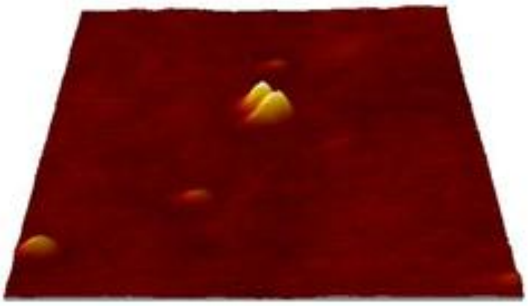

Figure 4.9 The 3D image showing the P3HT:PCBM thin layer's morphology given by AFM. It is usual to have some "hills" on the surface (shown in the image). The scanning area's dimension is 10 x 10 μm^2, Sq calculated with SPIP is 0.923nm.

4.3.4 PEDOT:PSS LAYER SPIN-COATING AND MORPHOLOGY

After spin-coating the active layer, a thin PEDOT:PSS layer ought be formed subsequently. Similar to the process of active layer's formation, the PEDOT layer is also made by spin-coating, and the process is present in Fig.4.10. I use the same rotating program (rotation: at 1000~1500 RPM for 45 sec) to form the thin PEDOT:PSS layer, while due to its own viscosity and wettability, the thickness of PEDOT:PSS layer is a bit smaller than the active layer, but it is still in the numerical range of 100~200 nm (measured with the Dektek profiler). It is also good to have a thinner PEDOT:PSS layer since this very layer's function is collecting positive charge carriers, so it doesn't need to be too thick, otherwise some light will be absorbed by this layer but not go through it and induce excitons in the active layer. However, if we go to the very contrary point, namely making the PEDOT:PSS layer extremely thin, that will also degrade the organic solar cells, because the thin layer will result in a foreseeable increase of the sheet resistance. So in a word, we need to minimize the unnecessary light loss in this process, and maximize the PEDOT:PSS thin layer's intrinsic function.

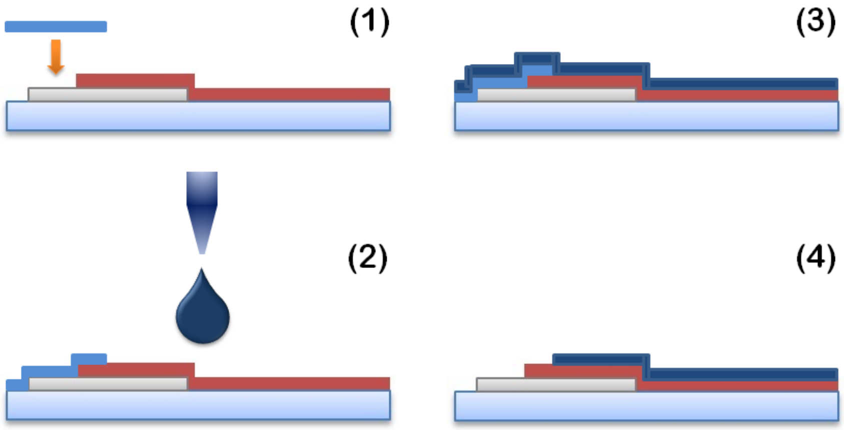

Figure 4.10 The process of forming PEDOT:PSS layer on top of the active layer. (1) Placing a tape to partially cover the active layer; (2) Vertically dropping a proper dose of PEDOT:PSS blend onto the substrate (with a plastic sucking pipe); (3) Spin-coating the PEDOT:PSS; (4) Peeling the tape off (with a pair of tweezers) and the substrate is ready to be sent for the second annealing. All the operations need to be done in the glove-box, too.

As can be seen, a special step-configuration is formed by shifting the assistant tape a bit. That is because both the bottom electrodes and PEDOT:PSS layer are conductive, if they are close to each other, potential short-circuit would be ignited. So in order to avoid any kinds of short-circuit, I moved the assistant tape downwards a bit while placing it. The performances have proved this step-configuration of the conjugated layers is rather helpful.

Same as the active layer, after an indispensable annealing, the morphology can be investigated with AFM and the software SPIP. The 3D image Fig. 4.11 shows the top surface of a well-annealed PEODT:PSS layer. Here, we can see the surface has got rougher than the active layer's, the Sq value given by SPIP is 1.86nm.

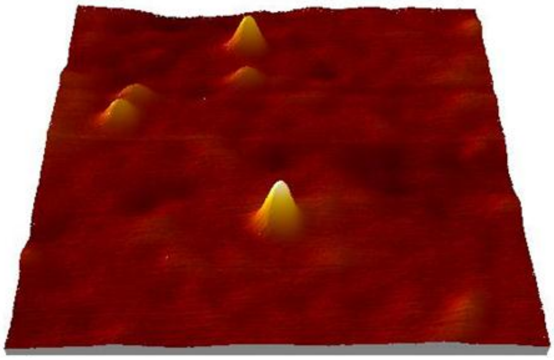

Figure 4.11 The 3D image showing the PEDOT:PSS thin layer's morphology given by AFM. More "hills" and pinholes appear on the top surface. The scanning area's dimension is 10 x 10 μm^2, Sq calculated with SPIP is 1.86nm.

Normally, we also expect a smooth PEDOT:PSS top layer, because the roughness is rather related to the final resistivity. Thus, we always need to reduce the roughness of PEDOT:PSS top layer. [31]

4.3.5 FINAL APPEARANCE OF THE SOLAR CELLS

After going through all the procedures above, we obtain the final rigid organic thin film solar cells, both the structural drawing and the real appearance are shown in Fig.4.12.

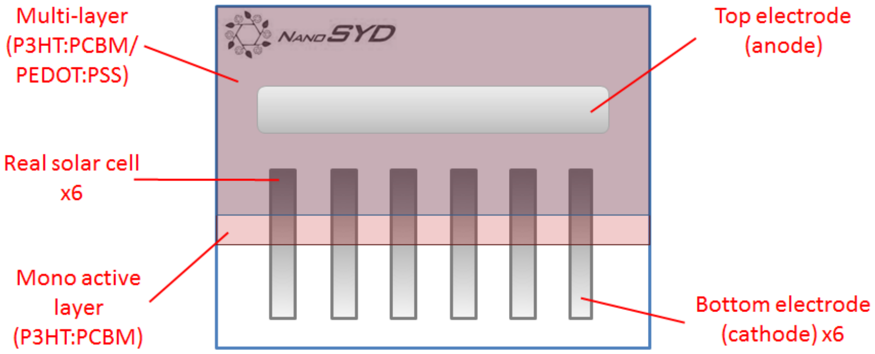

(a)

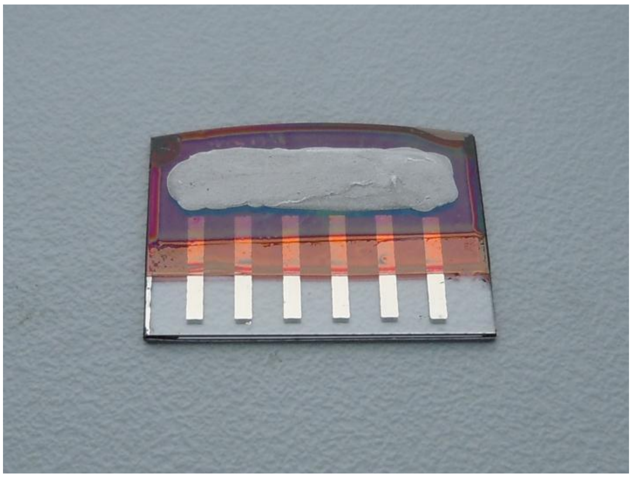

(b)

Figure 4.12 (a) Structural drawing of an organic thin film solar cell; **(b)** The solar cells in reality

4.4 PERFORMANCE

To organic solar cells, the essential parameters are short-circuit current or current intensity (Isc or Jsc), open-circuit voltage (Voc), fill factor (FF) and power conversion efficiency (PCE), which have been introduced and discussed in the theoretical interpretation in Chapter 3. Now, let us see the performance of the rigid organic thin film solar cells in reality, and conclude the electric behaviour to further modify or optimise the properties of the flexible organic thin film solar cells.

For obtaining good solar cells with good performance and stability, a proper annealing is necessary. Annealing enhanced the charge carriers' mobility[32] in combination with changing the recombination behaviour.[33] Normally, for the P3HT:PCBM active layer, the annealing is considered to take place in these three sequent steps: (i) the P3HT matrix is softened; (ii) PCBM molecules start to diffuse out of disordered P3HT clusters and form larger fullerene aggregates; (iii) the new fullerene-free P3HT matrix recrystallizes into larger fibroid type crystals, which are embedded in a matrix consisted of PCBM nano-crystals and amorphous P3HT. [5]

An adequately long heating will bring a big change to the morphology of active layer, and the morphology is quite related to the solar cells' electric performance. The longer of the annealing, the smoother the surface will be. On the other hand, the adequately high temperature can also eliminate the negative impact caused by the residual oxygen, so that avoid possible oxidation in some level. However, every coin has two sides, if we used too high temperature or too long annealing time, then we will hazard the intrinsic ability of the active layer, because that will degrade the active layers or even cause some serious damage to the solar cells. 140℃ has been proofed as a proper annealing temperature for the active layer, [34] and for the further comparison and optimization, the time varies from 15 to 30 minutes. But for the PEDOT:PSS layer, the annealing's function is more like hard-baking without harming it, so I kept the same annealing temperature, while shorten the time to 2 minutes and 30 seconds. All the annealing operations were fulfilled in the glove-box, which is full of protective N_2.

Before characterizing the I-V curve, let us get familiar with the measuring devices:

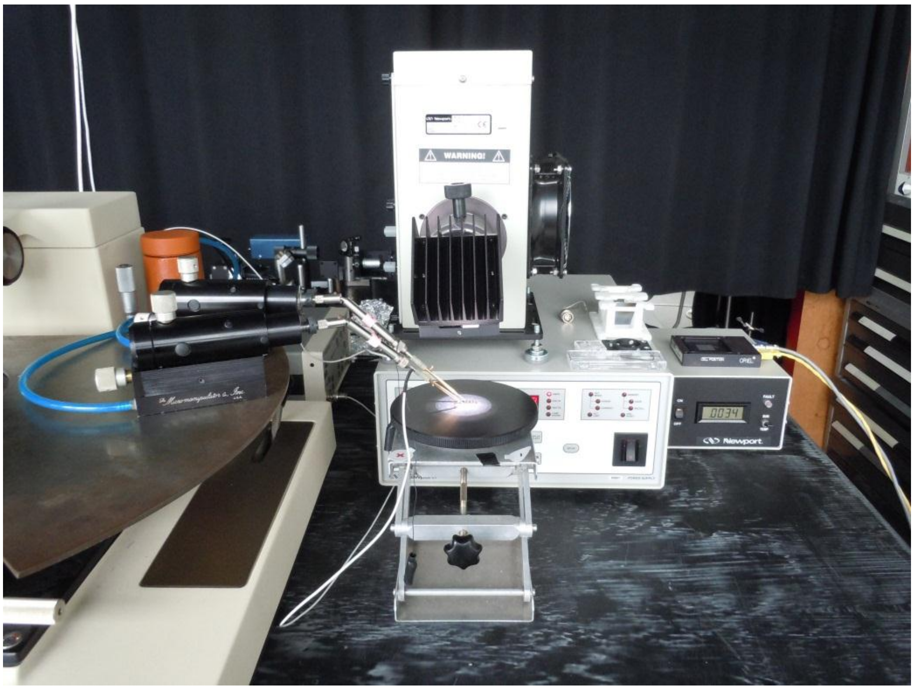

Figure 4.13 The devices for measuring. The electrical characterization was made using a custom-built, LabVIEW-controlled measurement setup, where the voltage is controlled by a 16-bit National Instruments DAQ card, which also samples the current measured by a Stanford Research SR 570 current amplifier. The measurements were performed under illumination of an Oriel lamp with an intensity of 100 mW/cm^2 using an AM 1.5G filter.

The illumination intensity measured with the reference cell is 1 Sun (equals to 100mW/cm2), used in all the experiments involved in this project. All the data are gathered and automatically plotted with the software LabVIEW 2009 SP1.

4.4.1 THE SOLAR CELLS WITHOUT NANOSTRUCTURES

For the further optimization and comparison, first of all, I tried to make some solar cells without any nanostructures. In this part, I made dozens of cells. However, due to some defects and damages, not all of them are taken into account, some of them have to be discarded. So I selected some trustable ones, processed the data and re-plotted them.

If we plot the current intensity and voltage data, the J-V curve can be achieved as following,

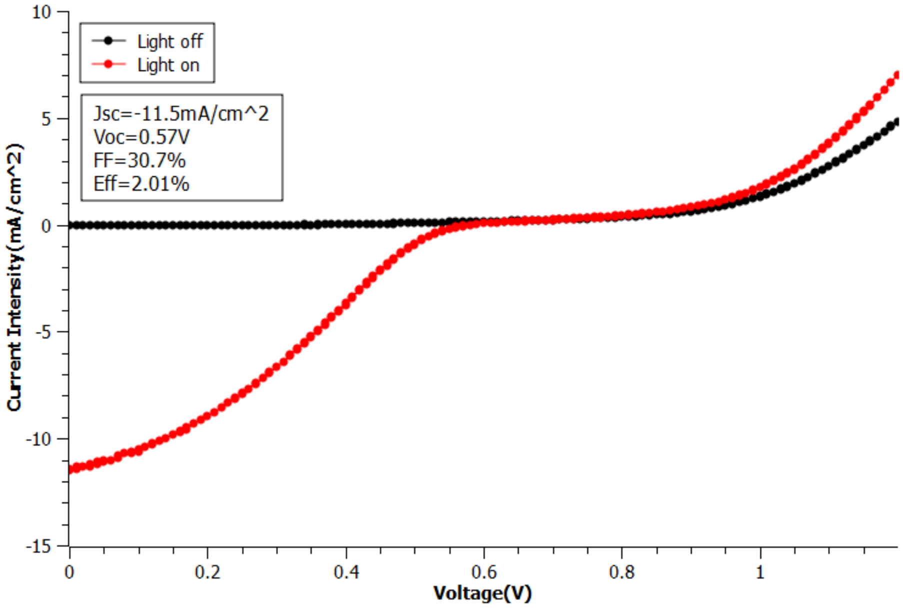

Figure 4.14 This is the J-V curve of one cell chosen from the samples. The black-dot one shows the current intensity & voltage relationship in the dark circumstance; the red-dot-line curve shows that in a light condition. (Incident light: 1 Sun)

In Fig4.14, we can tell that in the dark circumstance the solar cell behaves pretty like a diode, while in a light condition it turns into a real power-supplying device.

According to the formula (3.4), (3.5) and (3.6), we can work out the fill factors and the efficiencies, all the calculated results are listed in Appendix I(a).

From the data in Appendix I(a), we cannot clearly see the tendency of the FFs and PCEs varying as annealing time increasing. Even though I did my endeavour to keep all the experimental conditions (i.e. background light intensity, mechanical disturbance, nitrogen flush rate, etc.) constant, however, they were still hard to be utterly controlled. And these factors could possibly impact the solar cells' characteristics.

Well, we can still see that the best result shows up at the 20min annealing (YR-05), and the 15min-above annealing can provide relatively good outcomes. Besides, according to Ref[27], for obtaining good morphology of the active layer, 25min turned out to be reasonable, that is how long I use for the following experiments.

4.4.2 THE NANO-STRUCTURING ENHANCED SOLAR CELLS

As the description in Chapter 3, periodic nanostructures are able to enhance the light absorption within the organic solar cells. In principle, if we want to enhance the light absorption, then we have to know which wavelength range of the incident light is proper for the solar cells, so that we can make use of the nanostructures and try to expand the potential absorption range. In order to expand the light absorption range in the whole spectrum, we must consider which part of the spectrum is more absorbed by the colourful conjugated layers. Figure 4.15 shows the absorption curve of a 200nm-thick P3HT:PCBM active layer and reflection spectrum of the nano-structured electrode covered with 200nm thick P3HT:PCBM layer. The periodic pitch distance of the nano-gratings is 500nm which can lead the diffraction of incident light with this correspondent wavelength. [27] In Fig.4.15, the effect is visualized by the reflection spectrum, which showing a minimum point around 530nm. And, Fig.4.15 also provides an absorption spectrum which displaying the peak of light absorption matches the grating's dimension, this is what we expect to benefit the light absorption within the solar cells.

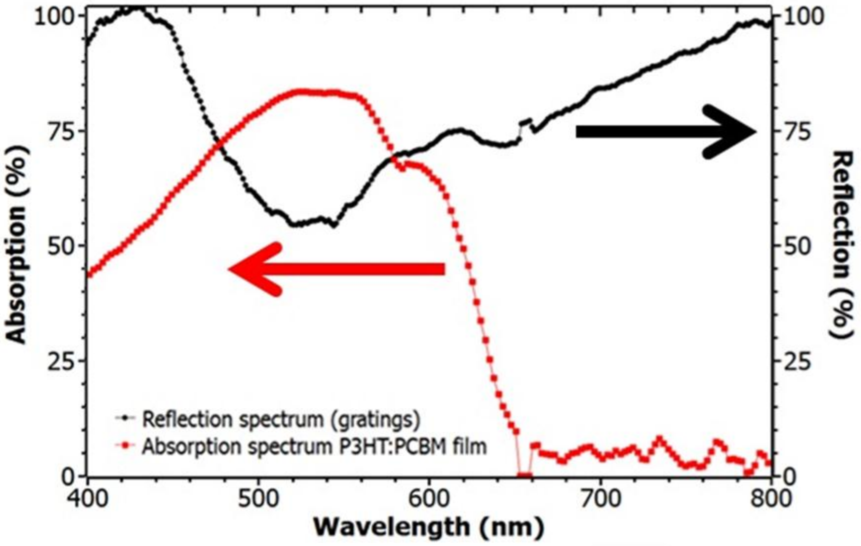

Figure 4.15 Light absorption curve of 200nm-thick P3HT:PCBM active layer on glass substrate and reflection spectrum of a nano-structured electrode with periodic metal gratings (covered with a 200nm-thick P3HT:PCBM film). The data are collected and analysed with spectroscopic ellipsometer (SE200BM, Ångstrom Sun Technologies).

Certainly, the shape of the applied nano-structures could be diverse, inspired by Ref[4] and[35], gratings could be adequately efficient, so that is the pattern what I chose for the design.

In order to clearly compare the solar cells with & without nano-gratings, I rearranged all the characteristics data and put them into a table (Appendix I(b)). From the comparison table there, we can see that in general the structured cells' short-circuit current intensities are higher than the ones of the unstructured cells, while the open-circuit voltages are somehow on the same level. These result in the increase of the fill factors and efficiencies. For representing the enhancement manifestly, I make a table of mean-value comparison as following,

Table 4.5 Enhancement of the structured sample

Sample/Cell	Average Jsc (mA/cm^2)	Average Voc (V)	Average Fill Factor (%)	Average Efficiency (%)
Structured 500-3	-9.93	0.57	35.80	2.04
Unstructured 500	-6.86	0.60	33.25	1.36
Enhancement	**44.75 %**	**-5%**	**7.70 %**	**50%**

Here, it is very clear to see that the enhancements of both the Jsc and the PCE (44.75% and 50%, respectively). It means the nano-structured back surface of bottom electrode does exert its specific function, namely trapping more light into the thin active layer. In a word, the application of periodic nano-structures is verified to be feasible and efficient, moreover, it is possible to further optimise this very process in future work.

4.5 DISCUSSION

4.5.1 FEASIBLE OPTIMIZATION OF THE CHARACTERISTICS

Actually, some feasible ways have already been referred for optimising the organic solar cells' properties, i.e. increasing the annealing time to get better surface morphology and employ nano-structures to enhance light absorption, etc. In reality, we may have quite a few different ways to optimise the organic solar cells' performance. Because of the large diversity, in the following content I would like to just briefly mention a few aspects.

The thicknesses of both the active and PEDOT:PSS layers are worthy of investigating. According to Ref[5], a 200nm thick

P3HT:PCBM (mixing ration1:1 by weight) layer can offer the optimum function in organic solar cells. And, a top PEDOT:PSS layer with the thickness around 220nm is corresponding to the optimum performance of organic solar cells. [36] So, basing upon these valuable experience, active layer and top PEDOT:PSS layer in the same thicknesses are also employed in my project.

Now, let's take a look at the annealing temperature. According to a plenty of work done by other researchers, the differential annealing temperatures for P3HT:PCBM active layer can be plotted in the graph as following,

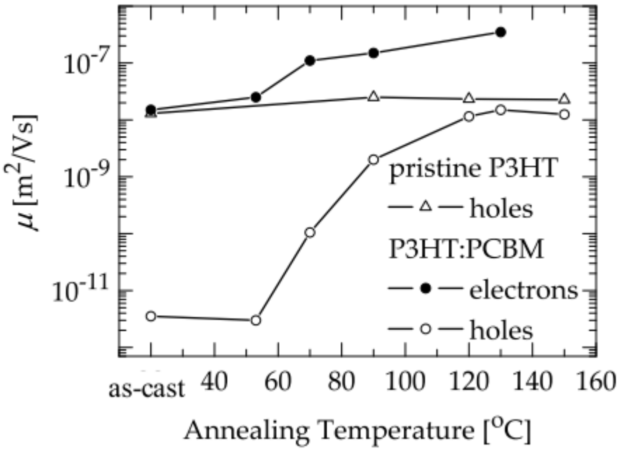

Figure 4.16 The hole's and electron's mobilities in P3HT:PCBM blends and pristine P3HT regarded as a function of annealing temperature. The graph is quoted from Ref[34].

According the curve which depicted in the graph, 140°C is used as a proper annealing temperature. [31, 34] the charge carriers' mobilities under this temperature are good enough to induce constant and reliable current. So, it is also used in this project.

Another active material, PCPDTBT, has been mentioned in Chapter3. As a promising candidate for fabricating organic thin film solar cells, it was also tested by me, all the calculated results are contained in Appendix I(c). As can be seen, the characteristics of the solar cells with PCPDTBT:PCBM performing not as good as the P3HT:PCBM ones. However, this kind of solar cells is supposed to be qualified and promising in a way. From the light absorption spectrum shown below (Fig.4.17), respecting to the active material, more light can be absorbed, especially the range of <420nm and 600~800nm. That would result in a potential increase of the light-trapping and further improve the conversion efficiency as well.

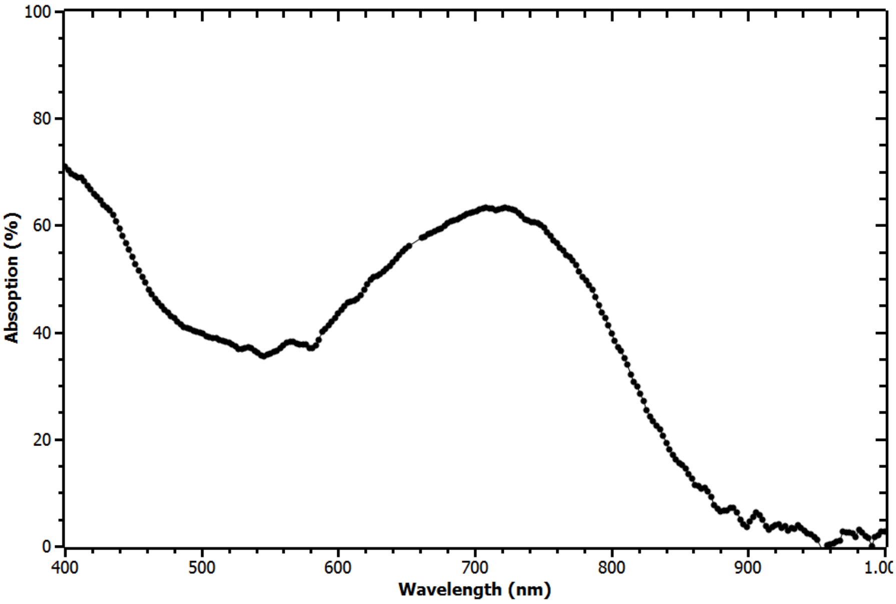

Figure 4.17 Light absorption spectrum of the solar cells with PCPDTBT:PCBM active layer.

In the spectrum above, the light in blue/green range and infrared range is relatively less absorbed, hence most of blue/green and infrared light is reflected, that makes the cells look green, even close to cyan somewhat.

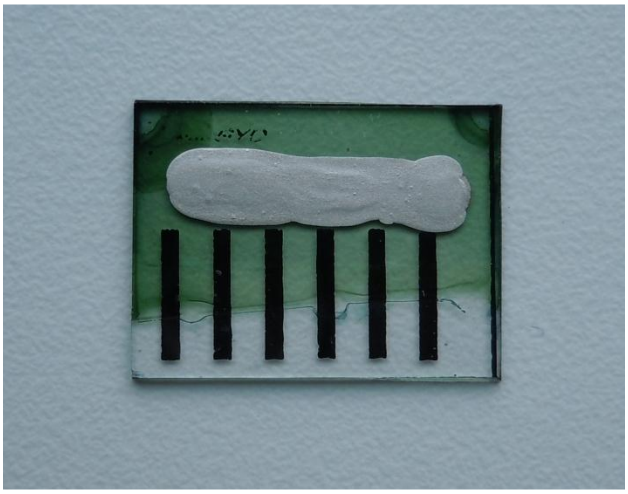

Figure 4.18 A sample fabricated with PCPDTBT:PCBM in reality.

Whilst doing this project, I also partially participated in the research about investigating the improvement of the efficiency by applying diffraction gratings on bottom electrodes and doping silver particles into the PEDOT:PSS solution. PCPDTBT:PCBM is the active blend which used in the objective solar cells in that research. The fruits of this research are presented in the reference article [27] which was published by SPIE, April, 2012. Basing on this article, the modifications for both of the bottom and top electrodes turn out to be efficient and prospective, PCEs of the solar cells which containing nano-gratings on bottom electrode or Ag nanoparticles doped in top PEDOT:PSS layer are enhanced by 20%~30% comparing to the unstructured and un-doped ones. In future, the combination of these two specific methods can be also realised, a foreseeable significantly improvement is around the corner, and it can also be applied for the P3HT:PCBM-based inverted organic thin film solar cells.

4.5.2 OTHER FACTORS

We all know that any measurements may contain untrue errors somehow, there is no exception in this project as well. Even a sequence of measurements with very short intervals to a same cell, we still cannot get two identical results. For this reason, I made two samples just for investigating how the difference of two measurements will be (Table 4.6).

Table 4.6 Characterisation of Sample YR-07 & Sample YR-08

Sample/Cell/ Measurement			**Anneanling**	**Jsc (mA/cm^2)**	**Voc (V)**	**FF (%)**	**Eff (%)**
YR-07	C1	M1	140°C A-Layer (P3HT:PCBH): 20min P-Layer: (PEDOT:PSS) 2min30sec	-4.36	0.57	33.7	0.837
		M2		-4.86	0.57	30.8	0.853
	C2	M1		-4.78	0.59	31.1	0.878
		M2		-4.73	0.58	29.2	0.8
	C3	M1		-4.12	0.59	28.7	0.698
		M2		-4.29	0.54	27.8	0.643
YR-08	C1	M1	140°C A-Layer (P3HT:PCBH): 25min P-Layer (PEDOT:PSS): 2min30sec	-6.48	0.6	35	1.36
		M2		-7.3	0.59	33	1.42
	C2	M1		-7.61	0.6	33.9	1.55
		M2		-8.19	0.59	31.7	1.53
	C4	M1		-6.39	0.59	34.5	1.30
		M2		-7.25	0.56	32.5	1.32
	C5	M1		-5.5	0.59	37.3	1.21
		M2		-6.21	0.61	31.9	1.21

* *Initial conditions of the glove-box:* O_2*: 555ppm;* H_2O*: 1655 ppm*

From the table above we can tell even two sequent measurements are still not able to provide identical results, but if the interval is relevantly small, the difference may not be too big. For instance, the C4 of Y8, if we take the first measurement's result as the reference, then the percentage difference is (1.32-1.30)/1.30≈1.54%, that can be negligible in same way; however, for C2 of YR-07, the percentage difference is |(0.8-0.878)/0.878|≈8.89%, that will depend on specific requests to judge whether it is still negligible or not.

The reasons to the difference could be diverse, i.e. temperature, humidity, contamination, mechanical disruption, etc. All of these could be the issues for researching in future. Now that we have seen the measuring errors, then what if we elongate the interval, can it be a hint of the lifetime of the organic solar cells?

I personally suppose the answer is "Yes". However, despite the lifetime is not one of the prominent aims of this project, it is still good to be investigated in some way, and it could also kindle some inspirations for the future researches.

Here, I choose two cells to see the differences between the initial measurement and the 5-days-later measurement.

Table 4.7 Decay levels of Cell3 & Cell4 of Sample YR-08

Cell	**Measurement**	**Jsc (mA/cm^2)**	**Voc (V)**	**FF (%)**	**PCE (%)**
3	Initial	-7.74	0.59	33.5	1.53
	5-days-later	-2.37	0.28	12.4	0.0824
	Decay level	**69.4%**	**52.5%**	**63.0%**	**94.6%**
4	**Initial**	**-6.39**	**0.59**	**34.5**	**1.30**
	5-days-later	-6.48	0.41	18.3	0.485
	Decay level	**1.4%**	**30.5%**	**47.0%**	**62.7%**

**The storage circumstance is dry, draughty, dark and under room temperature, whereas with some random mechanical vibrations sometimes.*

The data which listed in the table above show the decay levels in a way, we can see that the fill factors and efficiencies have dropped noticeably after 5 days (in the order of 50%~95%). Considering the storage circumstance, the main reason could be a possible oxidation, because the sample was utterly exposed to the ambient air, without any encapsulations. Hence, an effective method is proposed to avoid or slow down the decay process could be an oxygen-free encapsulation. Through getting rid of the negative oxidation's influence, the lifetime could be well elongated. This work is promising and valuable which can also be investigated in future.

CHAPTER 5.

FLEXIBLE SUBSTRATES FABRICATION AND APPLICATION FOR NANO-STRUCTURED ORGANIC THIN FILM SOLAR CELLS

Flexible substrates' bloom is coming to us apace, numerous new electronic applications are being proposed and realised based on these novel substrates, including the OPV of course. The advantages of flexible electronics are quite a few: can be used as a foil over variable surfaces, on irregular surfaces or to be folded into compact modules; besides, the flexible behaviour enables cheap production processes, such as roll-to-roll production. So, while lowering the consumption of both the material and the cost, decreasing the harm to the natural environment at the same time.

In the introduction part, I demonstrated the offbeat meaning of the flexible organic thin film solar cells' emergence. Due to the significant flexibility, portability, low cost, unbreakable property and so on, this kind of solar cells is rather promising and can magnificently benefit mankind in the near future.

In this chapter, I will concentrate on the fabrication process of flexible organic thin film solar cells, and the characterisation afterwards. Furthermore, analyse the data or phenomena and propose feasible optimising methods based on the very outcomes, then test in real experiments. At last, a conclusion will be given and relevant discussion will be presented.

5.1 FABRICATION OF FLEXIBLE POLYIMIDE SUBSTRATES

Referring to the materials which are able to be used as the substrates of organic thin film solar cells, the candidates could be quite diverse. In the past years, exponential amount of reports and patents' on the flexible optical transparent foil has been published. Nevertheless, the optical materials served on market are usually developed for implementation on rigid substrates, and have no remarkable mechanical characteristics in terms of flexible and strength. [38] But some flexible solar cells such as the plastic ones with carbon nanotube network electrodes,[39] the CdS/CdTe cells on molybdenum foil and Kapton polyimide, [40, 41] and the CIGS thin film solar cells which fabricated on polyimide foils[42] have already been researched and revealed good application potential. In this part of the project, I choose a spin-coat version of Polyimide PI2525. It has good properties and can also tolerate 350℃ (according to Ref[38, 41] the commercial polyimides' maximum tolerating temperature are usually around 400℃, but 350℃ is good enough to meet the requirement in my case), that makes an identical annealing as described in the last chapter possible. This kind of polyimide is often used as a stress buffer in the semiconductor industry due to its very good mechanical properties. For holding and adhering, silicon wafer P1 (525μm thick, one-side polished, without any adhesion layers) is used, all the fabrication process is done based on the Si handling wafer. [43, 44]

The Si wafer was cut into desired pieces of the dimension 20mmx15mm, then a PI substrate is fabricated with a single small Si piece. The PI layer fabrication procedures as following: (i) Spin-coating at speed 1000rpm for 5sec, then rotate at speed 2000rpm for 45sec; (ii) hard baking at 210℃ for 180 min, whereas the 210℃ temperature is reached after a slow temperature slope of 4℃/min. (iii) cooling down and ready to be delivered to the next step. [38] The thickness of a well-made PI2525 specimen is about 10μm, measured with the profiler (Veeco Dektak 150) at the cleanroom in Alsion. A well-made PI substrate is shown in Fig.5.1. More detail information of this PI substrate's fabrication process can be found in the Appendix VI.

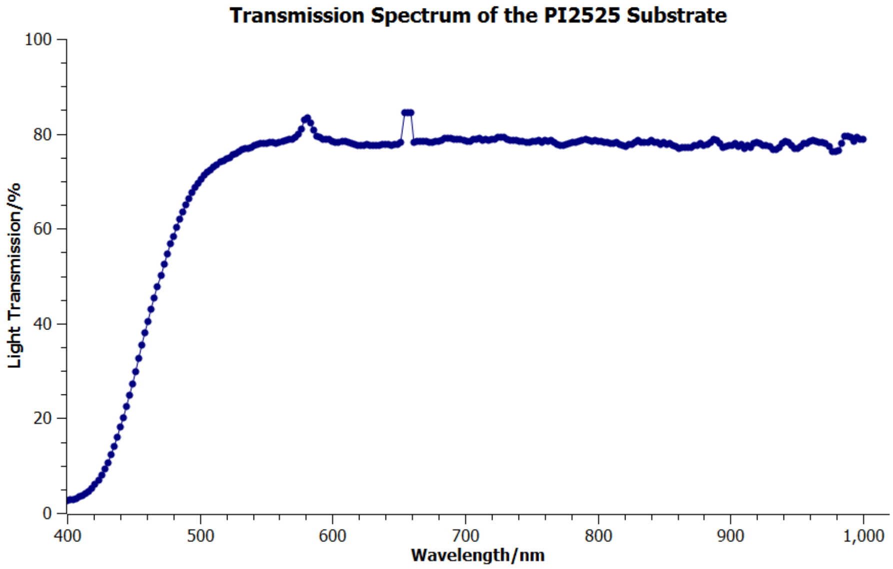

Figure 5.1 The light transmission spectrum of the flexible polyimide substrate. Measured with spectroscopic ellipsometer (SE200BM Ångstrom Sun Technologies).

From the light transmission spectrum (Fig.5.1) we can see that the light with the wavelength below 550nm cannot transmit through the PI substrate sufficiently, that makes the see-through PI substrate look somewhat yellow (Fig.5.2).

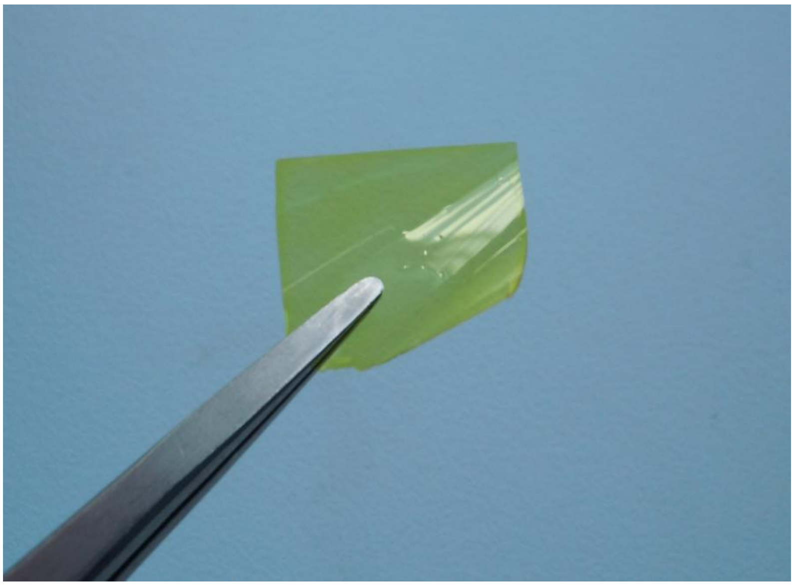

Figure 5.2 A well-made PI2525 substrate sample in reality. It is transparent-yellow and quite flexible.

After the preparation of the PI substrates, here comes the bottom electrode's deposition, subsequently. About this process, more detailed description will be mentioned in Section 5.2.

5.2 MORPHOLOGIES OF THE SUBSTRATES, BOTTOM ELECTRODES AND CONJUGATED LAYERS

5.2.1 MORPHOLOGY OF THE POLIMIDE SUBSTRATE

In common impression, the organic thin film soalr cells always look like a kind of foil. In fact, it is, indeed, a kind of power-supplying organic foil with the flat, smooth and transparent appearance. A planar surface of the PI substrate is always what we want. With the help of AFM, the morphology of the top surface can be investigated, and it is also essential to know.

For getting more convictive information of the top surface, I made 4 3D AFM images of different PI substrates to show the general morphology, all of them are listed in Table 5.1. From the mean value of parameter Sq (root mean square of the vertical height calculation, interpreted in subsection 4.3.2) given by the software SPIP, we can numerically tell the general morphology. The mean value of Sq is only 0.227nm (Table 5.1), that means the top surface of the PI substrates are quite smooth so that the flatness can be trusted for building organic thin film solar cells on.

Table 5.1 3D AFM images showing the morphologies of the PI substrates

3D AFM Images	1 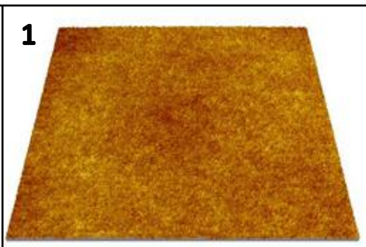	2 
Sq	0.267nm	0.213nm
3D AFM Images	3 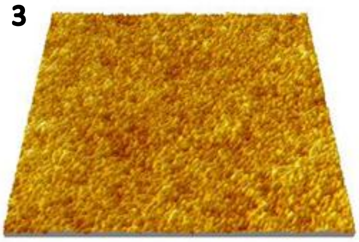	4 
Sq	0.200nm	0.229nm
Sq-mean=0.227nm		

**Scanning area's size: 20x20 μm^2*

5.2.2 MORPHOLOGY OF THE BOTTOM ELECTRODE

After the depiction of the PI substrates' morphology, let us have a look of the bottom electrodes'. With the help of AFM, the surface information can be investigated manifestly. Here, I put three 3D AFM images to show the scanning results, and get the individual Sq values with SPIP, then calculated the mean value of these Sq to estimate the roughness of the bottom electrodes' surface.

Table 5.2 3D AFM images showing the morphologies of bottom electrodes built on a PI substrate

Scan	**3D AFM images**	**Sq (nm)**	**Mean Sq value (nm)**
1	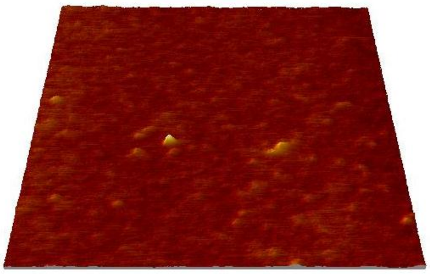	0.476	0.552
2	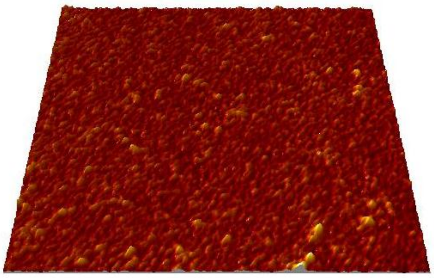	0.571	
3	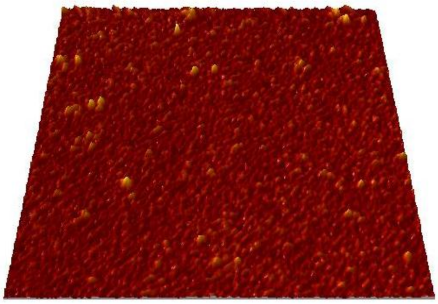	0.61	

** The scanning area's dimension is 10x10 μm², same for each single scan.*

5.2.3 MORPHOLOGIES OF THE CONJUGATED LAYERS

After the spin-coating of P3HT:PCBM blend, the morphology of this very important layer has become more serious. That is because the morphology is rather related to the performance of the solar cells, so there is in demand that investigating the conjugated layers.

Speaking of the morphology of the active layer, we must take the annealing into consideration. As mentioned in Section 4.4, an adequately long annealing can improve the morphology significantly. In order to verify this point, I made this test: investigating both of the morphologies of the pre- and post-annealing P3HT:PCBM active layers, and utilizing 3D AFM images to tell the difference. For getting more reliable numerical results, namely the Sq values, triple-time measurements were used for the pre- and post-annealing P3HT:PCBM active layers, respectively.

According the description, the annealing here is at 140℃ for 25 minutes, for both of these two cases.

Table 5.3 Comparison of the pre- & post-annealing P3HT:PCBM active layers' morphologies

	3D AFM images	**Sq/nm**	**Mean Sq value/nm**
Before annealing	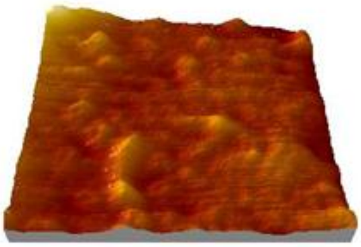	1.63	1.31
	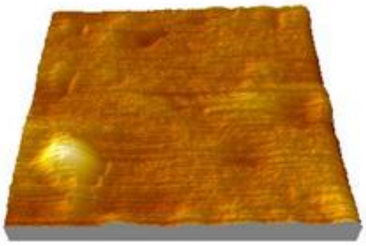	1.14	

	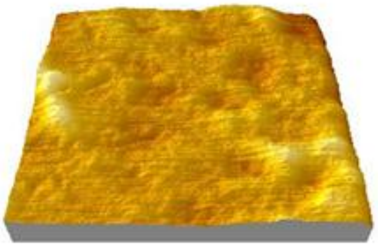	1.16	
After annealing	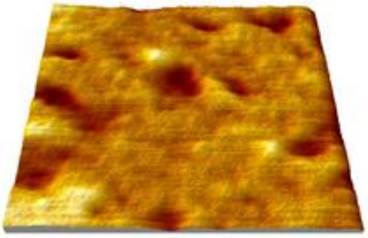	0.592	0.615
	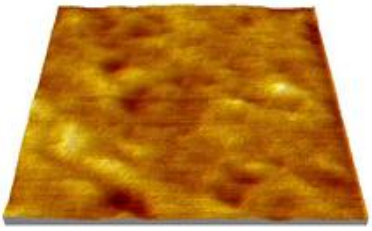	0.453	
	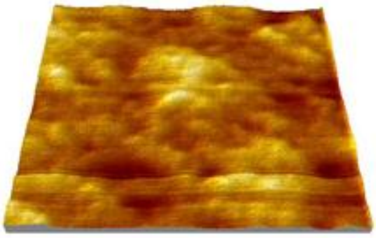	0.8	

** The scanning area's dimension is 5x5 μm^2, same for each single scan.*

** The annealing condition was fixed, at 140 ℃for 25 min.*

From the table above, we can see that a proper annealing dose change the morphology a lot. It turned out to be an efficient way to improve both the appearance and the performance of organic thin film solar cells. [7, 30, 31]

After spin-coating and annealing, the PEDOT:PSS needs to be spin-coated again to form a thin top conductive layer, and it is also necessary to be investigated. Still with the help of AFM, three scanning images were taken, so that the roughness information can be obtained with regard to the mean Sq value.

Table 5.4 3D AFM images showing the morphologies of PEDOT:PSS conductive layers

Scan	**3D AFM images**	**Sq/nm**	**Mean Sq value/nm**
1	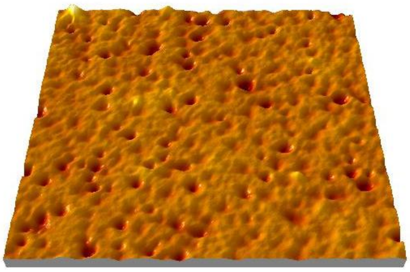	4.78	5.17
2	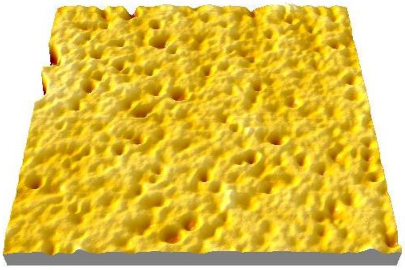	5.83	

3	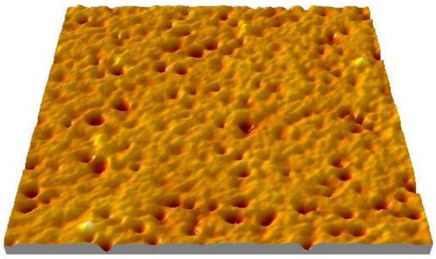	4.90	

** The scanning area's dimension is 10x10 μm², same for each single scan;*

** The AFM images are all obtained from well-annealed PEDOT:PSS top layer.*

Form the table above, The general morphology of the top PEDOT:PSS conductive layers are understood. Even the surface is rougher than the P3HT:PCBM active layers', that is still pretty flat. So, the solar cells' appearances are still good enough to show. Besides, a flat top surface also makes future encapsulation feasible, possibly minimises the negative impacts from the ambient circumstance.

Now, we have all the morphology information of all the flexible organic thin film solar cells' components, so the roughness variation is pretty clear to see. From the flow chart below, we can see the whole tendency of the roughness variation.

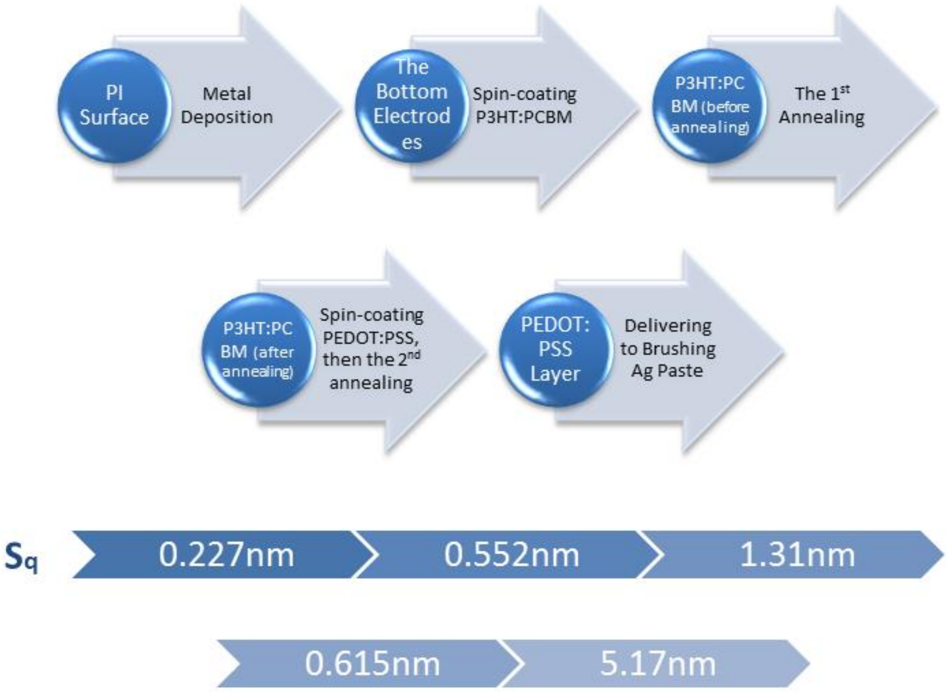

Figure 5.3 The variation tendency of the components' surface roughness of the flexible organic thin film solar cells.

5.3 PERIODIC NANOSTRUCTURES: DESIGN AND FABRICATION

5.3.1 DESIGN OF THE PERIODIC NANOSTRUCTURES

As mentioned in the former subsection, the nano-patterns were fabricated with the SEM. Essentially, the EBL process is employed to decompose the specific resist area which being exposed to the electron beam writing. Before the EBL process, a 150 nm thick PMMA A4 layer was applied by spin-coating and afterward was delivered to a hotplate for hard-baking, which is at 200℃ for 90 seconds. Then, the EBL was performed at 30keV in the Hitachi S-4800 SEM (shown in Fig.5.4) with a Raith ELPHY Quantum module. After the E-beam writing, the pattern was developed with being immersed in a 3:1 IPA:MIBK solution, rinsed, and dried, then was sent to the metal deposition.

As depicted in the former chapter, I employed the nano-gratings onto the bottom electrodes built on rigid substrates. For that part, the nano-pattern is the gratings with pitch distance of 500nm. Based on the experience, I chose the same design in the beginning for the bottom electrodes built on the flexible substrates, and subsequently proposed possible modifications and reengineered the nano-patterns.

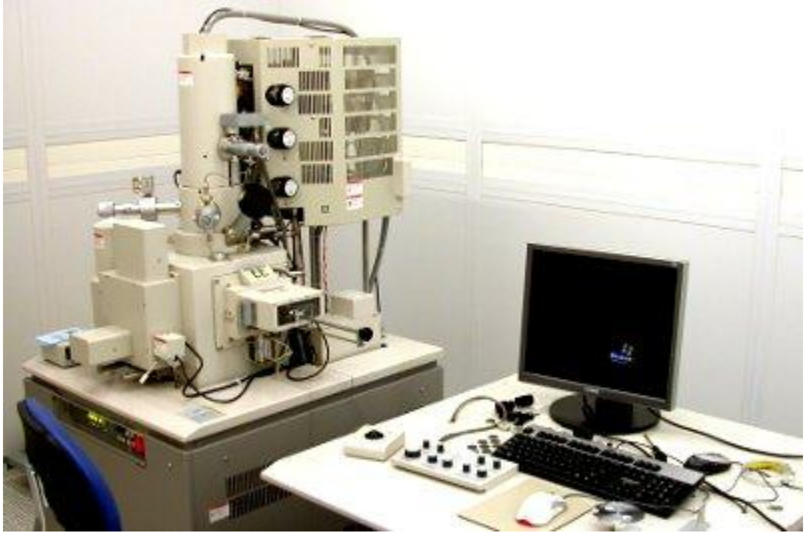

Figure 5.4 Hitachi S-4800 System, the scanning electron microscope (SEM) which is used for performing the EBL process in this project. The whole system is settled at the Cleanroom in Alsion.

Speaking of the EBL process, we must consider the dose factor for the electron-beam writing since it is quite related to the quality of the EBL's results. In formulas (5.1) and (5.2), F is the dose factor; I_{beam} is the beam current; T_{dwell} is the beam dwell time at each scanning step; T_{dwell}^{*} is the effective beam dwell time at each scanning step, and s is the step size of the dwell area. If the dose factor is chosen too high, then the design pattern will be over exposed to the E-beam; on the contrary, if the dose factor is too low, then the beam cannot utterly decompose the resist (PMMA (methyl methacrylate) A4 in my case) so that the structure cannot be formed after metal deposition and lift-off (more details depicted in Appendix VIII). So apparently, a proper dose factor is quite important.

$$Area\,Dose = \frac{I_{beam}T_{dwell}}{s^2} \quad (unit\ is\ \mu As/cm^2) \tag{5.1}$$

$$F = \frac{T^*_{dwell}}{T_{dwell}} = \frac{I_{beam}T^*_{dwell}}{AreaDose \cdot s^2} \tag{5.2}$$

In order to decide the proper range of dose factors, I made several tests. Here, some results are shown as below,

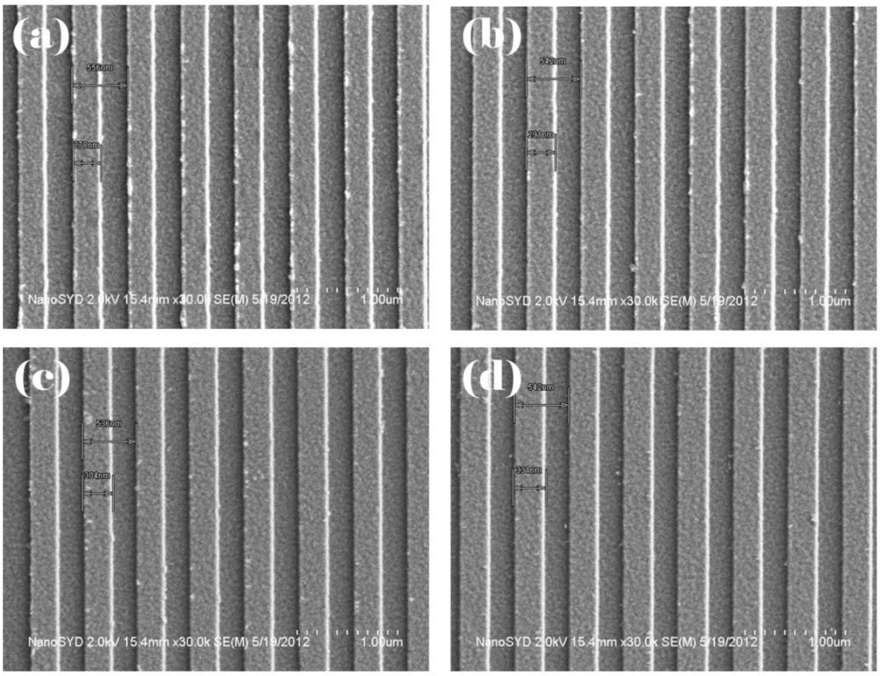

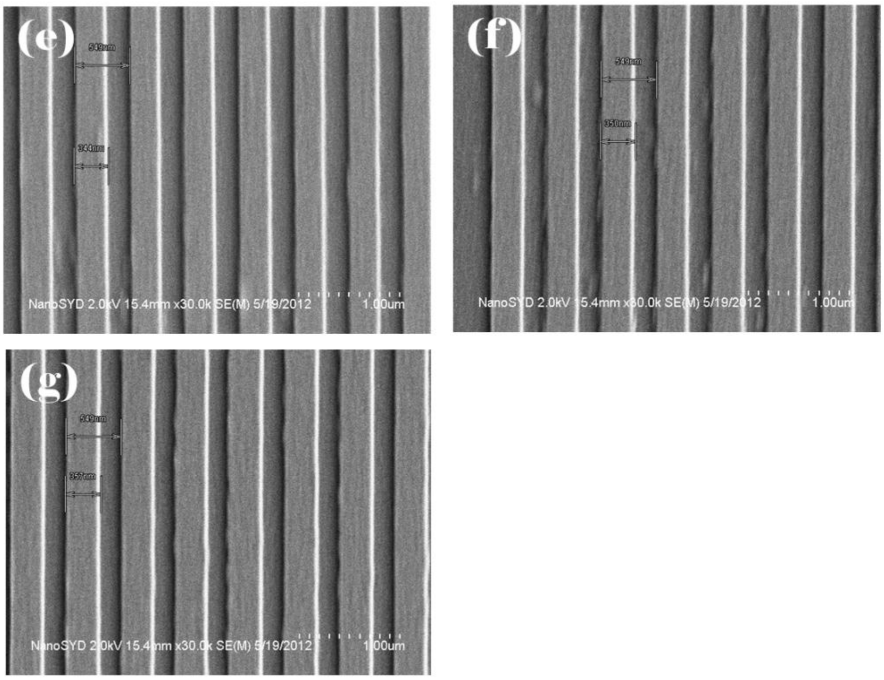

Figure 5.5 SEM images of a dose test's results. The designed pitch distance of a period is 550nm, designed width of a crest ("nano-stripe") is 275nm. Dose factor: (a)3, (b)3.5, (c)4, (d)4.5, (e)5, (f)5.5, (g)6.

From the SEM images above, we can see that when the dose factor varies in the range of 3~4 (Fig.5.5 (a)(b)(c)), the width of a crest, namely a "nano-stripe" is approximate to the design ((a)278nm; (b)291nm; (c)304nm). However, the width of the trough between each two neighbouring stripes gets smaller and smaller as the dose factor increases (Fig.5.5 (a)~(g)). So, in regard to the desired dimension, the proper dose factors could be tuned in the range of 3~4 for this very design.

After deciding the dose factor, fabrication of the nano-patterns on bottom electrodes with EBL should come onto the stage. However, we can only tell the planar information from the planform SEM images, so for investigating the profile information, I captured one AFM image to show (Fig.5.6).

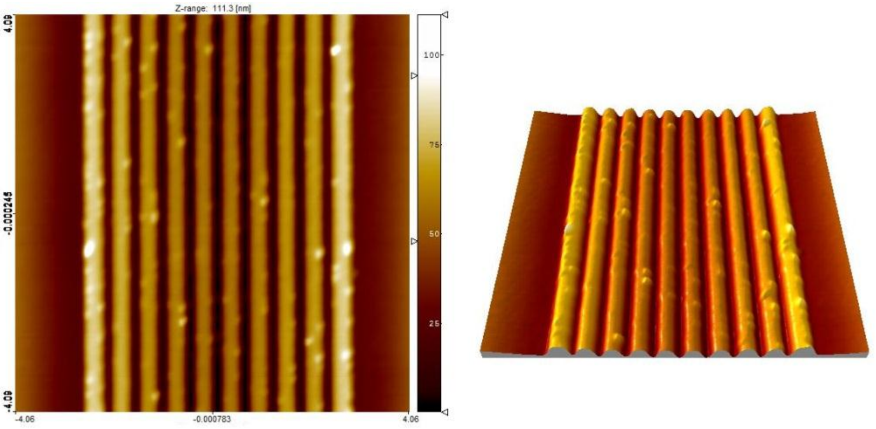

(a) **(b)**

Figure 5.6 AFM images for showing the nano-stripe arrays. (a) a 2D planform; (b) a 3D image. The scanning area's dimension is 10x10μm^2.

From the AFM image, the general height of these stripes is about 50nm, that quite corresponds to with the design height of the recipe (see Appendix VIII - Step 7).

With the help of the optical reflection spectrum in Fig.5.7, we can have some information about the light-trapping with the nano-gratings. Here, the reflection spectrum is taken on a bare nano-structured bottom electrode, the dip around 420nm implying that the light absorption around this specific wavelength is enhanced with the application of nano-gratings. However, as we know, the structured electrode should be covered by P3HT:PCBM thin film in a complete solar cell, which should definitely arise some changes to the spectrum. According to the equation (3.7), if we fixing $p=\lambda/n$, for normal incidence (m=0or±1), when the refractive index of material n increasing, the light should move to longer wavelength range. The refractive index of the active blend, P3HT:PCBM (1:1 by weight, dissolve in chlorobenzene or 1,2-dichlorobenzene) is around 1.9, [45] which means the spectrum in Fig.5.7 ought to red-shift after the P3HT:PCBM covering. That could also match the dimension of the nano-gratings (pitch dictance: 550nm) in a way. Therein, light absorption can be enhanced with the application of the nano-gratigns in the organic solar cells.

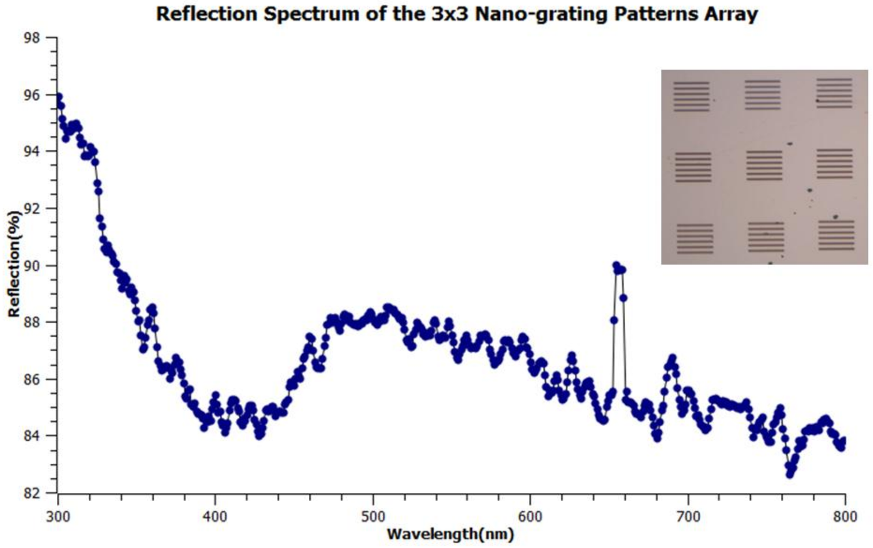

Figure 5.7 The reflection spectrum of the structured bottom electrode. The nano-structures are nine 100μmx100μm TiOx arrays composed of 550nm pitch distance gratings, shown in the inset photograph.

5.3.2 PATTERN FABRICATION WITH ELECTRON BEAM LITHOGRAPHY

Comparing to Au and Al/Ti layers, a mono Ti nano-gratings showed better capability of optical diffraction in experiments. That is why Ti became my option for the nano-structures. During the lift-off process, the unwanted Ti layer on top of the residue resist layer is stripped with immersing the sample in acetone, whereas the desired patterns can remain on top of the bottom electrodes. Considering the specialty of the PI substrates, a mild vibration was applied to instead of the common ultrasonic agitation, in case of the any possible peeling-off from the handling Si wafer.

In Appendix VIII, the fabrication process of the nano-patterns is listed step by step, with all the setup parameters.

5.4 PERFORMANCE

5.4.1 THE FLEXIBLE SOLAR CELLS WITH & WITHOUT NANO-STRUCTURES

With the utilization of EBL, nano-grating structures were engineered on the bottom electrodes. The flexible PI2525 substrates with these nano-structured bottom electrodes on were delivered to the solar cell producing process subsequently. The producing process is identical to the procedures of making rigid ones, which is depicted in Chapter4. (more detail is attached in Appendix VII)

With the same set-up displayed in Fig.4.13, I obtained the characteristics of the flexible organic thin film solar cells. All the initial data and calculated outcomes are listed in Appendix II(a). The data there are showing how the performance of the nano-structured flexible solar cell is, including the operating condition inside glove-box. Moreover, for further showing the enhancement of the nano-structures, some reference flexible organic thin film solar cells were fabricated as well. Those reference solar cells were fabricated without any nano-structures, whereas processed in the same operating conditions to the structured ones. Similar to the nano-structured solar cells, the initial data and calculated characteristics are also list in a table (Appendix II(a)). Discarding some invalid initial data, characteristics of 11 structured cells and 10 un-structured cells are collected and deployed.

From the table in Appendix II(a), we can roughly see that the improved Jsc and PCE with the nano-structured cells, but there is no obvious varieties of the Voc and FF, because Voc has a quite dependence on the ambient temperature and illumination intensity, and always in the range of 0.4 to 1 V. [12] In order to comprehend the performance of the solar cells, arithmetical average values of the solar cells' characteristics are necessary to be used to demonstrate the enhancement.

5.4.2 COMPARISON

For demonstrating the enhancement manifestly, arithmetical average values should be used because they are quite comparable and more reliable. Hence, I collect all the data of both structured & unstructured solar cells and list the averages of each characteristic (Jsc, Voc, FF and PCE) in the following comparison table.

Table 5.5 Comparison of the nano-structured & unstructured flexible organic thin film solar cells

Cells	**Mean Jsc (mA/cm^2)**	**Mean Voc(V)**	**Mean FF(%)**	**Mean PCE(%)**
Nanostructured	-4.90	0.58	20.72	0.55
Un-nanostructured	-3.62	0.54	21.29	0.38
Enhancement	35.36%	7.41%	2.77%	44.74%

From the table above we can conclude that the nano-gratings are surely helpful to enhance light absorption for improving PCE of the flexible organic thin film solar cell. The enhancements of Jsc and PCE can be up to around 35% and 45%, respectively. That proofs the feasibility of the combination between nano-structured electrode and flexible organic thin film solar cell, and also reveals a good potential of the application of the nano-gratings.

However, it is also clear to see the Jsc and PCE are still at low levels. But with the novel enhancement given by the nano-structures, this situation could be optimised in future work. Furthermore, we need to consider to improve the Voc and FF as well, in order to get even better performance of the flexible organic thin film solar cell. That is another milestone which has already been proposed, and could be fulfilled in the near future.

5.5 DISCUSSION AND SUMMARY

From the whole research we can see that both the Jsc and PCE can surely be improved with employing the periodic nano-structures. This fruitful research turns out to be meaningful and promising. Accompany with related researches, the flexible organic thin film solar cells can be further optimised and industrialized on a large scale in the near future. This inspired and remarkable creation will finally be significantly beneficial to our life.

During the whole process of making the flexible organic thin film solar cells, there showed up some issues. Here, I would like to present them briefly, and discuss the aftermaths they could result in.

5.5.1 THE DEVELOPER'S IMPACT ON POLYIMIDE SUBSTRATE

In the fabrication process, there are always some chances the developer (3:1 IPA:MIBK) for EBL can meet the polyimide substrates' surfaces directly. However the impact which this contact could result in is rarely published. With lacking of the references focusing on this very point, it is necessary to investigate what kind of influence the contact would bring. For this aim, several tests were made by myself.

Firstly, a neat PI2525 without any additional layers was prepared. Then, the test sample was sent to a proper photolithography process (Appendix III) while halted before metal deposition. Skip the step of metal deposition, I delivered the sample to developing directly, for comparing to the common 1min development, a 5min development was tested, the result AFM planform image with its profile curve are shown in the figure below.

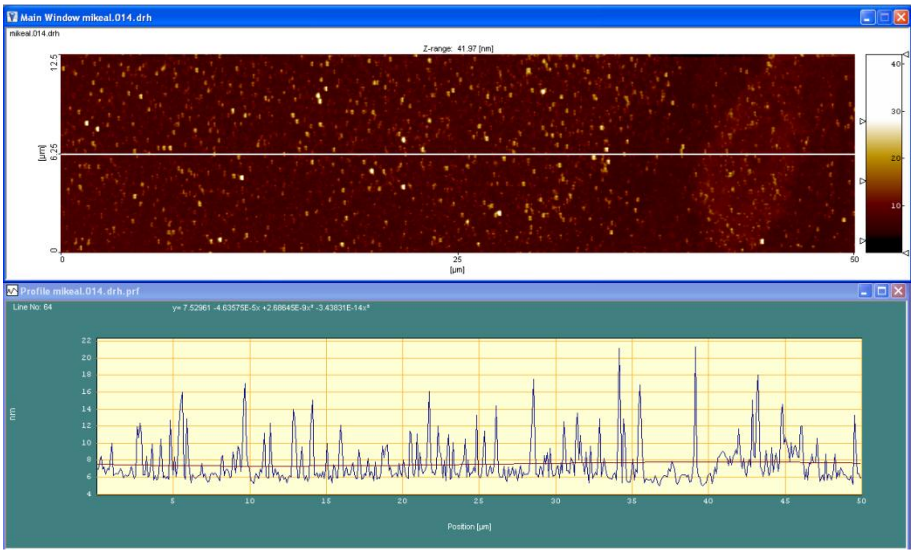

Figure 5.8 An AFM planform with its own profile curve for showing a 5min-developed PI2525 surface. We can hardly tell where the original boundary between UV-exposed and UV-unexposed areas locates.

Apparently, 5 minutes is long enough to overdevelop the unexposed photoresist (since AZ5214E is a typical negative photoresist material). However, there is no distinct difference in height between the UV-exposed and UV-unexposed areas even though after a relatively long time development. That means the developer doesn't damage the PI substrate's surface, thus the PI substrate can be trusted with the development. That also proves that the polyimide is a qualified material to be used as the flexible substrate of the organic thin film solar cell.

5.5.2 RESIST SHRINKAGE ON BOTTOM ELECTRODE

Before the EBL process, I need to spin-coat the resist material PMMA A4 on top of the bottom electrodes, after a subsequent hard-baking the sample can be sent to the E-beam writing. However, there were some phenomena caused my notice when the hard-baking process was done, that is the shrinkage in the electrodes. For displaying the corrugated surface, some images were taken with the optical microscope (Fig.5.9).

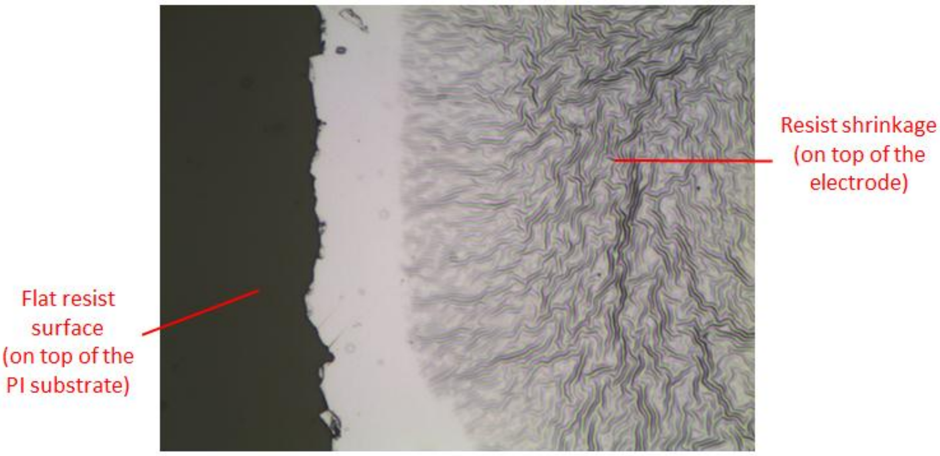

Figure 5.9 The shrinkage of PMMA A4 layer on top of bottom electrodes. Taken with digital inspection microscope (Nikon LV100D). Magnification: x20.

In fact, the aftermath might be quite serious. The experimental experience tells me that even though after doing the lift-off process followed by metal deposition, the corrugated surface may still exist so that cause surface tension concentration, therein can easily crack the delicate bottom electrodes (Fig.5.10).

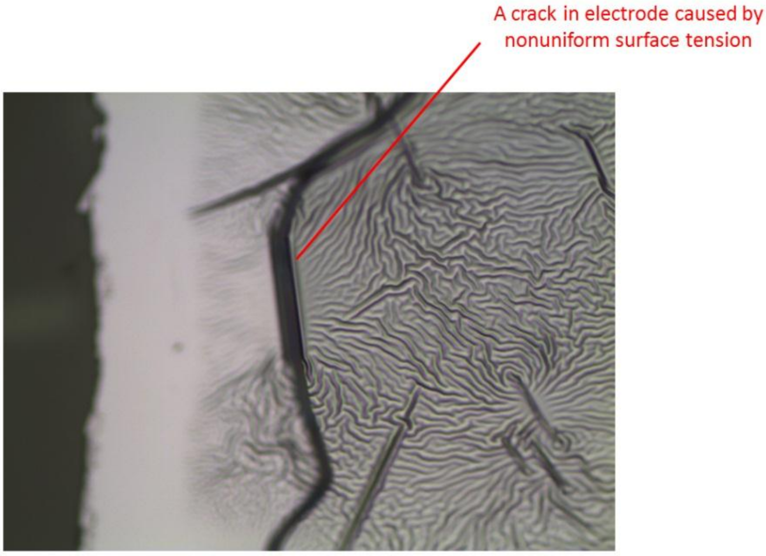

Figure 5.10 A typical crack in bottom electrode caused by nonuniform surface tension. Optical microscope image, magnification: x20.

But what could be the reason? Considering the specific area, the surface morphology, and the hard-baking process, I suppose there could be two possible explanations: the first, the reason could be the different coefficients of thermal conductivity (CTC) of the resist PMMA A4 and the bottom electrode. Comparing to the bottom electrode's coefficient of thermal conductivity (Aluminium-237 W/(m·K), TiOx- ≈11.7 W/(mK), the PMMA A4's is very small (normally 0.167~0.25W/(mK) [46]), which could result in different solidifying rates, and this difference would also lead to different shrinking rate so that finally cause the specific shrinkage. However, that could also due to the second reason, namely the different coefficients of thermal expansion (CTE). The CTE of polyimide is normally around 55ppm/℃ (or even higher, [47]), whereas the CTEs of aluminium and titanium oxide are usually 23.6ppm/℃ and 32.7ppm/℃, respectively. [48] Apparently, the PI has greater thermal expansion capability than the bottom electrode does. That could lead to different thermal expansions when the hard-baking is taking place so that resulting in the corrugations which look like shrinkages.

For verifying the hypothesises, I made other two tests. First, I heated up a PI substrate with bottom electrodes on as the normal hard-baking (200°C for 90 sec), but without the resist PMMA A4. The results can be seen that the corrugated surface showed up again after this simulating hard-baking. Second, I also did the normal hard-baking process for a complete solar cell sample with the resist PMMA A4 on. Certainly the corrugations showed up again. However, after a simulating lift-off, the corrugations still existed, even though the resist PMMA A4 was dissolved in acetone.

Hence, the corrugation does belong to the electrode while not the PMMA top layer. So, the main reason is the second hypothesis for sure, despite the thermal conductivities should also be considered.

In order to solve this problem, a slow baking could be helpful. From this assumption I did a long time test baking with a small increasing slope of temperature (2.3°C/min), from the room temperature (≈20°C) to 90°C. From the result (Fig.5.11(c)) we can easily see that after about 30min slow hard-baking, the electrode's surface didn't change too much, in fact, we can even barely see the changes. Comparing to the quick, high temperature hard-baking (200°C for 90 sec, Fig.5.11(b)), this one is doubtless much better without damaging the electrode's surface. Therein, all the PI substrate related baking were all fulfilled with this slow hard-baking process.

In fact, for the slow baking, higher temperature could also be reached. Since we need to anneal both the active layer and top contact PEDOT:PSS layer at 140 ℃ , so it is necessary to be tested. Experimentally, I tried the slow baking from room temperature to 140℃ in 30min as well, and it also turned out to be feasible.

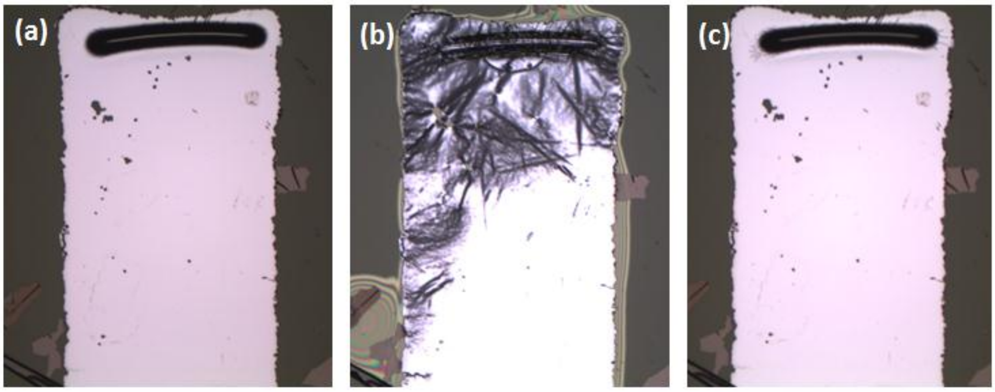

Figure 5.11 Results comparison between the quick hard-baking & the slow hard-baking of the bottom electrode on polyimide substrate. (a) the initial electrode with a mark, (b) after a quick hard-baking, (c) after a slow hard-baking. Images were taken with a digital inspection microscope (Nikon LV100D). Magnification: x10.

5.5.3 BEFORE & AFTER PEELING-OFF

Peeling-off is another important work in this project, it is rather worth being investigated. Experimentally, a mechanical peeling-off with tweezers has turned out to be an effective way to separate the flexible solar cells and the handling Si substrates. However, it is also a risky way which could cause mechanical damage to the solar cells.

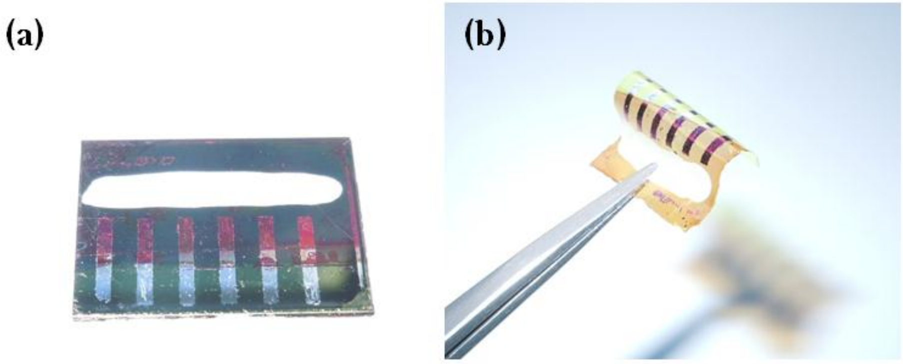

Figure 5.12 Appearances of the flexible organic thin film solar cell. (a)before peeling-off from a Si handling substrate; (b)after peeling-off from the Si handling substrate.

Ideally, we expect no difference of the solar cell's performance between before & after peeling-off. However, from the investigation, I found there is an obvious difference of the characteristics between two measurements (before & after peeling, timely). From the initial data and calculated outcomes, (Appendix II(b)), a rough decrease of the performance after peeling-off can be seen.

For clearly demonstrating the difference, arithmetical average values are used. All the results are listed in Table 5.6.

Table 5.6 Comparison of the flexible solar cells' characteristics between before & after peeling-off

Cells	**Mean Jsc (mA/cm^2)**	**Mean Voc(V)**	**Mean FF(%)**	**Mean PCE(%)**
Before peeling-off	-4.17	0.60	43.7	1.05
After peeling-off	-3.58	0.58	42.5	0.86
Degradation	14.15%	3.33%	2.75%	18.10%

As can be seen in the table above, the degradations of Jsc and PCE are 14.15% and 18.10%, which implying there was a loss took place in big extent during the mechanical peeling-off. If we plot one cell's J-V curves before & after peeling-off, we can directly see the degradation. (Fig.5.13)

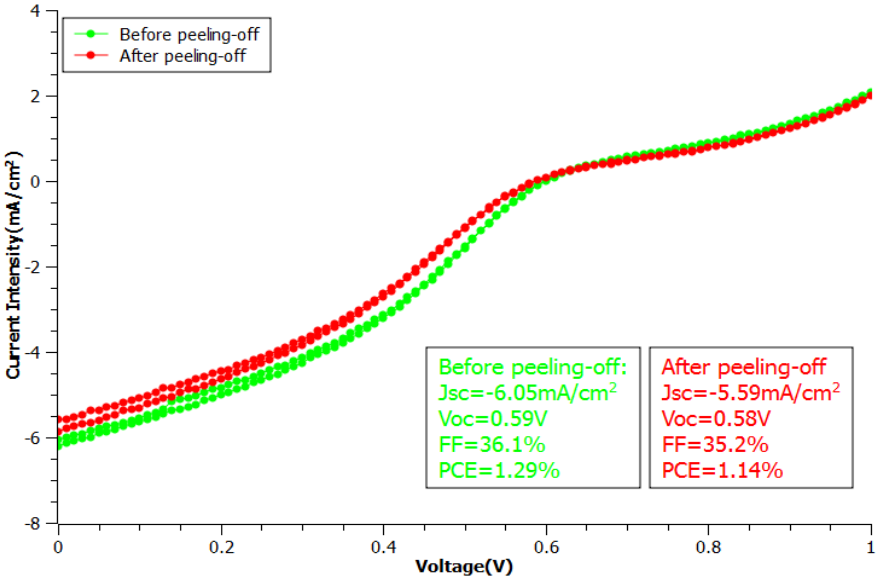

Figure 5.13 One cell's J-V curves showing the difference between before & after peeling-off.

Even though the reason to the performance degradation of flexible solar cells before & after peeling-off is not researched in this project, we can still assume that could be caused by some physical form changes which can impact the electric property of the solar cell. We may use some specific methods to eliminate this negative influence, for instance, using encapsulation to protect the delicate flexible solar cells. Some relevant work could also be performed in further, deeper following research.

CHAPTER 6.

CONCLUSIONS AND FUTURE WORK

6.1 CONCLUSIONS

In the Chapter 4 and 5, we have seen the fabrication processes of both the rigid thin film solar cells and the flexible organic thin film solar cells, and how to improve their performances theoretically and experimentally. During the whole project, quite a few state-of-the-art techniques were utilized, and combined with inspired ideas.

From the convictive experimental outcomes, we have seen the enhancements with those techniques and inspirations indeed. For the organic thin film solar cells built on rigid glass substrates, I demonstrated the experimental outcomes of the samples with & without nanostructures in Section 4.2, so that the enhancements can be seen easily with those data tables.

The improvements for the solar cells' characteristics are straightforward. With the nano-grating structures, the average power conversion efficiency (PCE) has been improved 11.5%. If we can further optimise the compound materials and encapsulate those samples to avoid any possible oxidations, the enhancements for PCE will be even greater.

Based on the experiences from the rigid solar cells, I continued improving the performance of the novel flexible organic thin film solar cells in Chapter 5. Effective methods such as proper annealing and light-trapping enhancement are integrated. Some issues and problems like the PEDOT:PSS's adhesion on the active layer and shrinkages of the bottom electrode on PI substrates were found and overcome in a way during this process.

Owing to the enhanced light-trapping by nano-gratings, Jsc and PEC are improved by 35.36% and 44.74%, respectively, which means the flexible organic thin film solar cell with nano-structured bottom electrode has a prospective potential for further optimisation. This valuable conclusion is significant to the possible application on large scale in future.

Another issue arose accompany with the mechanical peeling-off the flexible solar cell from Si handling substrate, degradation in performance in a way of the solar cell was discovered. This degradation is unnecessary and not what we expect, so it can be an issue which needs to be deeply investigated and overcome, could be presented in following work after this project.

Besides the content above, there are some other factors also presented and investigated in this thesis, i.e. morphologies of the component thin films in the rigid and flexible solar cells, proper dose factor test to the EBL process, optical absorption properties of the rigid and flexible solar cells, etc. Even though I have gotten abundant resources from the practical work and the comprehension of flexible organic thin film solar cell from the theoretical study, and, the initial objectives of this project have been achieved as well, however, it doesn't stand for the ending of this research. On the contrary, it is exact another starting point, plenty of interesting work in organic photovoltaic power generation awaits for being found and investigated, and the work will be significant and beneficial to the people. With the hard work of the talents, a foreseeable blooming era of its utilization is coming to us apace.

6.2 EMERGING ISSUES AND FEASIBLE COUNTERMEASURES

During this project process, I met a lot of challenges. However, in undertaking these challenges, in spite of some experimental issues tripped me a bit, nevertheless they were even more helpful to me for deeply comprehending organic thin film solar cells. During this process, some countermeasures or inspired methods were proposed and tested in a way.

6.2.1 S-SHAPE OF THE J-V CURVE

Among those emerging issues, the most important one should be the significant hump, which is the so-called “S-shape” of the measured J-V curve. Ideally, the J-V curve is supposed to have only one bend (Fig.3.11). However, in this project, this S-shape issue shows up very frequently (near Voc, for both of the rigid cells and the flexible ones). As can be seen in Fig.4.16, in the voltage range of 0.55~0.9V, the current intensity, or we can also say the current, is almost 0. That means in this voltage range the solar cell barely inputs current, in other words, we kind of “lose” this voltage range since it doesn’t dedicate anything to the circuit. Moreover, it is also easy to see that the FF and the PCE are reduced.

For solving this shape defect, I looked up some reference and tried to use different ways to eliminate it. In Ref[49, 50], a possible reason is explained, that should be related to an interfacial barrier for charge transport. Thus, an idea was inspired that is overcoming the barrier with external energy tuning. Interestingly, I tried to remove the AM 1.5 filter which for cutting off most of the UV light, then the “S-shape” got an apparent extinction. However, when the AM 1.5G filter was mounted back, the “S-shape” was observed again. So, generally speaking, this phenomenon was only observed when UV-light is cut off, that could be attributed to the increasing free charge carrier concentration in TiOx which can lower the carrier transport barrier across the interface when UV illumination is applied. [50]

At a routine academic seminar of SDU, Prof. Dr. Elizabeth von Hauff from Abert-Ludwigs-Universität Freiburg briefly presented a similar method to overcome the “S-shape” defect, namely lowering the interfacial barrier for charge transport with UV exposure. With the hint, I tested a few samples and did find this method is effective. From Fig.6.1, an obvious correction to the “S-shape” can be observed clearly, and in fact this effect gets increasingly stronger as time goes by. This phenomenon is worthy of investigation and very valuable to further researches.

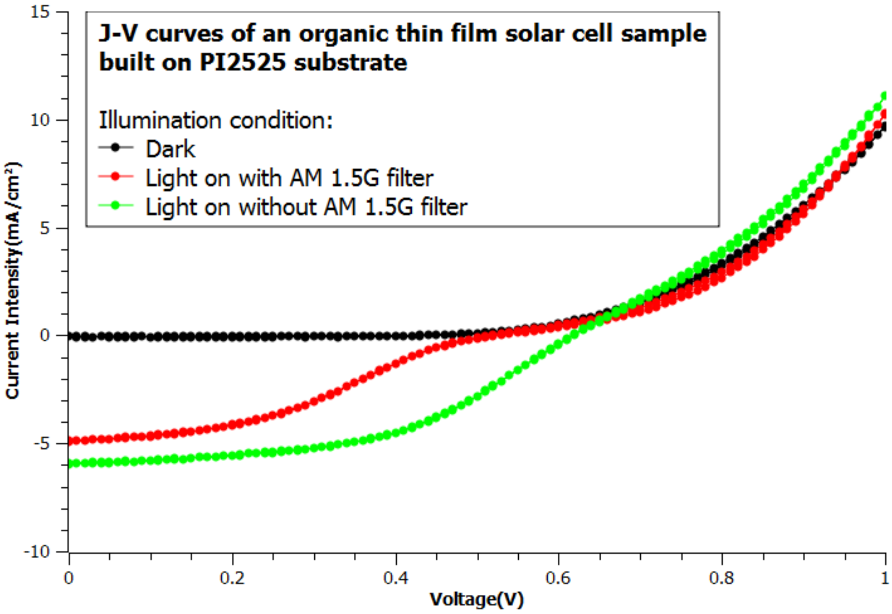

Figure 6.1 Comparison of J-V curves between with & without AM 1.5 cut-off filter under 1sun-illumination.

6.2.2 PEELING-OFF FROM THE HANDLING SILICON SUBSTRATE

As the handling substrates, Si wafer has been proved can offer a good adhesion to PI2525 thin film, but, even if the polyimide substrates can steadily adhere on, we still have to avoid any kind of disturbance which can cause peeling-off. For the investigating this issue, several tests were made by me.

First, a well-made flexible PI2525 on Si substrate was immersed into acetone for overnight to simulate a long time lift-off process (after the bottom electrodes deposition & the metallic nanostructures deposition). The result was the PI2525 substrate peeling off the Si substrate. So, it turned out that long time lift-off processes is not necessary and should be avoided as well. Normally, this process shouldn't longer than 15min in this polyimide substrate case.

Second, an ultra-sonic agitation was tested as well. Usually, metal lift-off process ought to be done with proper ultrasonications due to the high efficiency and high quality. However, in the polyimide substrate case, this method has been verified risky. When I initially tried to use ultrasonication for the lift-off process as before, the polyimide substrate was peeled off by the high frequent agitation. Unlike the rigid solar cells built on glass substrates, the flexible solar cells cannot tolerate such a high agitation. So I must manually shake the beaker with samples in for instead of ultrasonication. Even though it is an effective method, however, sometimes the manual shake could result in some defects due to the randomly varying vibration rate, i.e., partially missing electrodes or scratched electrodes (when several samples are being processed at the same time). Considering this issue, some feasible optimisations could be proposed and applied, like a mild, regular, proper-long agitation or some other novel organic solvents.

6.3 FUTURE WORK: HOW TO ELONGATE THE LIFETIME OF THE ORGANIC THIN FILM SOLAR CELLS

For a complete organic solar cell, the ability of offering high, constant power after a long-term usage is quite in demand. The life time is one of the most indexes to reflect organic solar cell's reliability, especially for the commercialisation. With the exposure to sun and the ambient increasingly heated circumstance, plus the organic nature and so on, the life time of organic solar cells could be concerned from diverse aspects. So far, plenty of work has been done by many researchers and lots of fruitful outcomes are well summarized. [51] Chemical, physical and mechanical degradation have been investigated and discussed within those research outcomes.

Essentially, the lifetime of the organic solar cells, is the time taken for the efficiency to drop below a predetermined percentage of its initial set value. Commonly, this life time is evaluated by indoor and more recently by outdoor testing. [51] The organic solar cell's life time is determined by both of the extrinsic and intrinsic stability factors. The active layer, the interface between active layer and electrode and the electrode's material, all of them can be the reason arising intrinsic instabilities; while the extrinsic instabilities can be arisen by lacking of encapsulation and some other external conditions such as weather, draught, humidity, contamination and the elevated temperature caused by illumination, etc. All the factors might result in serious degradation or even invalidation of the solar cells, let alone elongating the life time. Hence, for elongating the organic solar cell's life time, many factors should be taken into account.

As the temperature increasing due to a long time illumination, the PCE would drop mainly caused by a decrease in open-circuit voltage (Voc) as a function of increasing temperature, [52, 53] this instability would have negative impacts to the life time somehow. However, a good encapsulation can always avoid possible oxidations and pollutions, or, may also reduce some other negative factors, so that can elongate the solar cell's life time in a way. So for the flexible organic thin film solar cells built on PI2525 substrates, the encapsulation could be an effective option to minimise some serious negative impacts. Some deeper research would be interesting and meaningful on this topic.

Considering the speciality of the flexible thin film solar cell, the PI2525 substrate's life time should also be taken into account. Since as time goes by, there must be some changes take place in the polyimide thin film. Hence, for investigating the mechanical survivability of it, a fatigue test is necessary to be done. The results from the test could give us some hints for further optimising its mechanical property, and encourage us to keep seeking for other better materials for the flexible substrate as well.

BIBLIOGRAPHY

[1] Mario Pagliaro, Giovanni Palmisano and Rosaria Ciriminna; *Flexible Solar Cells*, 2008; Chap1: p.3, 4; WILEY-VCH Verlag GmbH & Co. KGaA, Weinheim; ISBN: 978-3-527-32375-3.

[2] Gang Li, Vishal Shrotriya, Jinsong Huang, Yan Yao, Tom Moriarty, Keith Emeryand and Yang Yang; *High-efficiency Solution Processable Polymer Photovoltaic Cells by Self-organization of Polymer Blends;* Nat. Mater. (Nov, 2005), Vol.4; DOI: 10.1038/nmat1500.

[3] Christoph J. Brabec, N. Serdar Sariciftci and Jan C. Hummelen; *Plastic Solar Cells;* Adv. Funct. Mater. 2001, 11.

[4] Vivian E. Ferry, Jeremy N. Munday, and Harry A. Atwater; *Design Considerations for Plasmonic Photovoltaics;* Adv. Mater. 2010, 22, 4794–4808; DOI: 10.1002/adma.201000488

[5] Christoph J. Brabec, Srinivas Gowrisanker, Jonathan J. M. Halls, Darin Laird, Shijun Jia, and Shawn P. Williams; *Polymer–Fullerene Bulk-Heterojunction Solar Cells;* Adv. Mater. 2010, 22, 3839–3856; DOI: 10.1002/adma.200903697

[6] Meng Tao; *Inorganic Photovoltaic Solar Cells: Silicon and Beyond;* The Electrochemical Society Interface (winter, 2008), p.30-35.

[7] Travis L. Benanti and D. Venkataraman; *Review: Organic Solar Cells: An Overview Focusing on Active Layer Morphology*; Photosynthesis Research (2006) 87, 73–81; DOI: 10.1007/s11120-005-6397-9.

[8] Chin-Yi Liu, doctoral thesis: *"Hybrid Solar Cells from Polymers and Silicon Nanocrystals"*; ASME 3rd International Conference on Energy Sustainability, ES2009, (July, 2009), 1, 985-987.

[9]http://www.konarka.com/index.php/site/pressreleasedetail/konarkas_power_plastic_achieves_world_record_83_efficiency_certification_fr; accessed on 22nd, May, 2012.

[10]http://www.heliatek.com/?p=199&lang=en; accessed on 22nd, May, 2012.

[11]http://www.electroiq.com/articles/sst/2011/july/organic electronics-workshop-day-2-pushing-organic-pv-performance.html; accessed on 22nd, May, 2012.

[12] Fan Yang, doctoral dissertation *"Thin Film Solar Cells Grown by Vapour Phase Deposition"*; Sep, 2008; Princeton University; UMI No. 3323172.

[13] S. R. Forrest, Chemical Review (1997); 97, 1793.

[14] Mario Pagliaro, Giovanni Palmisano and Rosaria Ciriminna; *Flexible Solar Cells*, 2008; Chap4: p.85; WILEY-VCH Verlag GmbH & Co. KGaA, Weinheim; ISBN: 978-3-527-32375-3.

[15] Mario Pagliaro, Giovanni Palmisano and Rosaria Ciriminna; *Flexible Solar Cells*, 2008; Chap2: p.33-34; WILEY-VCH Verlag GmbH & Co. KGaA, Weinheim; ISBN: 978-3-527-32375-3.

[16] *"Organic Heterojunctions in Solar Cells"*; on webpage: http://depts.washington.edu/cmditr/modules/opv/organic_heterojunctions_in_solar_cells.html; accessed on 23rd, May, 2012.

[17] Kittel Charles, Herbert Kroemer; *Thermal Physics (2nd Edition)*. W. H. Freeman. p.357; ISBN 978-0-7167-1088-2

[18] G. Yu, J. Gao, J. C. Hummelen, F. Wudl, A. J. Heeger, Science 1995; 270, 1789.

[19] J. C. Hummelen, B. W. Knight, F. Lepec, F. Wudl, J. Org. Chem. (1995), 60, 532.
[20] Nelson, J. *The Physics of Solar Cell*, 2003; Imperial College Press, London.

[21] L. Zeng, Y. Yi, C. Hong, J. Liu, N. Feng, X. Duan, L. C. Kimerling and B. A. Alamariu; *Efficiency Enhancement in Si Solar Cells by Textured Photonic Crystal Back Reflector*; American Institute of Physics 2006; DOI: 10.1063/1.2349845.

[22] Ying Zheng and Jiangeng Xue; *Organic Photovoltaic Cells Based on Molecular Donor-Acceptor Heterojunctions; 2010;* Polymer Reviews, 50: 420–453, ISSN: 1558-3724; DOI: 10.1080/15583724.2010.516051.

[23]Eugene Hecht; *Optics (fourth edition, 2002);* ISBN: 0-8053-8566-5.

[24] Xiong Gong, Ming-Hong Tong, Sung Heum Park, Michelle Liu, Alex Jen and Alan J. Heeger; *Semiconducting Polymer Photodetectors with Electron and Hole Blocking Layers: High Detectivity in the Near-Infrared,* Sensors 2010, 10, 6488-6496; DOI:10.3390/s100706488.

[25] David Mühlbacher, Markus Scharber, Mauro Morana, Zhengguo Zhu, David Waller, Russel Gaudiana, and Christoph Brabec; *High Photovoltaic Performance of a Low-Bandgap Polymer;* Adv. Mater. 2006, 18, 2884–2889; DOI: 10.1002/adma.200600160

[26] A. Baumann, J. Lorrmann, C. Deibel and V. Dyakonov; *Bipolar Charge Transport in Poly(3-hexyl thiophene)/Methanofullerene Blends: A Ratio Dependent Study,* (2008); Experimental Physics VI, Julius-Maximilians-University of Wurzburg, and Bavarian Center for Applied Energy Research e.V. (ZAE Bayern).

[27] Roana Melina de Oliveira Hansen, Manuela Schiek, Yinghui Liu, Morten Madsen and Horst-Günter Rubahn; *Efficiency Enhancement of ITO-free Organic Polymeric Solar Cells by Light Trapping, April;* NanoSYD, Mads Clausen Institute, University of Southern Denmark & Kekulé-Institute of Organic Chemistry and Biochemistry, Rheinische Friedrich-Whilhelms-University of Bonn; Proc. SPIE (2012) Vol. 8438 843813-1

[28] Zheng Tang, L. Mattias Andersson, Zandra Geroge, Koen Vandewal, Kristofer Tvingstedt, Patrik Heriksson, Renee Kroon, Mats R. Andersson and Olle Inganas; *Interlayer for Modified Cathode in Highly Efficient Inverted ITO-Free Organic Solar Cells;* Chamlers University of Technology, Sweden; DOI: 10.1002/adma.201104579.

[29] Sung Heum Park, Anshuman Roy, Serge Beaupré, Shinuk Cho, Nelson Coates, Ji Sun Moon, Daniel Moses, Mario Leclerc, Kwanghee Lee and Alan J. Heeger; *Bulk Heterojunction Solar Cells with Internal Quantum Efficiency Approaching100%;* Nature Photonics, (May, 2009) Vol 3; DOI: 10.1038/nphoton.2009.69.

[30] *Effect of Interfacial Polymer Morphology on Solar Cell Performance*; Sandia National Laboratory, USA.

[31] Claudio Girotto, Barry P. Rand, Soeren Steudel, Jan Genoe, Paul Heremans; *Nanoparticle-based, Spray-coated Silver Top Contacts for Efficient Polymer Solar Cells;* Organic Electronics 2009, 10, 735–740.

[32] V. D. Mihailetchi, H. Xie, B. de Boer, L. J. A. Koster, P. W. M. Blom, Adv. Funct. Mater. 2005, 15, 1260.

[33] A. Pivrikas, G. Juska, A. J. Mozer, M. Scharber, K. Arlauskas, N. S. Sariciftci, H. Stubb, R. Österbacka , Phys. Rev. Lett. (2005), 94, 176806.

[34] *"Chapter One: Introduction to Organic Solar Cells"* extracted from a thesis, anon.

[35] Harry A. Atwater and Albert Polman; *Plasmonics for improved photovoltaic device*; DOI: 10.1038/NMAT 2629.

[36] Steven K. Hau, Hin-Lap Yip and Alex K.-Y.Jen; *A Review on the Development of the Inverted Polymer Solar Cell Architecture;* Department of Materials Science and Engineering, University of Washington, Seattle, WA 98195-2120, USA; ISSN: 1558-3724 print/1558-3716 online; DOI: 10.1080/15583724.2010.515764

[37] Kai Frolic; *Developing Polymer Solar Cells – Morphology of the Photoactive Laye,* (2007); Department of Chemical Engineering and Chemistry, Technical University of Eindhoven.

[38] Erwin Bosman, Geert Van Steenberge, Bram Van Hoe, Jeroen Missinne, Jan Vanfleteren, and Peter Van Daele; *Highly Reliable Flexible Active Optical Links*; IEEE Photonics Technology Letters (March, 2010), Vol. 22, No. 5; DOI:10.1109/LPT.2009.2038797.

[39] Michael W. Rowell, Mark A. Topinka, Michael D. McGehee, Hans-Jürgen Prall, Gilles Dennler, Niyazi Serdar Sariciftci, Liangbing Hu and George Gruner; *Organic Solar Cells with Carbon Nanotube Network Electrodes;* App. Phy. Lett. (2006), 88, 233506; DOI: 10.1063/1.2209887.

[40] Jennifer Drayton, Anthony Vasko, Akhlesh Gupta, A.D. Compaan; *Magnetron Sputtered CdTe Solar Cells on Flexible Substrates;* Department of Physics and Astronomy, The University of Toledo; ©2005 IEEE, 0-7803-87074/05.

[41] A.C. Vasko, X. Liu, A.D. Compaan; *All-sputtered Cds/CdTe Solar Cells on Polyimide;* Department of Physics and Astronomy; ©2009 IEEE, 978-1-4244-2950-9/09.

[42] Tokio Nakada, Taku Kuraishi, Taku Inoue, and Takahiro Mise; *CIGS Thin Film Solar Cells on Polyimide;* Department of Electrical Engineering and Electronics, Aoyama Gakuin University; ©2010 IEEE, 978-1-4244-5892-9/10.

[43] Chi Hwan Lee, Dong Rip Kim, and Xiaolin Zheng; *Fabrication of Nanowire Electronics on Nonconventional Substrates by Water-Assisted*

Transfer Printing Method; Nano Lett. (2011), 11, 3435–3439; dx.doi.org/10.1021/nl201901z.

[44] Kuniharu Takei, Toshitake Takahashi, Johnny C. Ho, Hyunhyub Ko, Andrew G. Gillies, Paul W. Leu, Ronald S. Fearing and Ali Javey; *Nanowire Active-matrix Circuitry for Low-voltage Macroscale Artificial Skin*; Nat. Mater. (Oct, 2010), 9, 821-826; DOI: 10.1038/NMAT2835.

[45] W.H. Lee, S.Y. Chuang, H.L. Chen, W.F. Su, C.H. Lin; *Exploiting Optical Properties of P3HT:PCBM Flms for Organic Solar Cells with Semitransparent Anode*; Thin Solid Films(2010), 518, 7450–7454; DOI:10.1016/j.tsf.2010.05.021

[46]http://www.matbase.com/material/polymers/commodity/pmma/properties, accessed on 22nd, May, 2012

[47] J. Dolbow, M. Gosz; *Effect of Out-of-plane Properties of a Polyimide Film on the Stress Fields in Microelectronic Structures;* Mechanics of Materials (1996), 23, 311-321.

[48] H. Xie, X. T. Zeng, and W. K. Yeo; *Temperature Dependent Properties of Titanium Oxide Thin Films by Spectroscopic Ellipsometry;* SIMTech technical reports, Jan-Mar, 2008, Vol.9 -No.1.

[49] *Multi-layer Organic Thin Film Solar Cell;* Technology Offer; EMPA Technology Transfer; TT-Ref. 2009-085.

[50] Srinivas Sista, Mi-Hyae Park, Ziruo Hong, Yue Wu, Jianhui Hou, Wei Lek Kwan, Gang Li, and Yang Yang; *Highly Efficient Tandem Polymer Photovoltaic Cells;* Department of Materials Science and Engineering University of California Los Angeles; Adv. Mater. 2010, 22, 380–383; DOI: 10.1002/adma.200901624

[51] M. Jørgensen, K. Norrman, F. C. Krebs, Sol. Energy Mater. Sol. Cells 2008, 92, 686.

[52] Sewang Yoon and Vahan Garboushian *Reduced Temperature Dependence of High-concentration Photovoltaic Solar Cell Open-circuit Voltage (Voc) at High Concentration Levels;* CH 3365-4/94/0000-1500.

[53] Wang Jian-jun; *The Temperature Influence on Solar PV Generation;* Journal of Qinghai Normal University (Natural Science) (2005) No.1, p.28-30.

[54] Gilles Dennler, Markus C. Scharber, and Christoph J. Brabec; *Polymer-Fullerene Bulk-Heterojunction Solar Cells;* Adv. Mater. 2009, 21, 1323–1338; DOI: 10.1002/adma.200801283.

[55] Jeong Ah Chang, Jae Hui Rhee, Sang Hyuk Im, Yong Hui Lee, † Hi-jung Kim, Sang Il Seok, Md. K. Nazeeruddin, and Michael Gratzel; *High-Performance Nanostructured Inorganic-Organic Heterojunction Solar Cells;* Nano Lett. 2010, 10, 2609–2612; DOI: 10.1021/nl101322h.

[56] Neil D. Treat, Michael A. Brady, Gordon Smith, Michael F. Toney, Edward J. Kramer, Craig J. Hawker, and Michael L. Chabinyc; *Interdiffusion of PCBM and P3HT Reveals Miscibility in a Photovoltaically Active Blend;* Adv. Energy Mater. 2011, 1, 82–89; DOI: 10.1002/aenm.201000023.

[57] T. Aernouts, T. Aleksandrov, C. Girotto, J. Genoe, and J. Poortmans; *Polymer Based Organic Solar Cells Using Ink-jet Printed Active Layers;* App. Phy. Lett. 2008, 92, 033306; DOI: 10.1063/1.2833185.

[58] Elizabeth von Hauff, Vladimir Dyakonov, Jürgen Parisi; *Study of Field Effect Mobility in PCBM Films and P3HT:PCBM Blends;* Solar Energy Materials & Solar Cells 87 (2005) 149–156; DOI:10.1016.

[59] Christopher Palmer; *Diffraction Grating Handbook- 5th Edition;* Richardson Grating Laboratory, USA; Copyright 2002, Thermo RGL.

[60] Xuanhua Li, Wallace C. H. Choy, Lijun Huo, Fengxian Xie, Wei E. I. Sha, Baofu Ding, Xia Guo, Yongfang Li, Jianhui Hou, Jingbi You, and Yang Yang; *Dual Plasmonic Nanostructures for High Performance Inverted Organic Solar Cells;* Adv. Mater. 2012; DOI: 10.1002/adma.201200120.

Appendix I.

(a) Characterised Outcomes of the Rigid Unstructured Samples

Sample/Cell		**Annealing**	**Jsc (mA/cm^2)**	**Voc (V)**	**Fill Factor(%)**	**Efficiency (%)**
YR-01	Cell1	140°C Active layer: 5min; PEDOT:PSS 1: 2min30sec;	-5.51	0.62	34.8	1.190
	Cell2		-2.15	0.63	48.0	0.650
YR-02	Cell1	140°C Active layer: 7min; PEDOT:PSS: 2min30sec;	-4.73	0.62	33.8	0.991
	Cell2		-6.59	0.62	34.0	1.390
YR-03	Cell1	140°C Active layer: 10min; PEDOT:PSS: 2min30sec;	-5.20	0.62	43.7	1.410
	Cell2		-7.43	0.63	42.7	2.000
YR-04	Cell3	140°C Active layer: 15min; PEDOT:PSS: 2min30sec;	-5.90	0.57	24.2	0.814
	Cell4		-7.04	0.52	24.6	0.901
	Cell5		-6.58	0.59	20.0	0.777
YR-05	Cell2	140°C Active layer: 20min; PEDOT:PSS: 2min30sec;	-16.6	0.61	28.1	2.850
YR-06	Cell3	140°C Active layer: 25min; PEDOT:PSS: 2min30sec;	-6.33	0.58	22.9	0.839
	Cell4		-6.03	0.55	24.1	0.798

**Initial conditions of the glove-box:* O_2*: 510 ppm (parts permillion);* H_2O*: 2223 ppm.*

(b) Comparison Between Structured Organic Thin-film Solar Cells and the Unstructured Ones

Sample/Cell		**Annealing Time**	**Jsc (mA/cm²)**	**Voc (V)**	**Fill Factor (%)**	**Efficiency (%)**
Structured	Cell2	140℃ Active layer: 25min; PEDOT:PSS:2min30sec;	-9.54	0.58	37.4	2.07
	Cell3		-8.86	0.53	36.8	1.73
	Cell4		-11.4	0.61	33.2	2.31
Unstructured	Cell3		-6.36	0.58	34.4	1.27
	Cell6		-7.35	0.61	32.1	1.44

* *Initial conditions of the glove-box:* O_2*: 518 ppm;* H_2O*: 2036 ppm*

(c) Characterisation of the Solar Cells with 200nm Thick PCPDTBT:PCBM Layer

Sample/Cell		**Annealing**	**Jsc (mA/cm²)**	**Voc (V)**	**Fill Factor(%)**	**Efficiency (%)**
B01U	Cell 1	80°C Active layer: 25min; PEDOT:PSS:2min30sec;	-0.904	0.33	28.8	0.0862
	Cell 2		-0.955	0.33	27.2	0.0857
	Cell 3		-1.000	0.38	28.2	0.1070
	Cell 4		-1.000	0.37	28.4	0.1050
	Cell 5		-0.923	0.31	28.5	0.0816
	Cell 6		-0.803	0.26	28.1	0.0587

**Initial conditions of the glove-box:* O_2*: 530ppm;* H_2O*: 2150 ppm*

Appendix II.

(a) Characterised Outcomes of the Flexible Samples

Sample/Cell		**Jsc(mA/cm²)**	**Voc(V)**	**FF(%)**	**PCE(%)**
YF-01	C1(S)	-2.38	0.59	21.4	0.300
	C2(S)	-3.18	0.52	24.5	0.405
	C3(S)	-2.82	0.60	21.6	0.365
	C4(U)	-2.09	0.59	19.5	0.241
	C5(U)	-1.54	0.59	21.2	0.193
	C6(U)	-1.25	0.36	27.1	0.122
YF-02	C4(U)	-2.74	0.71	17.5	0.307
	C5(S)	-3.10	0.69	16.6	0.356
	C6(S)	-3.54	0.70	17.0	0.421
YF-03	C1(S)	-11.40	0.50	20.7	1.180
	C2(S)	-10.60	0.48	19.5	0.992
	C3(S)	-6.57	0.45	19.7	0.583
	C4(U)	-7.46	0.46	22.1	0.760
	C5(U)	-7.39	0.43	20.2	0.643
	C6(U)	-5.79	0.34	22.0	0.433
YF-04	C1(S)	-3.49	0.63	21.9	0.482
	C2(S)	-5.03	0.64	22.3	0.717
	C3(S)	-1.78	0.63	22.7	0.254
	C4(U)	-3.47	0.64	21.3	0.474
	C5(U)	-2.70	0.64	21.0	0.363
	C6(U)	-1.76	0.64	21.0	0.237

**(S) - nanostructured solar cell; (U)- un-nanostructured solar cell.*

**Conditions in glove-box: O_2:85ppm; H_2O: 11ppm.*

**Annealing conditions: For P3HT:PCBM active layer: 140 ℃ for 20min;*

For top PEDOT:PSS layer: 140 ℃ for 2min30sec.

(b) Comparison of the Flexible Solar Cell's Characteristics before & after Peeling-off

Sample/Cell		**Before Peeling**				**After Peeling**			
		Jsc (mA/cm²)	**Voc (V)**	**FF (%)**	**PCE (%)**	**Jsc (mA/cm²)**	**Voc (V)**	**FF (%)**	**PCE (%)**
YF-05	C1	-4.31	0.60	49.1	1.27	-2.84	0.57	45.8	0.74
	C2	-4.13	0.60	48.4	1.20	-3.30	0.57	50.3	0.95
	C3	-3.64	0.60	48.5	1.06	-3.22	0.58	44.8	0.84
	C4	-4.61	0.60	41.9	1.16	-4.81	0.58	42.3	1.18
	C5	-1.42	0.59	44.5	0.37	-1.45	0.58	44.6	0.38
YF-06	C1	-5.06	0.61	33.0	1.02	-3.87	0.59	34.2	0.78
	C2	-6.05	0.59	36.1	1.29	-5.59	0.58	35.2	1.14

**Conditions in the glove box: O_2-2.0ppm; H_2O-131.6ppm.*

**Annealing conditions: For P3HT:PCBM active layer: 140 ℃ for 20min;*

For top PEDOT:PSS layer: 140 ℃ for 2min30sec.

Appendix III - The Process Recipe of Photolithography

STEP	CONTENT	CONFIGURATION	DESCRIPTION
1	Starting Wafer		For the rigid solar cells, the glass wafer is BK7; for the flexible solar cells, the substrate is a 10µm thick PI2525 film on top of handling wafer P1(Si(100), 4'', single-side polished, thickness=525µm).
2	Deposit Adhesion Promoter	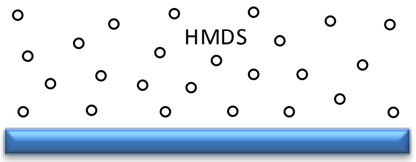	HMDS processing, for getting good photoresist adhesion in the following step.
3	Spin-coating Photoresist	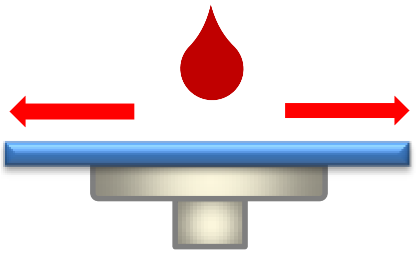	EBS11 spin-coater, photoresist: AZ 5214E, thickness=1.5 µm; 1 Automatic photo dispense; 2 Spin at 500rpm for 5s (acc.5000rps2); 3 Spin at 4000rpm for 30s;(acc.10000rps2)
4	Prebake	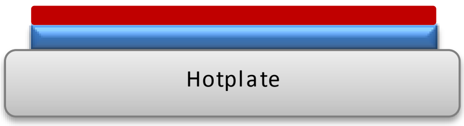	Hotplate, 90°C for 60s.
5	UV Exposure	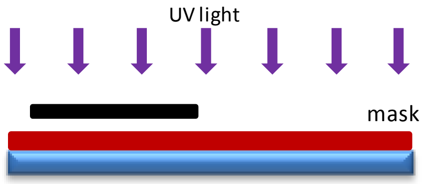	KS mask aligner, exposure time=35s.
6	Inversion Bake		Hotplate, 140°C for 120s.
7	Flood Exposure	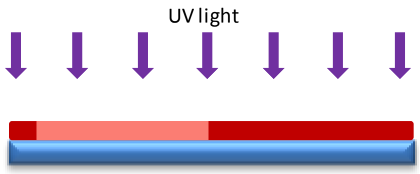	KS mask aligner, exposure time=45s, without mask.

8	Development	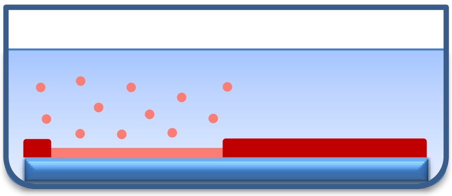	Developer: AZ 351B (mixed with DI water, ratio=1:4), agitation for 60s.
9	Air-blow Drying	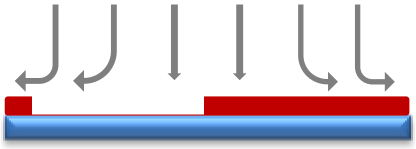	Blow-drying with clean dry air.
10	Inspection		With optical microscope and profiler.
*11	Metal deposition	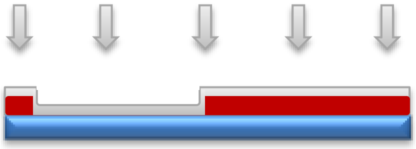	The metal deposition depends on the designed architecture of the bottom electrodes
*12	Lift-off	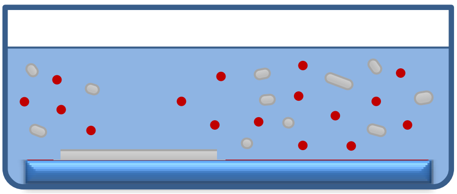	Immerse into acetone for a certain while: For the rigid solar cells, ultrasonication is possible, but for the flexible solar cells, only mild shaking is acceptable.
*13	Air-blow Drying	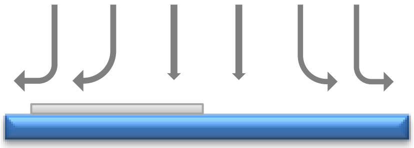	Blow-drying with clean dry air.

** Actually, the Step 11, 12 and 13 shouldn't to be counted as a part of the photolithography process. However, in order to make the process integrated and manifest, I still put them into this recipe.*

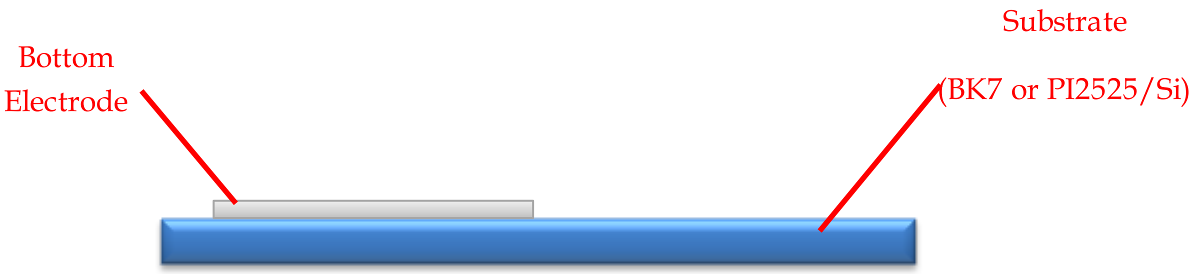

Appendix IV- The E-beam Recipes of Bottom Electrode Deposition

A. The Initial Architecture

LAYER (FROM THE BOTTOM UP)	MATERIAL	BASE PRESSURE	DESIGNED THICKNESS	DEPOSITION RATE	CONFIGURATION
1	Ti	3x10^{-5}mbar	3nm	1Å/s	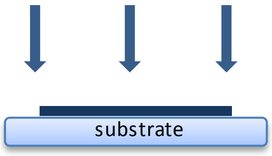
2	Al	3x10^{-5}mbar	80nm	2Å/s	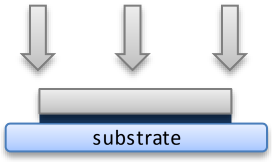
3	Ti	3x10^{-5}mbar	20nm	2Å/s	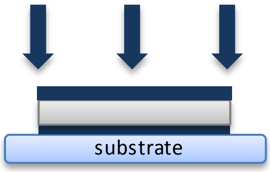

B. The Latter Architecture

LAYER (FROM THE BOTTOM UP)	MATERIAL	BASE PRESSURE	DESIGNED THICKNESS	DEPOSITION RATE	CONFIGURATION
1	Al	3x10^{-5}mbar	80nm	2Å/s	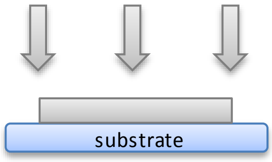
2	Ti	3x10^{-5}mbar	2nm	1Å/s	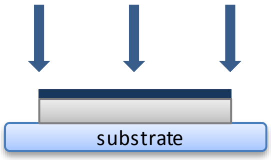

**1mbar=100Pa(SI)*

Appendix V - Solar Cell Fabrication (on BK7 glass substrate)

STEP	CONTENT	CONFIGURATION	DESCRIPTION
1	Substrate Cleaning		Clean the substrate (with bottom electrodes on) with acetone and IPA, clean air blow-dry.
2	Tape1 Covering	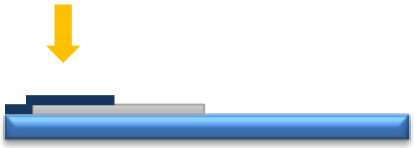	The tape needs to be sticky properly, while cannot leave any contamination which may degrade the solar cells' performance.
3	Spin-coating Active Material	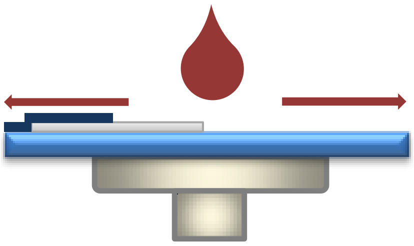	At 1500~2500rpm for 45sec(depending on specific requirements).
4	Tape1 Removal	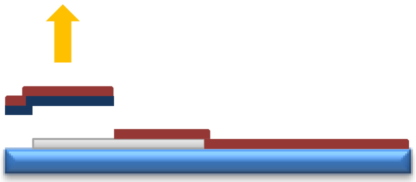	With the help of tweezers.
5	1st Annealing		140℃ for a certain time. Normally from 10 to 45 min.
6	Tape2 Covering	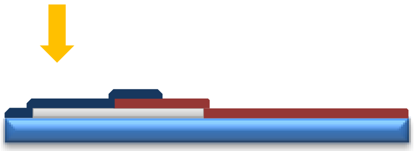	Same as Step2.

7	Spin-coating PEDOT:PSS blend	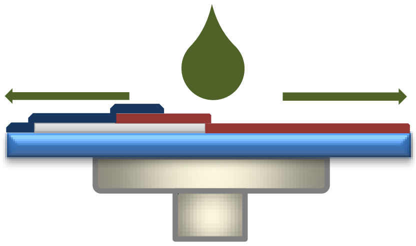	At 1500~2500rpm for 45sec (Also depending on specific requirements).
8	Tape2 Removal	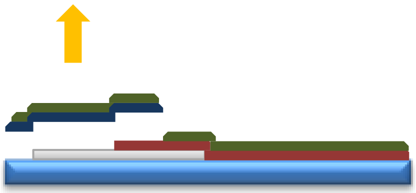	Same as Step4.
9	2nd Annealing		140℃ for a certain time. Normally 2.5min.
10	Ag Paste Laying	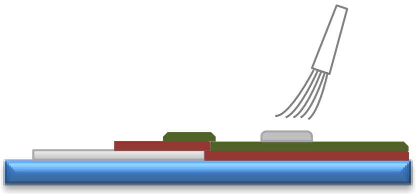	Ag paste is brushed on top of the PEDOT:PSS layer.

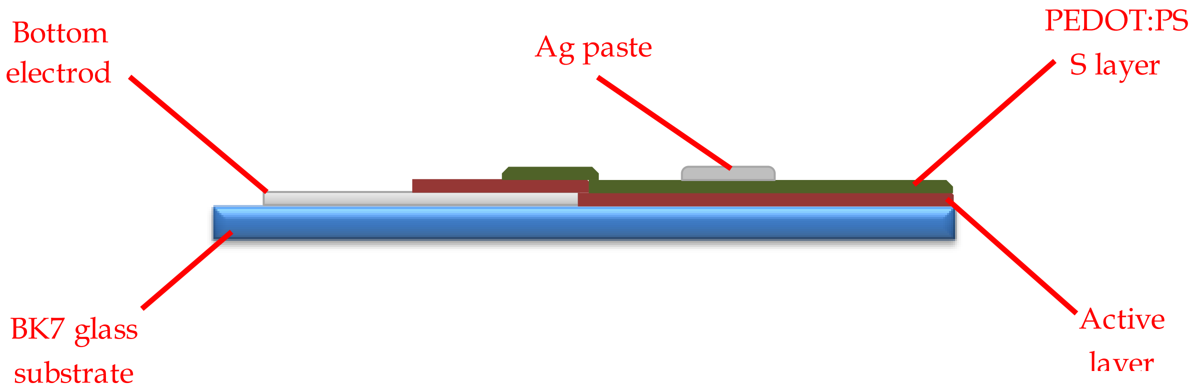

Appendix VI - PI2525 Substrate Fabrication

STEP	CONTENT	CONFIGURATION	DESCRIPTION
1	Si Substrate Preparation		Before dispensing polyimide on, the Si wafer needs to be cut in designed dimension. Pre-cleaning is necessary before starting the fabrication process. (Acetone-IPA-DI water-Clean air blow)
2	Spin-coating PI2525	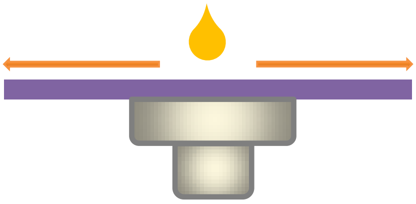	1. 1000rpm for 5sec; 2. 2000rpm for 45sec. PI 2525 solution needs to be stored in a cold, dark, steady circumstance and well-sealed before & after using.
3	Heating-up from RT to 210℃		The 210℃ temperature is reached after a slow temperature slope of 4℃/min. Hence this process lasts around 47mins
4	Staying at 210℃		Staying at 210℃ for around 2h 13min, so that the whole process is approximately 3 hours.
5	Cooling Down		Cooling down to the RT.

Appendix VII-Solar Cell Fabrication (on PI2525 substrate)

STEP	CONTENT	CONFIGURATION	DESCRIPTION
1	Substrate Cleaning		Clean the substrate (with bottom electrodes on) with acetone and IPA, clean air blow-dry.
2	Tape1 Covering	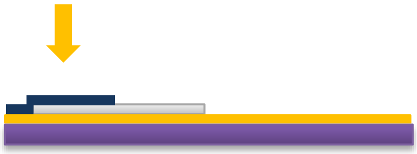	The tape needs to be sticky properly, while cannot leave any contamination which may degrade the solar cells' performance.
3	Spin-coating Active Material	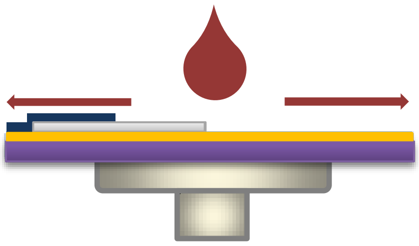	At 1500~2500rpm for 45sec(depending on specific requirements).
4	Tape1 Removal	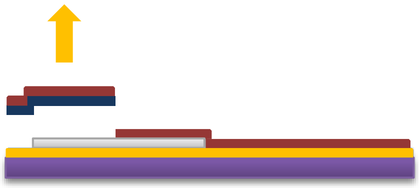	With the help of tweezers.
5	1st Annealing		140℃ for a certain time. Normally from 10 to 45 min.
6	Tape2 Covering	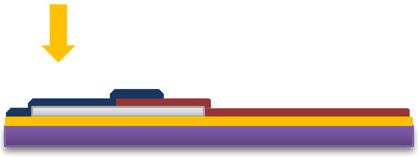	Same as Step2.

7	Spin-coating PEDOT:PSS blend	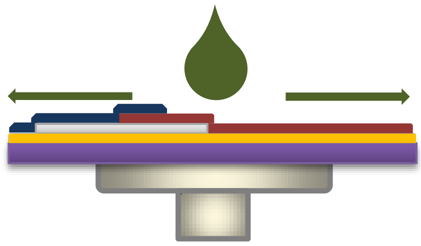	At 1500~2500rpm for 45sec (Also depending on specific requirements).
8	Tape2 Removal	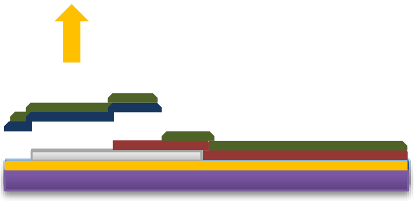	Same as Step4.
9	2nd Annealing		140℃ for a certain time. Normally 2.5min.
10	Ag Paste Laying	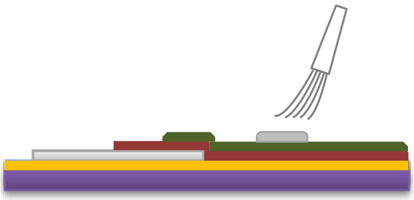	Ag paste is brushed on top of the PEDOT:PSS layer.
11	Peeling-off	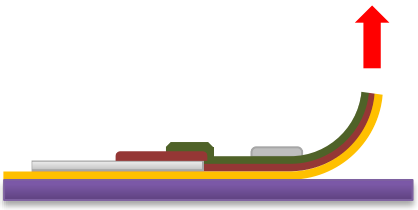	Peeling the solar cell off from the handling Si substrate.

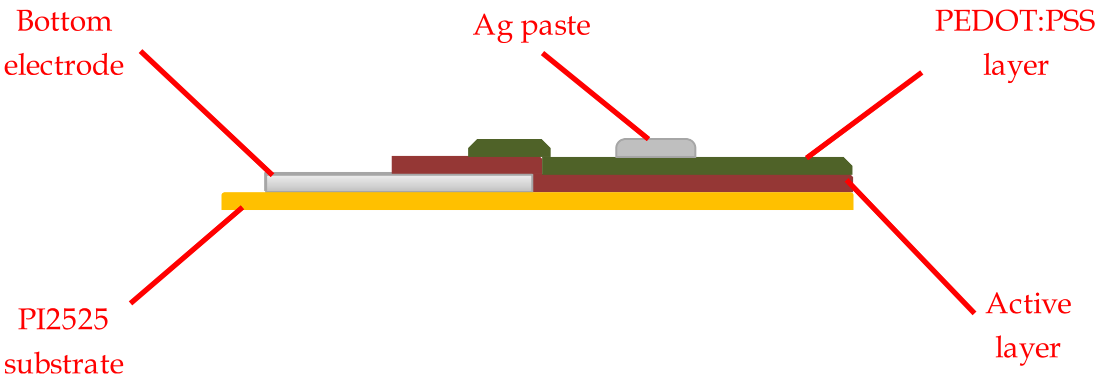

Appendix VIII - Periodic Nanostructure Fabrication with EBL

STEP	CONTENT	CONFIGURATION	DESCRIPTION
1	Substrate Cleaning		Clean the substrate (with bottom electrodes on) with acetone and IPA, clean air blow-dry.
2	Spin-coating Resist	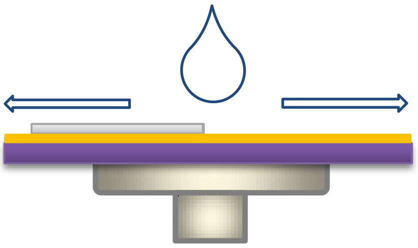	Resist: PMMA A4, thickness≈150μm. 1, 1500rpm for 5sec; 2, 7000rpm for 45sec;
3	Hard-baking	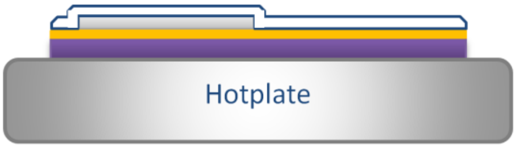	200℃ for 90sec.
4	E-beam Writing	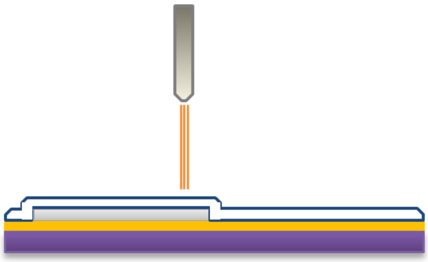	Electron beam photolithography (EBL) process.
5	Development	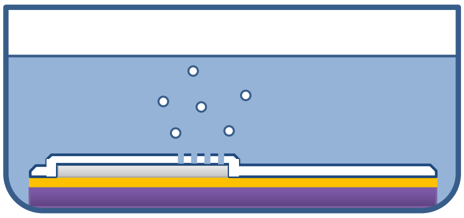	1, Develop in the developer MIBK:IPA(1:3) for 40sec; 2, Dip in the stopper IPA for 30sec.

6	Air-blow Drying	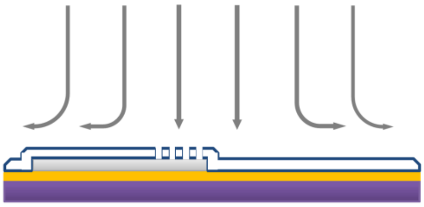	Blow-drying with clean dry air.
7	Metal Deposition	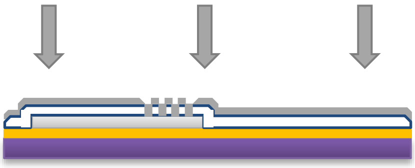	50nm thick Titanium layer in this project.
8	Lift-off	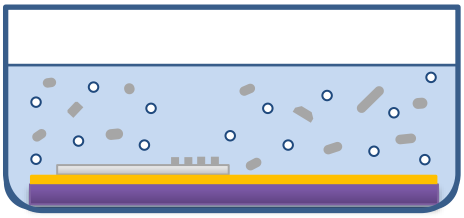	Lift-off with acetone, a mild vibration is used instead of ultrasonication.
9	Inspection	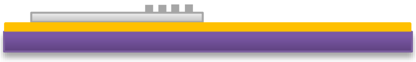	Optical microscopy, AFM or SEM.